Centre for Ecology & Hydrology

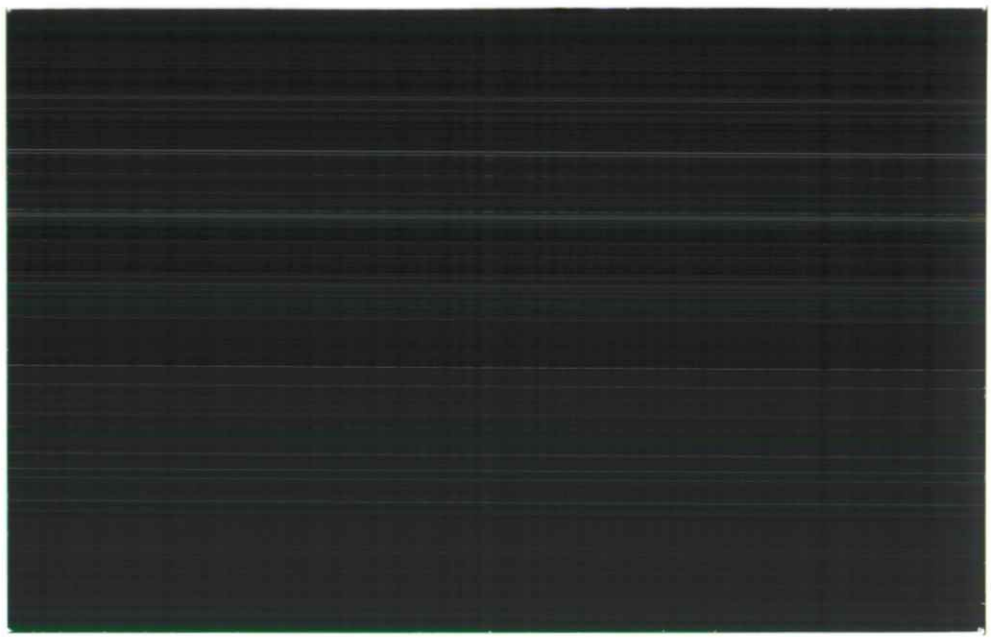

Natural Environment Research Council

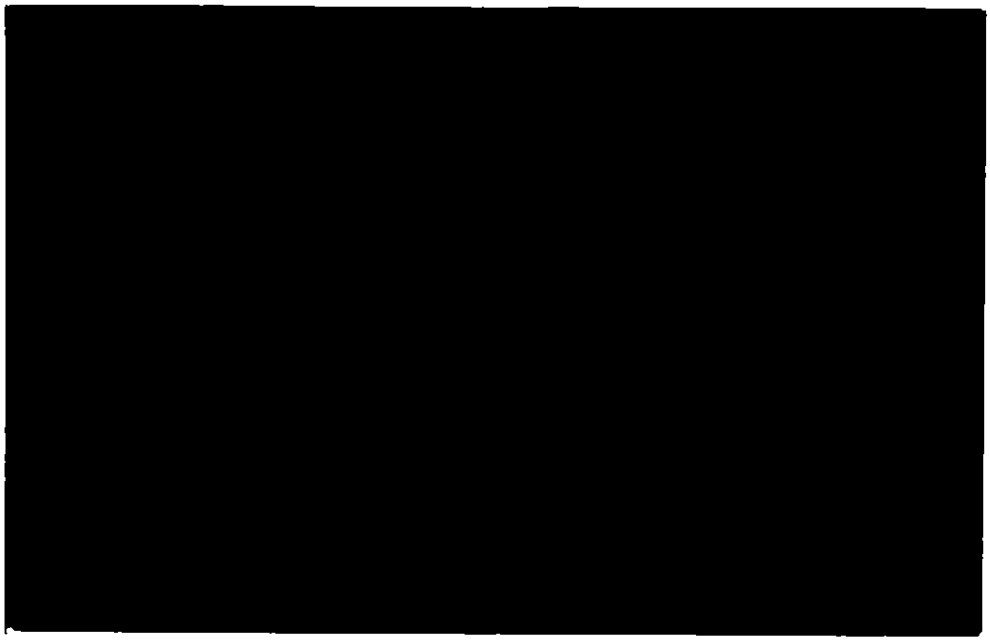

Development of an Integrated Hydro-Ecological Model (IHEM)

First Year Report

C. Huntingford
October 1999

Please accept this report as "provisional". The two manuscripts Huntingford and Smith, and, Huntingford and White, should be nearer to publication in about a month. I would be grateful if I could resubmit the report then for formal CEH archiving.

First Year Report

Development of an Integrated Hydro-Ecological Model (IHEM)

C. Huntingford
October 1999

The structure of this report is to summarise activities undertaken within the first year of this CEH Integrating Fund project. A brief outline of activities undertaken to date are presented here, but the bulk of the report consists of manuscripts that are either accepted for publication, or near to submission.

Brief overview of project description

The following text is contained within the original project description:

The IHEM project will exploit existing component modelling approaches at IH and ITE to:

1. Develop an efficient integrated model, capturing the essential elements of plant growth and surface-atmosphere gas exchange including atmospheric and soil feedbacks.
2. Investigate ecosystem responses over a wide range of environmental conditions and anthropogenic forcings.
3. Significantly increase the confidence with which land-surface responses to atmospheric changes may be predicted.

Such a model (IHEM) will:

1. Explicitly characterise all important inter-component feedbacks.
2. Demonstrate if such feedbacks simplify behaviour of the surface-atmosphere system.
3. Be succinct and parameter-scarce, as opposed to a complicated series of individual component models.

First year activities

The very first task of the project was to spend a few days working on the final galley proofs of paper **Huntingford** (IH) and **Monteith** (ITE Bush) "The behaviour of a mixed-layer model of the convective boundary layer coupled to a big leaf model of surface energy partitioning". This outlines a methodology to reduce land surface and boundary-layer feedbacks so a single equation. The Penman Monteith and Convective

(atmospheric) Boundary Layer equations may be formally combined to a single functional form, mainly dependent upon stomatal resistance. The resultant form demonstrates a surprising reduction in variability in land surface energy partitioning (as a function of other environmental constraints) into latent and sensible heat fluxes.

A key task of the project is to develop a land surface description capable of predicting potential changes in land surface cover within a warmer, CO_2 enhanced atmosphere. This has been achieved through simplification of the Hadley Centre GCM land surface model, and a new description developed representing a single vegetation type. Model thresholds are found within a prescribed changing climate that allow either 1) a new vegetation type to emerge, 2) an existing vegetation type that is robust to climate change and 3) an existing vegetation type that will "die-back" (re: similar work by **Andrew Friend (ITE, now NASA-GISS)** on die-back within the Amazon rainforest). An interesting finding is that the onset of "die-back" is highly dependent upon the functional form prescribed for plant respiration. Traditionally, such fluxes are given less attention that photosynthetic activity. This paper demonstrates that this could be a dangerous approach when predicting future global change. The work is summarised in **Huntingford (IH), Cox (Hadley Centre) and Lenton (ITE Bush)**, and has been submitted to Ecological Modelling.

The ability of the convective boundary layer to mitigate (or otherwise) changes in surface energy fluxes, as a function of variation in the land surface, are formally classified within a statistic *s*. If *s* is greater than 100%, then the atmospheric boundary layer will enhance any changes in the land surface. This work undertaken here extends that by Jacobs and DeBruin (J. Climate, **5**, p693), but within a more formal framework. It provides a linkage with the work of Huntingford and Monteith (1998). The atmospheric boundary-layer is found to suppress changes in stomatal resistance and roughness length, but enhances the impact of variation in surface albedo on surface flxues. This has implications for changes in land surface cover and land degradation. A paper has been written **Huntingford (IH) and White (ITE Bush, now Herriot Watt university)** which is near to internal review and hopefully submission to Boundary-layer Meteorology.

To develop a balanced model of boundary-layer feedbacks, the land surface description must retain a simple framework. It is very easy to develop more and more complicated land surface models, sometimes with each vegetation biome retaining it's own characteristics. However, even at very low levels above the ground, the individual fluxes can be aggregated to just a few parameters. To demonstrate this (and the ability to transfer parameterisations between surface scheme of different complexities), a test case of heat fluxes for a Sahelian savannah are investigated. This is summarised in a manuscript (accepted, subject to minor revision) by **Huntingford (IH), Verhoef (IH, now Reading university) and Stewart (IH, retired)**.

The most important control upon land surface energy partitioning (and associated energy fluxes into the atmosphere, controlling boundary layer development) is stomatal resistance. Many authors have modelled this as a function of microclimate, and notably temperature, vapour pressure deficit, soil moisture content and atmospheric CO_2

concentration. However Monteith (1995, Plant Cell Env., **18**, p357) suggest that the vapour pressure deficit response is actual a proxy variable for vegetation response to the water fluxes. In addition, Leuning (1995, Plant Cell Env., **18**, p339) suggest that the temperature and light responses are a proxy variable for response to net photosynthesis. Finally, work of Tardieu (1993, Phil. Trans. R. Soc. Lond., **341**, p57) suggest that stomatal behaviour is due to chemical signalling (ABA), alerting stomatal controls to soil water status. This Integrating Fund project has allowed a comparison to be made between such models. Mathematical analysis has highlighted that all three models can in fact be related, and formally shown to be nearly equivalent. Extending this analysis further shows that in fact stomatal control can be shown to be a function of BOTH water and carbon dioxide fluxes, and the two other external variables of soil water status and atmospheric CO_2 concentration only. This work is currently given within a draft manuscript by **Huntingford (IH) and Smith (IH)**, which we hope to place within internal review shortly. If physically correct, then this will greatly reduce the complexity of land surface schemes needed, and could change our current perception of how vegetation responds to both short timescale weather, and longer term climate change. Indeed, the mathematical analysis has generated a major surprise here. It is just possible that all short term dependence of stomatal control to "weather" is contained within explicit responses to the water and photosynthetic fluxes, whilst the long term behaviour is given through two environmental conditions with "memory", namely soil water status and atmospheric CO2 concentration. We certainly look forward to seeing what the referees make of it – the intention is to submit to Plant Cell and Environment.

In a final development, a piece of work has started looking at the dependence of surface energy partitioning as a function of stomatal control, but based upon the extensive data held at IH. Both papers (Huntingford and Monteith, and, Huntingford and White) hopefully generate new insights into boundary-layer feedbacks, but they are quite idealised in concept. In a research paper (**Huntingford (IH) and Harding (IH)**), data from four sites that range across geographical extremes will be collated and combined into a single study. These sites are a) tundra site, North Norway, b) UK grassland site, c) Sahelian site, SW Niger and d) Amazonia, Rondonia, Brazil. A riddle needs to be addressed. The previous papers suggest that, apart from initial temperature and humidity at sunrise, surface energy partitioning is almost independent of all other initial or boundary conditions. If this is the case, then it should be possible to characterise water use efficiency almost totally as a function of mean climatology. Careful (and consistent) analysis of these datasets will hopefully confirm the validity of these findings.

Other project activities have included:

- Retaining and developing all numerical code used within the manuscripts. This code is very carefully documented (including all variable descriptions, units and appropriate "comment" statements), which will allow for a final IHEM model to be distributed.

- Full literature searches undertaken and maintained using the BIDS system, with references then filed locally in Reference Manager. This electronic structure of information (and the associated references themselves) allows for a CEH database on land-atmosphere feedbacks to be developed.

- The creation of a project web site, for cross access with ITE (Bush).

- The project now has file space and access to the full ECMWF Re-analysis database, which will be of importance within year 2 of the project.

- Implementation of the Met Office Single Column Model on the Institute of Hydrology computers.

- Visits by staff between Wallingford and Edinburgh (and vice versa).

Perhaps the most helpful contribution to this project that is not currently available is further details ecological information on vegetation change and structure that may occur within a perturbed climate. This information could be used to further enhance/calibrate the physiological aspects of the IHEM model. It is certainly a loss that both collaborators from ITE Bush (Andrew Friend and Andy White) have accepted posts elsewhere. However, once the ITE Bush modelling group is rebuilt, I believe there will be some superb opportunities to develop the biological aspects further.

Proposed activities in year two

I am hopeful that the manuscripts outlined above have generated a framework of modelling components that are of "intermediate complexity" inasmuch as they are 1) parameter scarce, 2) when coupled together generate a well-balanced (IHEM) model, but most importantly, 3) still retain all the salient features expected in land-atmosphere feedbacks. However, it is not enough to simply create "conceptual" models, and I hope this project will place a high emphasis upon comparison with actual data.

The Institute of Hydrology has a long history of land surface measurements, using eddy correlation devices to relate local microclimate to surface fluxes of water and carbon. These provide good understanding of land surface processes, but of course they are uncoupled from the atmosphere above. The intention is to use these measurements in conjunction with the Met. Office Single Column Model, thereby combining surface behaviour with atmospheric feedbacks. A missing component is prescription of atmospheric fluxes of heat and vapour into the column of air above. These will be derived from the ECMWF re-analysis data. The latter is based upon real data, as the ECMWF analysis includes meteorological measurements to "nudge" their model output to be more realistic. The combination of all these components will allow the issue of local atmospheric feedbacks to be reduced to a closed system.

The work undertaken within the first papers outlined above do rely on the models applied to clear and sunny days. A major step forward will be to use the Met .O. Single Column Model to investigate feedbacks during periods of cloudiness and even rainfall. Classification of advective fluxes will play a very important role in this case.

A further hope is to continue collaboration with **Mark Smith (IH),** and test the ideas outlined in the Appendix against data collected from the Blackwood field site. If it is confirmed that vegetation response is based far more upon surface fluxes (as opposed to microclimate), then a unique opportunity opens to revisit and extend the optimisation ideas of Farquhar (Canberra University), as already started by **Huntingford (IH), Raupach (CSIRO) and Cox (Hadley Centre)**. This earlier work is outlined within the Appendix to "Combined growth and water use modelling of mixed vegetation", *CEH Integrating Fund Project T06050P2*. Many of these new ideas are written out in note form. Their further extension provide a fantastic opportunity for the new CEH Bush staff to develop under this project.

Within the Institute of Hydrology, colleagues are undertaking equilibrium GCM simulations with different land surface descriptions. A hope is that this project (by year three) will be of use of such colleagues by providing some simplified insight into the full GCM simulations.

I do believe that this project will enhance the CEH science base. Much comes down to finding to correct balance between providing the "glue" between other CEH science activities, developing conceptual models that are a distinct product of this project itself, and then relating such models to the extensive datasets held within the separate CEH labs.

Contrasting responses of a simple terrestrial ecosystem model to global change

Huntingford, C.

Cox, P.M.

Lenton, T.M.

SUBMITTED TO "ECOLOGICAL MODELLING"

Contrasting responses of a simple terrestrial ecosystem model to global change

C. Huntingford[+], P.M. Cox[++] and T.M. Lenton[+++]
[+] *Institute of Hydrology, Wallingford, OX10 8BB, U.K.*
[++] *Hadley Centre, Bracknell, RG12 2SY, U.K.*
[+++] *Institute of Terrestrial Ecology, Edinburgh Research Station, Bush Estate, Penicuik, Midlothian, EH26 0QB, U.K.*

September 14, 1999

Abstract.
A simple parameter-scarce model of vegetation dynamics is introduced which describes a single dominant vegetation type using three equations for vegetation carbon, fractional coverage by the vegetation and soil carbon. Three categories of response to prescribed increases in atmospheric CO_2 concentration and temperature are identified:

(1) The emergence of a new dominant vegetation type in a cold environment. When the vegetation is establishing, there is a long period (dependent upon the "seeding" fraction) of slow vegetation spread. This is followed by a rapid increase in fractional cover as the vegetation moves to being in near equilibrium with the perturbed climate, causing a large pulse of positive net ecosystem productivity (carbon uptake from the atmosphere).

(2) Robust behaviour of an established vegetation in a warm environment. Extra carbon assimilated is mostly allocated to spreading, but because the fractional cover is nearly complete, the carbon is further diverted into extra litter fall ("self shading"). The soil carbon reservoir grows and net ecosystem productivity is initially weakly positive. However, soil respiration increases more rapidly with warming than net primary production, causing a gradual switch to weakly negative net ecosystem productivity.

(3) "Die-back" can occur at high temperatures. Net primary productivity starts to decrease causing a decline in litter supply and shrinkage of the soil carbon reservoir. Eventually, there is not enough incoming carbon to match natural disturbance rates, and the vegetation rapidly decreases in fractional coverage until it disappears. This causes a large pulse of negative net ecosystem productivity (releasing carbon dioxide to the atmosphere). In the simulations undertaken, the assumption that dark and plant respiration do not "cut-off" at high temperatures allowed sufficient decrease in net primary productivity to trigger such "die-back". The description of respiration strongly influences the predicted behaviour of the terrestrial ecosystem model.

KEYWORDS: Biomass, Growth modelling, CO_2 fertilisation, Respiration, Climate Change

1 Introduction

Anthropogenic fossil fuel emissions are increasing atmospheric carbon dioxide concentrations, and are likely to cause associated increases in mean atmospheric temperature (the "greenhouse" effect). The uptake or release of carbon by terrestrial ecosystems depends upon both ambient carbon dioxide and temperature as these directly affect ecosystem productivity.

The next generation of General Circulation Models (GCMs) will include the global carbon cycle, and as such will require a description of the changes in terrestrial carbon budget. A GCM coupled to a land surface model can predict changes in terrestrial carbon which might result from perturbations in atmospheric green-

house gases. Associated increases in radiative forcing are balanced by changes in surface microclimate (most notably temperature, T (K)), which impacts upon the fluxes of both photosynthesis, and vegetation and soil respiration. Photosynthetic activity is also a function of ambient CO_2 level c_a (ppm), and this concentration may itself be enhanced or offset by changes in terrestrial carbon content.

Coupled GCM simulations include land-atmosphere feedback mechanisms, which influence the response of terrestrial ecosystems to changing climate. However, in this fully coupled context, it may be difficult to isolate and understand particular modes of vegetation behaviour. For example, ecosystem change as a consequence of land-atmosphere feedbacks may be difficult to distinguish from characteristics of the terrestrial carbon cycle model.

It is necessary to understand generic behaviours of the terrestrial carbon cycle that can occur within a changing climate, and can then be classified and related to thresholds in climatic forcing. To develop this categorisation, it is sensible to study the different behaviours of any proposed land surface model "off-line", driven by representative changes in microclimate due to increased radiative forcing.

In this paper, a simple description of vegetation dynamics is presented which is a subset of the "TRIFFID" dynamic global vegetation model currently being introduced within the Hadley Centre GCM (Cox and Palmer, 1996). This simple model captures the gross ecosystem changes that may be expected within a CO_2 enriched climate. The model is deliberately simple and parameter-scarce, but dynamic, allowing the investigation of vegetation "lags" when responding to a changing climate. The vegetation may grow vertically (thereby changing the vegetation carbon), and may also spread at higher net primary productivity values (thereby adjusting the fractional coverage). The main driving variable is net primary productivity, supplied by a model of photosynthesis and plant respiration. Two different descriptions of vegetation respiration as a function of temperature are analysed, which differ as to whether a high temperature "cutoff" exists. A complete mathematical description is provided, onto which more complicated dynamic terrestrial ecosystem models can potentially be mapped.

The equations of the model are described in Section 2. Section 3 presents numerical solutions for three case studies, in which the initial atmospheric (leaf level) temperature is prescribed different values, thereby representing different climatic regimes. These include cases representing vegetation emergence and "dieback". Section 3.4 also discusses the critical CO_2 concentration beyond which ecosystem carbon storage is modelled to decrease. The model is tractable to analytical methods, which are used to contrast the equilibrium and dynamic solutions in Section 4. In equilibrium mode, all behaviour is described through a series of derived algebraic solutions. In dynamic mode, "order-of-magnitude" analyses allow lags in the system (the differences between dynamic and equilibrium response) to be mathematically described and predicted. The relevance of the results to future global change are discussed in Section 5.

2 The governing equations

2.1 Ecosystem model

The status of a dominant vegetation type is described by just three key controlling variables, namely vegetation carbon, C_B (kg C (m^2 vegetation)$^{-1}$), fractional coverage ν (m^2 vegetation (m^2 land surface)$^{-1}$) and soil carbon C_S (kg C (m^2 land surface)$^{-1}$). Vegetation is allowed to grow or shrink "vertically" (within a fixed area), through variations in C_B. The rate of change of C_B is modelled as the balance between net carbon accumulation by the vegetation and natural turnover thus:

$$\frac{\mathrm{d}C_B}{\mathrm{d}t} = (1 - \lambda_\nu)\,\Pi - \gamma_c C_B \tag{1}$$

where Π (kg C (m^2 vegetation)$^{-1}$ s^{-1}) is Net Primary Productivity (NPP), $(1-\lambda_\nu)$ is an allometric constant for the fraction of NPP directed to vegetation growth, γ_c (s^{-1}) is vegetation turnover timescale and t (s) is time.

Vegetation is also allowed to spread or retract in spatial coverage. The rate of change of fractional coverage is a balance between the remaining NPP (after growth) that is available for spreading minus any disturbance. Hence

$$C_B \frac{\mathrm{d}\nu}{\mathrm{d}t} = \lambda_\nu \nu(1 - \nu)\Pi - \gamma_\nu \nu C_B \tag{2}$$

where γ_ν is the disturbance rate. The factor $(1 - \nu)$ represents additional disturbance due to "self-shading", and is consistent with the Lotka-Volterra equation for ecosystem competition.

The spatial (patch) scale associated with vegetation coverage is considered small, and as such soil carbon is assumed to be everywhere (and hence the units of C_S being per unit of land surface). Soil carbon is a balance between incoming vegetation litter Λ (kg C m^{-2} vegetation s^{-1}) and soil respiration rate R_s (kg C m^{-2} land surface s^{-1}). That is

$$\frac{\mathrm{d}C_S}{\mathrm{d}t} = \nu\Lambda - R_s \tag{3}$$

The total carbon content C_T (kg C m^{-2} ground) is therefore given by $C_T = \nu C_B + C_S$.

The litter flux is composed of biomass falling to the ground through both turnover and disturbance. Conservation of vegetation carbon gives (from combining Eqs (1) and (2))

$$\frac{\mathrm{d}}{\mathrm{d}t}(\nu C_B) = \nu\Pi - \nu\left[C_B(\gamma_c + \gamma_\nu) + \lambda_\nu \nu \Pi\right], \tag{4}$$

and so $\Lambda = C_B(\gamma_c + \gamma_\nu) + \lambda_\nu \nu \Pi$.

2.2 PARTITIONING PARAMETER, λ_ν

A dimensionless partitioning parameter, $0 \leq \lambda_\nu \leq 1$, determines how available carbon is split into growth or spreading. A number near unity implies that most NPP is directed into "spreading", whilst a number near zero implies that most NPP is directed into "vertical" growth. In this model, vegetation needs to grow to a critical biomass, expressed as a minimum leaf area index, L_{min} (m^2 leaf (m^2 vegetation)$^{-1}$), before spreading can occur. For an emerging vegetation that attains L_{min} (due to a changed climate resulting in increased NPP), the carbon available for spreading is modelled as increasing linearly in leaf area index, L (m^2 leaf (m^2 vegetation)$^{-1}$). That is

$$\lambda_\nu = \begin{cases} 0 & L \leq L_{min} \\ \frac{L - L_{min}}{L_{max} - L_{min}} & L_{min} < L < L_{max} \\ 1 & L \geq L_{max} \end{cases} \tag{5}$$

where L_{max} (m^2 leaf (m^2 vegetation)$^{-1}$) is a maximum attainable leaf area index. Here, the dominant vegetation type is considered to be mainly representative of trees, and L_{min} and L_{max} are set as 4 and 10 respectively. Leaf area index and vegetation carbon are related in a simple linear fashion as

$$C_B = \sigma L \tag{6}$$

where σ (kg C (m^2 vegetation)$^{-1}$) is a constant of proportionality. For this exercise, a value of σ is found through comparison with the main TRIFFID model for a high LAI value (representative of forest). This gives a value of $\sigma = 1.72$, although Eq. (6) represents a significant simplification of the full TRIFFID model.

Equations (1) to (6) provide a complete and parameter-scarce dynamic vegetation model for given carbon dioxide fluxes into and out of the system, namely net primary productivity, Π and soil respiration R_s.

2.3 LEAF PHOTOSYNTHESIS AND RESPIRATION

Top-leaf net photosynthesis, A_l (kg C (m^2 vegetation)$^{-1}$ s^{-1}), is given by

$$A_l = P_l - R_{d,l}$$

where P_l (kg C (m^2 vegetation)$^{-1}$ s^{-1}) is the top-leaf gross photosynthesis and $R_{d,l}$ (kg C (m^2 vegetation)$^{-1}$ s^{-1}) is the top-leaf dark respiration. Many authors propose that gross photosynthesis is the minimum of three rates, each representing a "light limited", "Rubisco limited" and "transport limited" solution, whilst Collatz *et al.* (1991) propose a gradual transition between such limits. This latter approach is adopted here, with the parameterisations described in full in Cox *et al.*, 1999. In particular, P_l is dependent upon photosynthetically active radiation, I_{par} (W m^{-2}), leaf level temperature, (assumed to be the ambient temperature, T (K)) and intercellular CO_2 concentration, c_i (ppm). Stomatal conductance g_s (m

s^{-1}) is based upon the description of Jacobs (1994) and implemented by Cox *et al.*, (1998), which relates c_i to leaf level specific humidity deficit, D (kg kg^{-1}), and the ambient CO_2 concentration, c_a (ppm), as $(c_i - \Gamma)/(c_a - \Gamma) = f_0[1 - (D/D_*)]$. Constants $D_* = 1.0$ (kg kg^{-1}) and $f_0 = 0.875$ are representative of broadleaf trees, and Γ (ppm) is the photorespiration compensation point. When combined with the equation for diffusion of CO_2 through the stomata, this "closure" enables g_s to be derived from net photosynthesis. This "closure" shows that gross photosynthesis also depends upon temperature and leaf level humidity, q (kg kg^{-1}) via D and also the ambient CO_2 concentration, all by influencing intercellular CO_2 concentration, c_i. In the event that $R_{d,l} > P_l$, then stomatal conductance is fixed at a minimum value.

Although the dependence of P_l upon the combination of T, I_{par}, c_a and q is complicated, a dominant feature throughout is a strong response to temperature. In particular (for small variations in c_i and high values of I_{par}), there is a near proportionality to the maximum rate of carboxylation of Rubisco, $V_{c,max}$ (mol (m^2 vegetation)$^{-1}$ s^{-1}). Expressed through parameter ζ, normalised to unity at $T = 298.15$K, then for C_3 plants this is given as

$$\zeta = 1.037 \frac{2.0^{0.1(T-298.15)}}{1 + e^{0.3(T-309.15)}}.$$

This functional form, including the higher temperature cut-off implicit within the denominator, is based on the work of Collatz (1991).

A model is required for top-leaf dark respiration, $R_{d,l}$. Within the literature, there are a range of different temperature dependent functions to describe dark respiration fluxes. Many models describe dark respiration as increasing continuously as temperatures rise (eg Lloyd *et al.*, 1995, Friend *et al.*, 1995), and where the latter uses a function that (for a broad range of temperatures) is the equivalent to a "Q10" function of value near two. Other authors perturb these functions to include a high temperature cutoff (eg Collatz *et al.*, 1991), and many authors relate $R_{d,l}$ directly to $V_{c,max}$ (Sellers *et al.*, 1996, Cox *et al.*, 1999). These functions contain quite different behaviour, particularly at higher temperatures.

An estimate of the sensitivity of the dynamic terrestrial ecosystem model to the description of dark respiration is sought. Hence, two possible functional forms are considered that represent different behaviours at higher temperatures. These describe R_d as either linear in ζ or ζ', where the latter is a "Q10" function. The two functions are made to be equal at $T = 298.15$K, and so ζ' is given by

$$\zeta' = 2.0^{0.1(T-298.15)}. \tag{7}$$

The final respiration term that requires calculation is non-leaf plant respiration (at the top of the canopy), $R_{p,l}$ (kg C (m^2 vegetation)$^{-1}$ s^{-1}), and this is modelled as linear in dark respiration. That is $R_{p,l} = \mu R_{d,l}$. The value of μ is related to the ratio of nitrogen contents of stems and roots to leaves, and vegetation

biomass. Here, μ is set to a single value based upon comparison with the full TRIFFID model using typical parameter values and for an LAI value of eight. In these circumstances, this gives $\mu = 3.85$ which is used here. It is now possible to calculate top-leaf level NPP,

$$\Pi_l = P_l - R_{d,l} - R_{p,l}. \tag{8}$$

The behaviour of Π_l for variations in temperature are shown in Figure 1a,b. These correspond to the two forms of respiration (linear in ζ and ζ'), and for different values of atmospheric CO_2. As expected, there are major differences between predictions of Π_l at high temperatures between the two forms of respiration.

For all temperatures, a higher atmospheric CO_2 concentration results in higher values of Π_l. Although not shown here, Π_l also quickly saturates in increasing I_{par} (around 100 W m^{-2}) and is very weakly dependent upon variations in q (kg kg^{-1}) (through D and c_i).

2.4 Scaling to canopy level

A scaling law is required between leaf and canopy level NPP. This is provided by Sellers *et al.*, (1992), where it is assumed that the relative importance of all limiting factors is the same at every depth. Therefore, NPP is regarded as linear in available light, which decays exponentially throughout the canopy (Beer's Law). Integration through the canopy gives a multiplicative parameter f_{par} given by

$$f_{par} = \frac{1 - e^{-kL}}{k} \tag{9}$$

where k (set here to 0.5) is a canopy light extinction coefficient. Hence, net primary productivity, Π, is calculated as

$$\Pi = f_{par}\Pi_l. \tag{10}$$

2.5 Soil respiration

Soil respiration is modelled as a "Q10" function in temperature and linearly dependent on soil carbon, thus

$$R_s = \kappa_s C_S 2.0^{0.1(T-298.15)} \tag{11}$$

where $\kappa_s = 1.0 \times 10^{-8}$ (s^{-1}) is a constant of proportionality.

2.6 Predictions of temperature change as a function of increased atmospheric CO_2

The growth model is assumed to respond to changes in annual mean temperature and atmospheric CO_2 concentration. As such, no account is made of the diurnal cycle, seasonality or inter-annual variability, which are regarded as "integrated

out" of this modelling exercise. An estimate of the mean impact of increased greenhouse gas concentrations upon temperature is frequently expressed through a climate sensitivity parameter λ_s (W m^{-2} K^{-1}). This relates radiative forcing anomaly ΔQ (W m^{-2}) to the global mean temperature anomaly ΔT (K) as

$$\Delta Q = \lambda_s \Delta T. \tag{12}$$

Huntingford and Cox (1999) investigate three transient experiments from Version 3 of the Hadley Centre coupled land-atmosphere-ocean GCM, HadCM3, which suggest that $\lambda_s \approx 0.94$ (W m^{-2} K^{-1}). For climate change predominantly driven by the accumulation of extra atmospheric CO_2 (assumed to be representative of surface level CO_2 concentrations, c_a), then this may be expressed as (Shine *et al.*, 1990)

$$\Delta Q \approx 5.4 \ln\left(\frac{c_a}{c_{a0}}\right).$$

The multiplicative factor of 5.4 is diagnosed from HadCM3 (W.J. Ingram, personal communication) and c_{a0} is an initial atmospheric CO_2 concentration of 280 ppm, representing pre-industrial conditions. Here, atmospheric CO_2 concentration is modelled as increasing by 1% (cumulative) per annum, which broadly corresponds to a future "business as usual" scenario. Thus

$$c_a = 1.01^{\tau} c_{a0}, \qquad T = T_0 + \Delta T = T_0 + 0.0572\tau, \tag{13}$$

where τ (yr) is the time in years since the start of the model run and T_0 (K) is the initial unperturbed temperature for the model simulation. This is not regarded as the global mean temperature, but instead, varies, acting as a proxy variable for spatial position.

Eqs (13) provide the two driving conditions to the NPP model (for fixed I_{par} and q), and therefore drives the vegetation growth model. No account is taken here of possible revised soil moisture stresses upon Π which may occur within a perturbed climate.

3 Numerical solutions

Numerical simulations using the model described in Section 2 are undertaken. The model is operated in the more physically realistic dynamic mode, and also in equilibrium mode, where intercomparison indicates the importance of system "lags". The equilibrium state corresponds to setting all time derivative terms to zero in Eqns (1) to (4). By definition, Net Ecosystem Productivity (NEP) (equal to $\nu\Pi - R_s$) is uniformly zero for the equilibrium case. The dynamic solutions are all initialised from an equilibrium state. Throughout all runs, $I_{PAR} = 200$ W m^{-2} and $q = 0.005$ kg kg^{-1}. Three distinct behaviours are simulated.

3.1 AN EMERGING VEGETATION TYPE

Figure 2 corresponds to model behaviour for increasing CO_2 and increasing temperature (both satisfying Eqs (13)), starting from an initial low temperature value of T_0 =276.15 K (3°C). In the equilibrium solution, a threshold in NPP, Π, is passed such that some carbon can then be allocated to spreading (that is, $\lambda_\nu > 0$). There then follows a general increase in fractional coverage, and therefore total vegetation carbon (νC_B), along with a corresponding increase in litter flux $\nu\Lambda$ (kg C (m^2 ground cover)$^{-1}$ s^{-1}). The latter balances soil respiration, giving a general increase in soil carbon. For this newly emerging and unestablished vegetation, the turnover and disturbance rate are high (both 0.1 yr^{-1}).

The dynamic solution in Figure 2 behaves somewhat differently. The threshold passed by NPP (such that $L > L_{min}$) also allows the vegetation to start to spread. However, it takes a long time (approximately 100 years) before the vegetation can really develop, due to the large lags in fractional coverage. This is then followed by a rapid increase in fractional coverage (corresponding to a positive pulse in NEP). For periods beyond 150 years, the dynamic solution maintains only a small lag behind the equilibrium solution. The pulse in NEP demonstrates the ability of even a simple dynamic terrestrial ecosystem model to exhibit potential "surprises" through its nonlinear behaviour. In this simulation, such behaviour could be defined as beneficial, as any positive values of NEP will absorb some future CO_2 emissions. For the low initial temperature, this model run could be representative of the northward migration of the boreal forest under a changed climate.

The numerical simulation presented in Figure 2 adopts respiration functions that are linear in ζ. Using linearity in ζ' for this low temperature simulation results in a model output (not presented here) that is virtually identical to that of Figure 2.

3.2 AN INVARIANT VEGETATION TYPE

In the second numerical run, presented in Figure 3, the model is initialised at a higher temperature of T_0 = 293.15K (20°C). The model now corresponds to a well established vegetation and turnover and disturbance rates are accordingly reduced to 0.02 yr^{-1}. Throughout the numerical run, NPP increases. The vegetation has established a high leaf area index, and as such, the model attempts to direct any extra carbon to spreading. However, the fractional coverage is near to unity, and so the vegetation is unable to spread further. As a consequence, self-shading forces most of the increased available carbon directly into litter. This extra litter initially enhances the soil carbon content. However, later in the simulation and as the temperature rises, this effect is overtaken by higher soil respiration. The ecosystem therefore switches from being a carbon sink (positive NEP) to a carbon source (negative NEP).

This simulation has many interesting aspects. The vegetation carbon content is almost invariant throughout, and implies that should vegetation reach this state,

then its existence is stable and robust. For almost all the key model variables and diagnostics presented in Figure 3, the equilibrium and dynamic runs are virtually indistinguishable, implying that system lags are negligible. The peak in soil content suggests that enhanced carbon uptake by vegetation in a warming climate may eventually be lost in the future should even higher temperatures be encountered.

Using the alternative form of respiration being linear in ζ' does not significantly alter the results.

3.3 VEGETATION DIE BACK

In a final two simulations, the model is initialised from a very high temperature of $T_0 = 305.15$K (32^0C), and so is likely to describe semi-arid regions. As may be expected from comparing Figures 1a,b (whereby the major differences in leaf NPP occur at higher temperatures), then model predictions differ greatly depending upon whether dark and plant respiration are linear in ζ or ζ'. Using functional form ζ (see Figure 4), then this solution has similar properties to the simulation described in Section 3.2. That is, changes in NPP affect the litter flux, and therefore soil carbon. However, the vegetation itself retains an almost invariant carbon content, C_B with a fractional coverage near unity.

The model using a respiration flux that is monotonically increasing in temperature behaves very differently (see Figure 5). Now, net primary productivity starts to decrease at very early times, until eventually temperatures are sufficiently high that respiration is larger than photosynthetic uptake (resulting in negative NPP values). As NPP decreases, the litter flux initially decreases (causing a gradual decrease in soil carbon, C_S) but with the fractional coverage remaining near to unity. However, when the carbon directed into spreading is no longer sufficient to balance both the natural disturbance rate and the creation of litter through self-shading, then ν starts to decrease rapidly. Around the same time, there is a rapid drop in vegetation carbon, C_B (as shown through the figure for LAI), until eventually the vegetation disappears. In the dynamic solution, the loss of fractional coverage falls behind the loss of LAI, eventually leaving a vegetation with very little carbon per unit area to slowly reduce in prevalence. As the vegetation "dies-back", there is a large negative NEP, corresponding to a pulse of carbon into the atmosphere. The internal dynamics extend the period during which the vegetation dies by a factor of about two compared to the equilibrium solution (consider, for instance, the vegetation carbon, νC_B). This simulation demonstrates how the modelled vegetation can initially be robust to variations in driving conditions, but once the key threshold is passed where there is no excess assimilation of carbon to form litter, then the vegetation can "die-back" very quickly.

It is noted that even within Figure 4 (that is, with respiration linear in ζ), NPP deceases rapidly towards the end of the simulation. Eventually "dieback" occurs in this example too (should the simulation be continued for further times), and so the timing of modelled "die-back" depends crucially upon the form of the respiration terms.

3.4 Critical conditions for terrestrial carbon loss

Vegetation dieback is a special case of the loss of total terrestrial (that is soil plus vegetation) carbon C_T, which is predicted at high CO_2 concentrations in models of this type. As atmospheric CO2 concentrations increase the climate is expected to warm as a result of the greenhouse effect, with a subsequent increase in both photosynthetic rates (mainly due to CO2-fertilsation) and also respiration rates (owing to the higher temperatures). Initially, the ecosystem may act as a net carbon sink, as photosynthesis increases faster than plant or soil respiration. However, CO2-fertilsation is expected to saturate at high CO2 concentrations, and photosynthesis will ultimately decrease at very high temperatures. By constrast, in most models, plant or soil respiration (or both) continue to increase monotonically with temperature. These models must therefore pass a critical CO2 concentration beyond which terrestrial carbon begins to decrease.

Figure 6 shows results from a family of equilibrium simulations which are undertaken to examine the critical conditions for this "sink-to-source" transition, as a function of the initial temperature T_0. In each case the turnover and disturbance rates (γ_c and γ_v) are fixed at 0.02 yr^{-1}, and the CO2 concentration increased until the total soil plus vegetation carbon is a maximum. Beyond this point the modelled ecosystem would provide a positive rather than a negative feedback on CO_2-induced climatic change. The two lines in Figure 6 demonstrate the sensitivity of this critical point to the parameterisation of dark and plant respiration. In both cases the critical atmospheric CO_2 concentration (Figure 6(a)) decreases strongly with (initial) temperature, but the values are lower if dark and plant respiration are assumed to increase monotonically with temperature. There are turning points for terrestrial carbon as a function of CO_2 even in the other model (dark and (non-leaf) plant respiration linear in ζ), largely because soil respiration is still assumed to follow the standard "Q10" dependence on temperature.

4 Solution Analysis

The four runs described in Section 3 demonstrate how even a simple terrestrial carbon cycle model can be used to generate many possible responses of vegetation to a perturbed climate. Here, exact solutions are given for the terrestrial ecosystem model when in equilibrium mode (corresponding to the dotted lines within Figures 2 to 5). In addition, an investigation of the "magnitude of terms" within the full dynamic model allows inferences to be made of the importance of lags, when compared to the equilibrium solution.

These analyses allow more insight into the specific runs described in Section 3. However, by generating a fuller understanding of the system, it is then possible to predict behaviours for a broad range of possible initial conditions and parameters. This has the potential to confirm whether effects seen from a small number of numerical simulations are general, or whether they are a consequence of particular combinations of driving parameters. Throughout this section, the unit of time is

years.

4.1 Equilibrium solutions

Equilibrium solutions correspond to setting all transient terms within Eqs (1) to (3) to zero. By definition, $\nu\Pi = \nu\Lambda = R_s$.

4.1.1 Vegetation carbon

In equilibrium, vegetation carbon (per unit area of vegetation cover) satisfies $C_B = (1 - \lambda_\nu)\Pi/\gamma_c$. Combined with Eqns (5) and (6), this gives

$$C_B = \begin{cases} \frac{\Pi(t)}{\gamma_c} & \text{for } \Pi(t) \leq \sigma\gamma_c L_{min}, \\ \frac{\sigma L_{max}\Pi(t)}{\sigma\gamma_c(L_{max}-L_{min})+\Pi(t)} & \text{for } \Pi(t) > \sigma\gamma_c L_{min}. \end{cases} \tag{14}$$

The first solution corresponds to $L < L_{min}$ and $\lambda_\nu = 0$ (that is, all carbon is put into growth) whilst the second solution corresponds to $L_{min} < L < L_{max}$. There is no solution $L \geq L_{max}$ as this requires $\Pi \to \infty$. For increasing values of Π, it is observed that C_B increases linearly until $L = L_{min}$, beyond which the vegetation carbon content saturates towards a theoretical limit of σL_{max}.

4.1.2 Fractional coverage

Equilibrium vegetation fractional coverage satisfies $\nu = \max\{0, [1 - (\gamma_\nu C_B/\Pi\lambda_\nu)]\}$. After some algebra, incorporating Eqs (5) and (14), this gives

$$v = \max\left\{0, 1 - \left(\frac{\sigma\gamma_\nu L_{max}}{\Pi - \sigma\gamma_c L_{min}}\right)\right\}. \tag{15}$$

Through the definition of λ_ν, a necessary condition for vegetation to exist is that $L > L_{min}$. In fact this is not a sufficient condition for $\nu > 0$, and from Eq (15), it may be seen that the condition for vegetation to exist is

$$\Pi(t) > \sigma(\gamma_c L_{min} + \gamma_\nu L_{max}). \tag{16}$$

For vegetation to sustain a non-zero equilibrium fractional coverage, there must be sufficient carbon available to both allow $L > L_{min}$, and to overcome the self-shading disturbance rate implicit within the model for spreading. This effect can be observed within Figure 2, whereby $L > L_{min} = 4$ before spreading occurs.

For very high values of net primary productivity, $\nu \to 1$. Combined with the similar observation for saturation of vegetation carbon, then should environmental conditions become very favourable for the uptake of carbon, a point is reached where the dominant vegetation type is no longer able to grow or spread. This is the stable state that may be observed for the simulations given in Figures 3 and 4.

4.1.3 Soil carbon

In equilibrium, soil carbon is given by

$$C_S = \frac{\nu\Pi(t)}{\kappa_s 2.0^{0.1(T-298.15)}}. \tag{17}$$

The equilibrium soil carbon is therefore a balance between changes in NPP and fractional coverage and the temperature influence upon soil respiration. As noted for the simulation in Figure 3 and Figure 4, the soil carbon initially gains from the increase in litter (equal to $\nu\Pi$ in equilibrium mode), before increases in soil respiration are sufficient to overtake and force a decrease in soil carbon content.

4.2 Dynamic solutions

Equilibrium solutions reveal much about the terrestrial carbon cycle system. However, they ignore transient effects due to the implicit timescales inherent within vegetation dynamics. From observing Figures 2-5, during most periods, there is a very small lag of the dynamic solution behind the equilibrium case. However, this is not true for the examples of a newly emerging vegetation type and the "die-back" event. Although exact solutions are not available for the dynamic case, significant understanding of the terrestrial behaviour may be achieved by "order of magnitude" arguments. Smith and Shugart (1993) suggest that in periods of change, the longest timescales will dominate behaviour. The analysis below provides a more formal basis for such conclusions.

4.2.1 Vegetation carbon

Suppose NPP is changing throughout a run of length t^* (yr) and at a rate of order χ (kg C $m^{-2}yr^{-2}$). That is $d\Pi/dt \sim O(\chi)$. If it is initially assumed that the lags are relatively small, then the dominant model terms will be those on the right-hand side of Eqs (1) to (3). Hence, from Eq (1), the change in vegetation carbon is of magnitude $\chi t^*(1-\lambda_\nu)/\gamma_c$. Nondimensionalising variables (where ' means dimensionless) gives

$$t' = \frac{t}{t^*}, \qquad C'_B = \frac{\gamma_c C_B}{(1-\lambda^*_\nu)\chi t^*}, \qquad \Pi' = \frac{\Pi}{\chi t^*}. \tag{18}$$

Hence Eqn (2) may be written as

$$\delta_1 \frac{dC'_B}{dt'} = \frac{(1-\lambda_\nu)}{(1-\lambda^*_\nu)}\Pi' - C'_B, \qquad \delta_1 = \frac{(1-\lambda^*_\nu)}{(\gamma_c t^*)}, \tag{19}$$

where λ^*_ν is a typical value of the partitioning coefficient during the simulation. An explicit scaling could also be found for λ_ν (using the equilibrium solutions given in Section 4.1.1), although the resultant algebra then detracts from the transparency of Eqs (19). Instead, it is assumed that during any different period of interest, $(1-\lambda_\nu)/(1-\lambda^*_\nu)$ is of order unity.

If $|\delta_1| \ll 1$, this confirms the hypothesis that over the timescale of interest, then the lag (expressed as a fraction of change in the equilibrium solution) is small. The absolute value of the lag, $C_{B,lag}$ (kg C (m^2 vegetation)$^{-1}$) is then δ_1 multiplied by the scaling for C_B. That is

$$C_{B,lag} \sim O\left(\chi(1-\lambda_\nu^*)^2/\gamma_c^2\right). \tag{20}$$

In Figure 2, $1-\lambda_\nu$ is approximately 0.5, and so $\delta_1 = 0.025$, which corresponds to a very small lag in C_B (see plot for LAI). Similar calculations may be made in Figure 3 and Figure 4.

Within Figure 5, consider the period as "die-back" occurs. Let $t^* = 50$ yr, and as now LAI is near to L_{min}, then $1-\lambda_\nu \sim O(1)$. Hence $\delta_1 = 1.0$. This value implies that all terms in Eq (1) balance, and so the lag will be as large as variation in the equilibrium solution. This may be observed for the LAI values in Figure 5.

4.2.2 Fractional coverage

For fractional coverage ν, a scaling for the change in equilibrium value of ν is required. Using the scalings presented in Eq (18), then from Eq (2) this gives for $w = 1-\nu$

$$w' = \min\left[\frac{w}{w^*}, 1\right] \qquad w^* = \frac{\gamma_\nu(1-\lambda_\nu)}{\gamma_c\lambda_\nu} \tag{21}$$

and so Eq. (2) may be written in nondimensional form as

$$\delta_2 C_B' \frac{\mathrm{d}\nu'}{\mathrm{d}t'} = \left(\frac{\lambda_\nu}{\lambda_\nu^*}\right)\nu' w' \Pi' - \nu' C_B' \qquad \delta_2 = \frac{1}{\gamma_\nu t^*}. \tag{22}$$

In a similar way to the analysis for C_B, δ_2 represents the ratio of lag to overall change in fractional coverage, and so if the value is small, then the solution is in near equilibrium. For δ_2 small, and from the scaling for w converted to a scaling for ν, the absolute lag in ν given as $\delta_2 \max\left[1-\{\gamma_\nu(1-\lambda_\nu)/\gamma_c\lambda_\nu\}, 0\right]$.

In Figure 2, for the complete run, $\delta_2 \sim O(0.05)$, and indeed the lag in fractional coverage is small at the end of the run. However, the scaling is not valid during the early period of this simulation. At this point, it is noted that the lower limit of fractional coverage is not zero, but instead a "seeding fraction" ϵ, where $0 < \epsilon \ll 1$ (thereby preventing the trivial solution $\nu \equiv 0$ for dynamic simulations). The emergence of the new dominant vegetation starts at the same time as the equilibrium equations can admit a solution; that is, the right hand side of Eq (2) becomes positive. However, the fractional coverage falls immediately out of equilibrium, and instead (from the Appendix) satisfies approximately

$$\frac{\mathrm{d}\nu}{\mathrm{d}\tilde{t}} = \omega\tilde{t} \tag{23}$$

which has solution

$$\nu = \epsilon e^{\omega\tilde{t}^2/2} \tag{24}$$

and where $\omega = [(\gamma_c + \gamma_\nu)\chi] / [\gamma_c \sigma(L_{max} - L_{min}) + \Pi_0]$. This solution demonstrates that for an emerging vegetation type, there is a strong dependence upon prescribed initial seeding fraction ϵ. The timescale associated with this "inner" timescale, before ν becomes of order unity, is given by $\sqrt{-2\ln(\epsilon)/\omega}$ yr. For the run presented in Figure 2, $\epsilon = 0.01$ and $\omega \approx 5.6 \times 10^{-4}$ yr^{-2} which implies a timescale of 128 yr. Linking this solution to the long term situation, whereby a small lag pervails, is an "intermediate" period when all the terms in Eq (2) balance. Fixing $\delta_2 = 1$ implies (for $\gamma_\nu = 0.1$), a short timescale of just ten years. From Figure 2, this appears to occur around year 120.

In Figure 3 and Figure 4, the small changes in equilibrium fractional coverage, combined with $\delta = 0.25$ suggest that the absolute values of the lag in fractional coverage are very small. However, for the "die-back" case in Figure 5, lags in fractional coverage are important. The equilibrium fractional coverage exhibits very large variability over a period of just twenty years, until the equilibrium solution reaches the seeding fractional coverage. This period ($t^* = 20$ yr) corresponds to a value of $\delta_2 = 2.5$, and as such, the transient term is large and lags will occur. For the dynamic solution, a short period occurs when Π is negative, but $\lambda_\nu > 0$, and as such, the vegetation is able to retract quickly due to the high respiration rates. When λ_ν becomes zero (around year 155 and due to $L < L_{min}$), the fractional coverage then continues to decrease, but due to disturbance only and satisfying $\mathrm{d}\nu/\mathrm{d}t = -\gamma_\nu \nu$. During this period, the vegetation LAI decreases towards zero.

4.2.3 Soil content

Finally, lags within soil content, C_S, require consideration. If the change in litter term is such that $\mathrm{d}(\nu\Pi)/\mathrm{d}t \sim O(\beta_s)$, then an appropriate scaling for litter, and therefore the change in C_S, is given by

$$(\nu\Lambda)' = \frac{\nu\Lambda}{\beta_s t^*} \qquad C_S' = \frac{C_S \kappa_S 2.0^{0.1(T_0 - 298.15)}}{\beta_s t^*} \tag{25}$$

This leads to the nondimensional equation for soil carbon as

$$\delta_3 \frac{\mathrm{d}C_S'}{\mathrm{d}t'} = (\nu\Lambda)' - C_S' 2.0^{0.1(T - T_0)} \qquad \delta_3 = \frac{1}{\kappa_s 2.0^{0.1(T_0 - 298.15)} t^*}. \tag{26}$$

There are two ways in which the solution for the soil carbon, C_S, may differ between the equilibrium and dynamic solutions. Either δ_3 becomes of order unity (or greater), or there are significant differences in $(\nu\Lambda)'$ depending upon whether in equilibrium or dynamic mode. For the full 200 yr, $\delta_3 \sim O(10^{-2})$. Even for smaller (decadal) time periods, δ_3 is still small, and as such the majority of lags are due to lags within the litter flux. This in turn is a consequence of lags in C_B and ν.

5 Discussion and Conclusions

The case of an emerging vegetation type in a cold environment (Figure 2) is somewhat analogous to northward migration of the boreal forest. As the temperature and CO_2 concentration increases eventually NPP becomes sufficiently high that it overcomes both turnover and disturbance rate, and the vegetation is able to spread. However, with operation in the (more physically realistic) dynamic mode, there is a long period whilst the vegetation becomes established. Further, the initial rate of spreading has a strong dependence upon a prescribed initial "seeding fraction". After a substantial period (after about one hundred years in Figure 2) the vegetation becomes partially established. There is then a rapid change in fractional coverage as the vegetation expands to near equilibrium with the new climate. During this period of rapid colonisation, there is a large positive pulse in net ecosystem productivity, implying net carbon uptake from the atmosphere. Finally, the dynamic solution settles to a state of a small lag behind the predicted equilibrium state, with weakened, but still positive, Net Ecosystem Productivity (NEP). This simulation illustrates a climate change induced "surprise" involving large changes in ecosystem structure and carbon cycling.

The case of well established vegetation in a warm environment (Figure 3) with a high leaf area index, and a fractional coverage near to unity may be analogous to tropical forest in an unstressed condition. Increasing temperature and atmospheric CO_2 concentration drive increasing net primary productivity. However, as the vegetation is near to maximum height and almost completely fills the available space, then the excess fixed carbon is directed immediately into litter. The major changes within this simulation are therefore observed within the soil carbon pool. Within the simulation given in Figure 3, NEP is initially positive, with enhanced carbon input causing the soil pool to grow. However, as temperatures increase, enhanced soil respiration overtakes carbon input to the ecosystem, NEP becomes negative and there is marked shrinkage of the soil carbon reservoir. This simulation suggests that there are likely to be vegetation types which are robust within a perturbed climate; that is, they are unaffected by carbon dioxide and temperature induced changes in net primary productivity (which are transferred directly to the soil). In this case, the main changes in carbon storage occur within the soil, which becomes as important for carbon cycling as the physiological controls on the vegetation itself.

If a particularly high initial temperature is adopted the model can be likened to semi-arid conditions. When a respiration function with a high temperature "cutoff" is adopted (Figure 4), net primary productivity peaks and then declines but (in a similar fashion to the previous simulation), this change only significantly affects the litter flux and the soil carbon pool. In this case it is not possible to induce a major reduction in overall vegetation carbon content. However, if respiration terms that monotonically increase with temperature are adopted (Figure 5), net primary productivity reaches a maximum earlier and eventually becomes

negative (that is, respiration exceeds gross photosynthesis). In this case, after an initial period in which (again) any variation in NPP is reflected in just the litter term, there is a very short period of rapid variability during which there is vegetation "die-back". Both the fractional coverage of vegetation and its carbon content (per unit area of vegetation) decline very rapidly. This is true for both the dynamic and equilibrium solutions, although significant lags do occur in the dynamic case. The loss of vegetation carbon results in a large pulse of carbon to the atmosphere (negative NEP). This phenomenon of "die back" has also been simulated in the more complex "Hybrid" vegetation model (White *et al.*, 1999). Our study suggests that the predicted occurrence of "die-back" depends heavily on the model formulations of dark and plant respiration. This is also true for the critical atmospheric CO_2 concentration above which vegetation changes from being a sink to a source of carbon.

The growth model lacks many features, including phenology, other competing species and any dependence of soil respiration on water stress. However, a relatively simple group of governing equations for terrestrial behaviour have been shown to exhibit a range of possible effects. The simplicity of this model allows a comprehensive analytical study to be undertaken, building both a full understanding of the different possible behaviours and a rapid methodology to extend such understanding to a continuum of different boundary conditions. The study has shown the relative importance of all the model parameters, and the dependence upon the behaviour of the "driving" model for net primary productivity.

It is hoped that this model, and the associated analysis, will provide a structure on to which other more complicated growth models can be mapped in order to summarise their gross features. It is also hoped that this essentially off-line analysis will be of use in diagnosing features of ecosystem models when fully implemented within a coupled GCM.

6 Acknowledgements

Chris Huntingford acknowledges both the CEH Integrating Fund, and the NERC science budget for funding. The terrestrial ecosystem model is based on the "TRIFFID" dynamic global vegetation model, developed at the Hadley Centre under the UK DETR Climate Prediction Programme (contract PECD 7/12/37). Tim Lenton acknowledges the CEH Integrating Fund.

Appendix

The initial behaviour of an emerging vegetation

A solution is found for the initial period after the emergence of a new dominant vegetation type, based upon linear perturbation analysis. When conditions become appropriate for vegetation to emerge, the r.h.s. of Eqns (1) and (2) are zero. Hence,

for short periods after this, NPP, vegetation carbon and the partitioning parameter may be written as

$$\Pi = \Pi_0 + \Delta\Pi \qquad C_B = C_{B,0} + \Delta C_B \qquad \lambda_\nu = \lambda_{\nu,0} + \Delta\lambda_\nu \tag{27}$$

where

$$(1 - \lambda_{\nu,0})\Pi_0 - \gamma_c C_{B,0} = 0 \qquad \lambda_{\nu,0}\Pi_0 - \gamma_\nu C_{B,0} = 0 \tag{28}$$

and it is assumed that $|\Delta\Pi/\Pi_0| \ll 1$, $|\Delta C_B/C_{B,0}| \ll 1$ and $|\Delta\lambda_\nu/\lambda_{\nu,0}| \ll 1$. It is observed (from Figure 2) that the LAI values (and therefore C_B and λ_ν) are almost identical between the equilibrium and dynamic simulations. Hence, linearisation of the equilibrium solution to Eq. (1), and from the definition of λ_ν in Eq. (5),

$$(1 - \lambda_{\nu,0})\Delta\Pi - \Pi_0\Delta\lambda_{\nu,0} = \gamma_c\Delta C_B \qquad \Delta\lambda_\nu = \frac{\Delta C_B}{\sigma(L_{max} - L_{min})}. \tag{29}$$

The change in NPP is given by

$$\Delta\Pi = \chi\tilde{t} \tag{30}$$

where $\tilde{t}$ (yr) is time since vegetation emergence. Linearisation of the equation for fractional coverage gives

$$C_{B,0}\frac{\mathrm{d}\nu}{\mathrm{d}\tilde{t}} = \nu\left[\Delta\lambda_{\nu,0}\Pi_0 + \lambda_{\nu,0}\Delta\Pi - \gamma_\nu\Delta C_B\right]. \tag{31}$$

Eqs (29) and (30) may be combined to give all the perturbed quantities within Eqs (27) as multiplicative in $\chi\tilde{t}$. Further combination with Eq. (29)a gives after some algebra

$$\frac{\mathrm{d}\nu}{\mathrm{d}\tilde{t}} = \frac{(\gamma_c + \gamma_\nu)\chi\tilde{t}}{\gamma_c\sigma(L_{max} - L_{min}) + \Pi_0} \tag{32}$$

A References

Collatz, G.J., Ball, J.T., Grivet, C. and Berry, J.A.: 1991. 'Physiological and environmental regulation of stomatal conductance, photosynthesis and transpiration: a model that includes a laminar boundary-layer'. *Agr. For. Met.*, **54**, 107-136.

Cox, P.M., Betts, R.A., Bunton, C., Essery, R.L.H., Rowntree, P.R. and Smith, J.: 1999, 'The impact of new land surface physics on the GCM simulation of climate and climate sensitivity,' *J. Climate*, **15**, 183-203.

Cox, P.M., Huntingford, C. and Harding, R.J.: 1998. 'A canopy conductance and photosynthesis model for use in a GCM land surface scheme.' *J. Hydrol.*, **213**, 79-94.

Cox, P.M. and Palmer, 1996. 'Global carbon cycle modelling.' Hadley Centre Report to the DoE, The Hadley Centre, London Road, Bracknell, RG12 2SY, UK.

Friend, A.D.: 1995. 'PGEN: An integrated model of leaf photosynthesis, transpiration and conductance' *Ecol. Modelling*, **77**, 233-255.

Huntingford, C. and Cox, P.M., 1999. 'An analogue model to derive additional climate change scenarios from existing GCM simulations.' *Clim. Dyn.* Accepted.

Jacobs, C.: 1994. 'Direct impact of atmospheric CO_2 enrichment on regional transpiration'. PhD Thesis, Wageningen Agricultural University.

Lloyd, J., Grace, J., Miranda, A.C., Meir, P., Wong, S.C., Miranda, H.S., Wright, I.R., Gash, J.H.C. and McIntyre, J.: 1995, 'A simple calibrated model of Amazon rainforest productivity based on leaf biochemical properties', *Plant Cell Environ.* **18**, 1129-1145.

Sellers, P.J., Berry, J.A., Collatz, G.J., Field, C.B. and Hall, F.G.: 1992 'Canopy reflectance, photosynthesis, and transpiration. III. A reanalysis using improved leaf models and a new canopy integration scheme', *Remote Sens. Environ* **42**, 187-216.

Sellers, P.J., Randall, D.A., Collatz, G.J., Berry, J.A., Field, C.B., Dazlich, D.A., Zhang, C., Collelo, G.D. and Bounoua, L.: 1996. 'A revised land surface parameterisation (SiB2) for atmospheric GCMs. Part I: Model Formulation.' *J. Climate* **9**, 676-705.

Shine, K., Derwent, R., Wuebbles, D. and Morcrette, J.J.: 1990. Radiative forcing of climate. In: Houghton, J., Jenkins, G. and Ephraums, J. (eds), Climate Change. The IPCC scientific assessment, Chapter5, 45-68. Cambridge University Press, Cambridge.

Smith, T.M. and Shugart, H.H.: 1993, 'The transient response of terrestrial carbon storage to a perturbed climate', *Nature* **361**, 523-526.

White, A., Cannell, M. G. R. and Friend, A. D.: 1999. 'Climate change inputs on ecosystems and the terrestrial carbon sink: a new assessment' *Global Environmental Change*, in press.

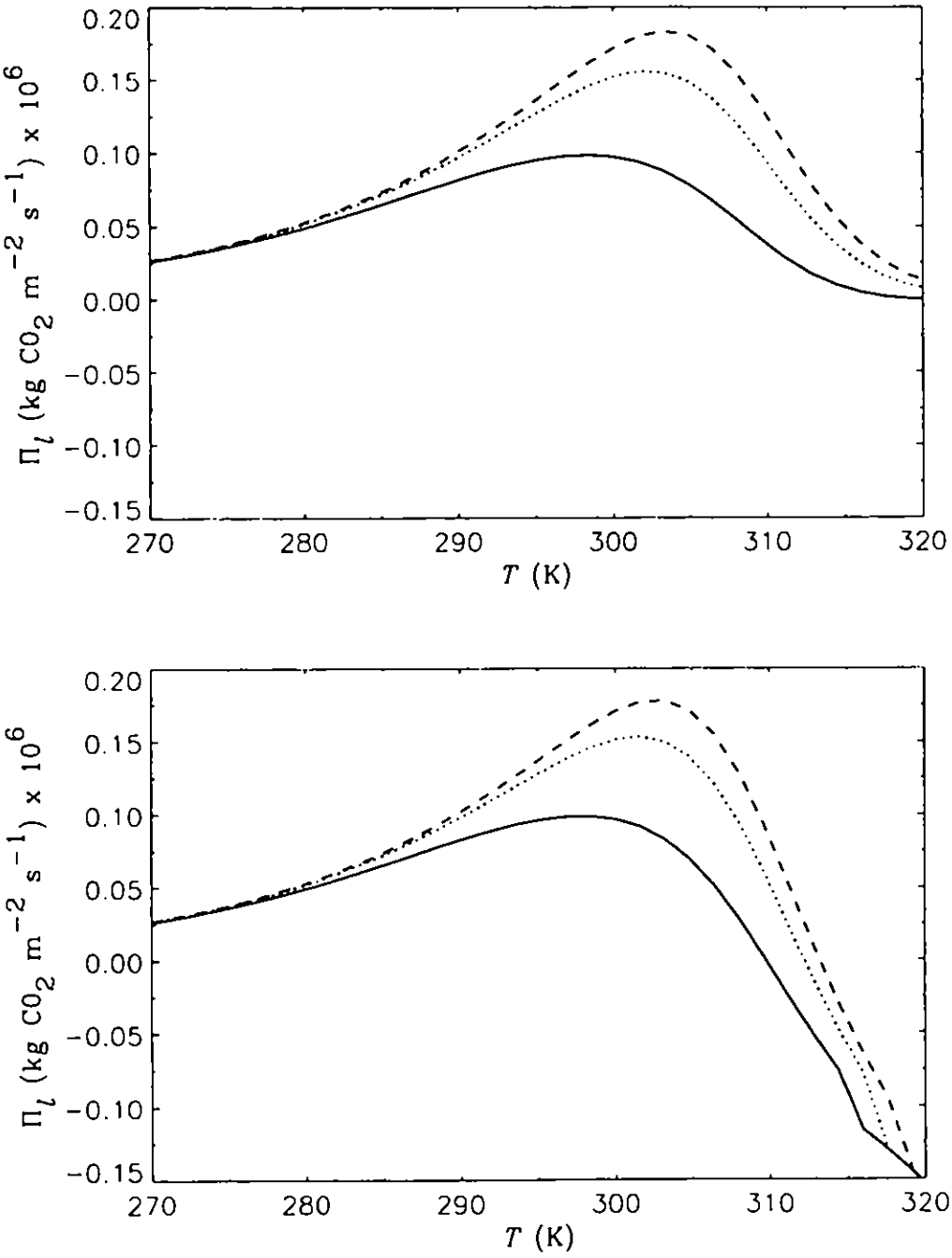

Figure 1. Leaf Net Primary Productivity, Π_l, as a function of leaf temperature for c_a = 350 ppm (continuous line), c_a = 700 ppm (dotted line) and c_a = 1050 ppm (dashed line). The plots correspond to dark and plant respiration being linear in ζ (see Equation (2.3)) within plot a) and linear in ζ' (see Equation (7) within plot b). In all cases, I_{PAR} = 200 W m^{-2} and q = 0.005 kg kg^{-1}.

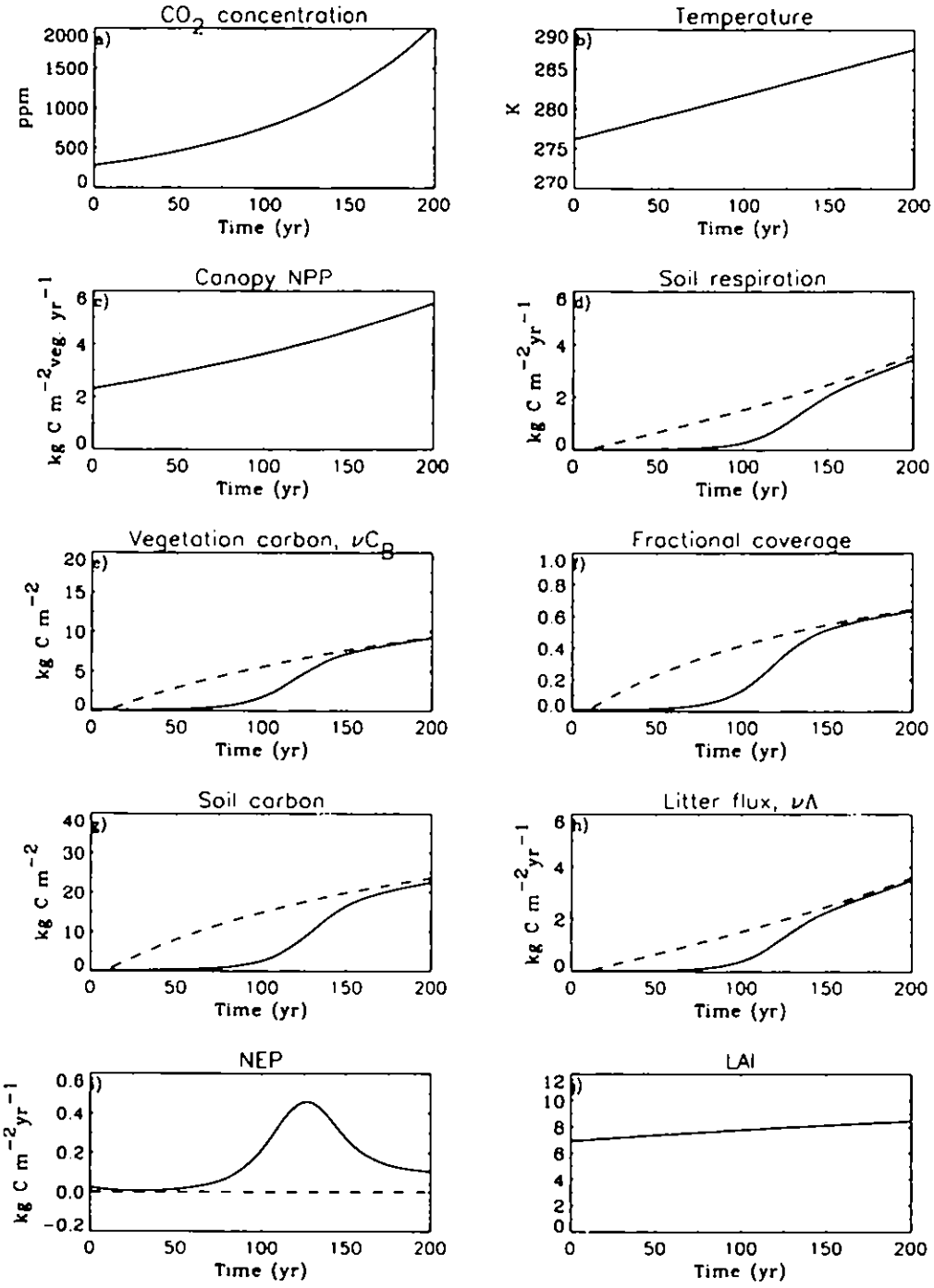

Figure 2. The prediction of c) NPP and d)-j) properties of the terrestrial carbon model for a) prescribed CO_2 concentration and b) associated temperature. This corresponds to $\gamma_c = 0.1\ \mathrm{yr}^{-1}$, $\gamma_\nu = 0.1\ \mathrm{yr}^{-1}$ and $T_0 = 276.15$ K. Dark respiration is linear in ζ, as given in Equation (2.3). The continuous line represents the dynamic solution and the dashed line the equilibrium solution. Fluxes are in units of yr^{-1}, and areal properties (except NPP) have units m^{-2} of ground cover (that is d), e), g), h) and i)).

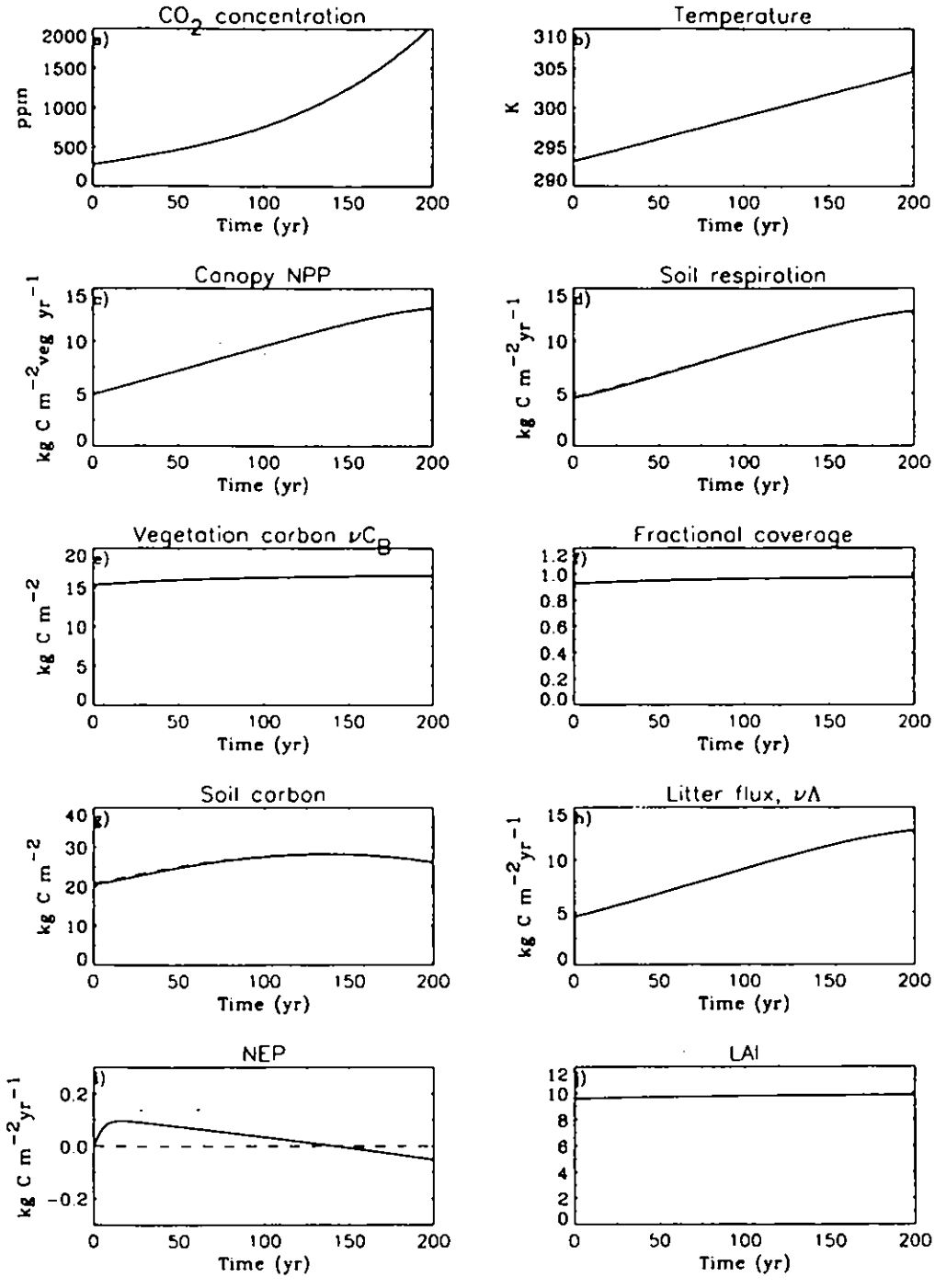

Figure 3. The prediction of c) NPP and d)-j) properties of the terrestrial carbon model for a) prescribed CO_2 concentration and b) associated temperature. This corresponds to $\gamma_\epsilon = 0.02\ \mathrm{yr}^{-1}$, $\gamma_\nu = 0.02\ \mathrm{yr}^{-1}$ and $T_0 = 293.15$ K. Dark respiration is linear in ζ, as given in Equation (2.3). The continuous line represents the dynamic solution and the dashed line the equilibrium solution. Fluxes are in units of yr^{-1}, and areal properties (except NPP) have units m^{-2} of ground cover (that is d), e), g), h) and i)).

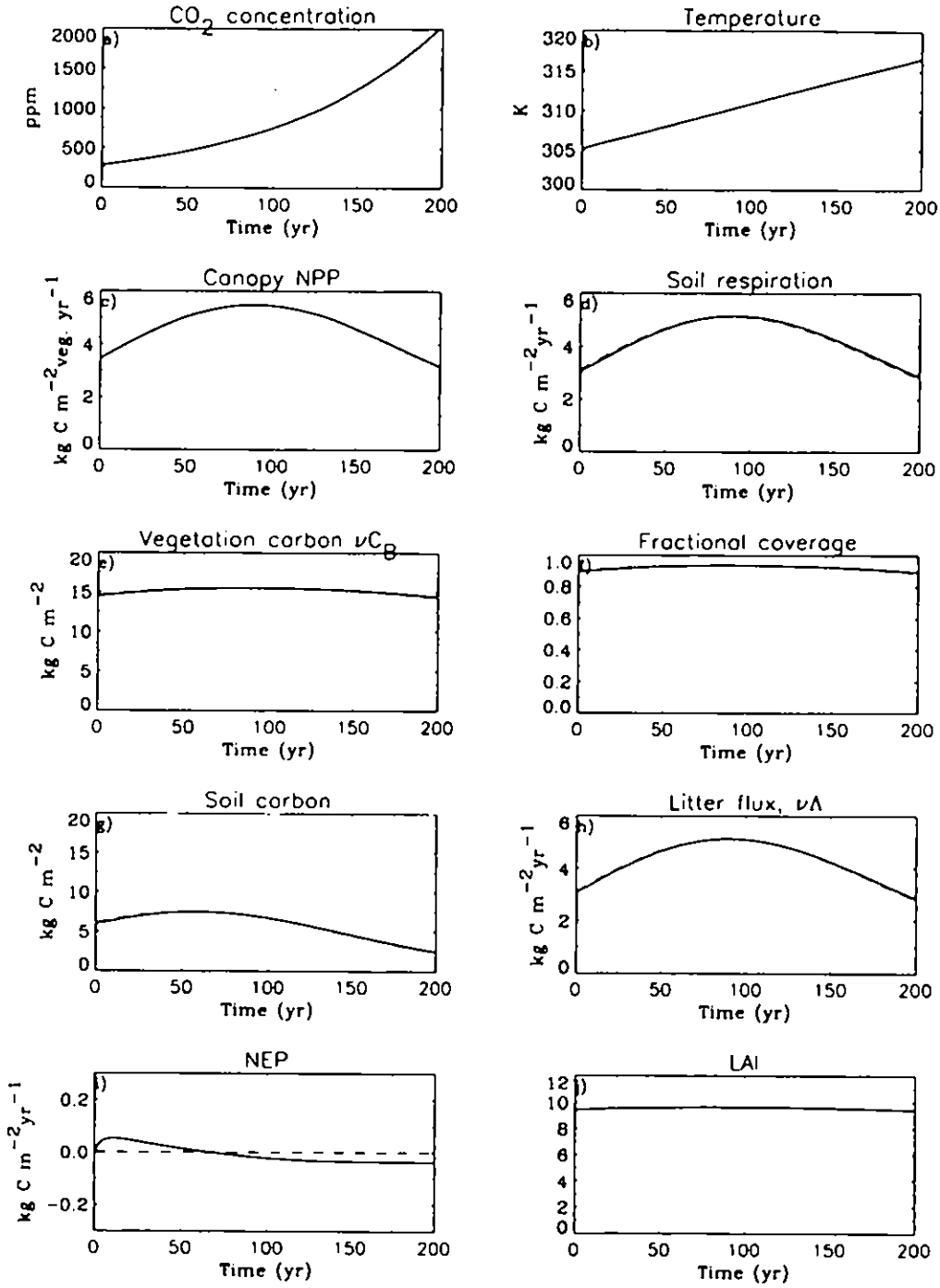

Figure 4. The prediction of c) NPP and d)-j) properties of the terrestrial carbon model for a) prescribed CO_2 concentration and b) associated temperature. This corresponds to $\gamma_c = 0.02$ yr^{-1}, $\gamma_\nu = 0.02$ yr^{-1} and $T_0 = 305.15$ K. Dark respiration is linear in ζ, as given in Equation (2.3). The continuous line represents the dynamic solution and the dashed line the equilibrium solution. Fluxes are in units of yr^{-1}, and areal properties (except NPP) have units m^{-2} of ground cover (that is d), e), g), h) and i)).

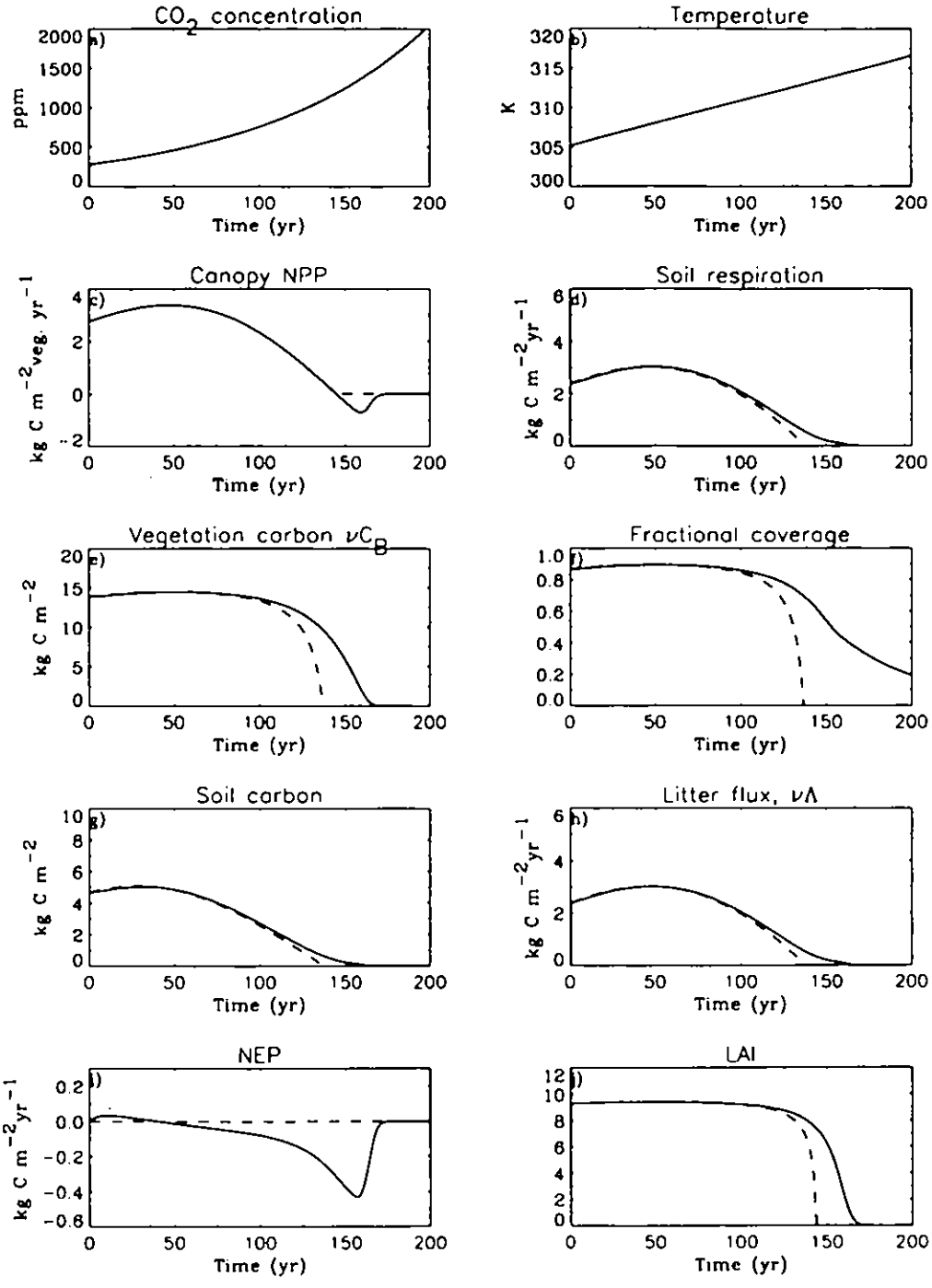

Figure 5. The prediction of c) NPP and d)-j) properties of the terrestrial carbon model for a) prescribed CO_2 concentration and b) associated temperature. This corresponds to $\gamma_c = 0.02$ yr^{-1}, $\gamma_\nu = 0.02$ yr^{-1} and $T_0 = 305.15$ K. Dark respiration is linear in ζ', as given in Equation (7). The continuous line represents the dynamic solution and the dashed line the equilibrium solution. Fluxes are in units of yr^{-1}, and areal properties (except NPP) have units m^{-2} of ground cover (that is d), e), g), h) and i)).

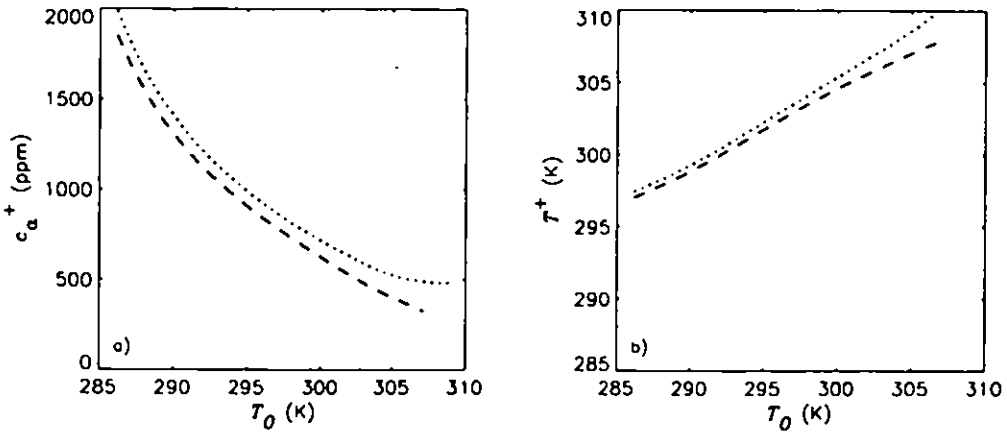

Figure 6. Values of (a) ambient CO_2 concentration, c_a^+ (ppm), and (b) temperature, T^+ (K), at which $dC_T/dt = 0$. These correspond to equilibrium simulations with a range of initial temperatures, T_0. In all simulations, $\gamma_c = \gamma_v = 0.02$ yr^{-1}, and the dark and plant respirations are linear in either ζ (dotted curves) or ζ' (dashed curves).

Planetary boundary-layer feedbacks on surface energy fluxes due to changes in land surface prescription.

Huntingford, C.

White, A.

Early notes, but hopefully submit to Boundary-layer Meteorology by Jan 2000

Planetary boundary-layer feedbacks on surface energy fluxes due to changes in land surface prescription

C. Huntingford[+] and A. White[*]
[+] *Institute of Hydrology, Wallingford, OX10 8BB, U.K.*
[*] *Institute of Terrestrial Ecology, Penicuik, EH26 0QB, U.K.*

October 21, 1999

Abstract. A family of numerical experiments demonstrate that the Convective Boundary-Layer (CBL) suppresses potential variation in both the Priestley-Taylor coefficient and evaporative flux that may otherwise be expected due to changes in surface resistance. This is also true for changes in roughness length, but in keeping with the analysis of Jacobs and DeBruin (1992), boundary-layer feedbacks enhance surface evaporation when a change in surface albedo is made. Theorectical considerations allow the study of Jacobs and DeBruin (1992), and the numerical work presented here, to be mapped onto the closed land surface plus CBL system encapsulated within the simple equation of Huntingford and Monteith (1998), linearly relating the inverse of the Priestley-Taylor coefficient to stomatal resistance.

KEYWORDS: Surface resistance, Diurnal variability, Latent heat flux, Atmospheric feedback, Priestley-Taylor coefficient.

1 Introduction

The Penman Monteith equation (Monteith, 1981) describes the partitioning of available energy at the land surface into sensible and latent heat fluxes as a function of surface resistance r_S (s m^{-1}) and microclimate, the latter prescribed at a reference height z_r (m) (Monteith, 1981). Models of the Convective Boundary Layer (CBL) relate land surface fluxes to the diurnal evolution of atmospheric temperature and humidity (eg McNaughton and Spriggs, 1989). As such, surface-atmosphere energy fluxes of heat and vapour are a function of the two-way coupling between the land surface and the growing CBL. In a theoretical modelling context, this coupling may be expressed as a relation between the Priestley-Taylor coefficient, α (Priestley and Taylor, 1972) and any prescribed value of r_S. Such a correspondance is found to lie between small bands of variation in α for even quite large changes in prescribed initial conditions. This has been demonstrated in graphical format by McNaughton and Spriggs (1989). Meanwhile Huntingford and Monteith (1998) show that, to a good approximation, the mean Priestley-Taylor coefficient during a daytime period satisfies $1/\overline{\alpha} = 1/\alpha_0 + m r_S$. Parameters α_0 and m show little dependence upon changes in prescribed initial conditions (except initial surface temperature, θ_{s0} (K) and initial surface specific humidity, q_{s0} (kg kg^{-1}).

Jacobs and DeBruin (1992) characterise the importance of boundary-layer feedbacks on surface fluxes. They do this by changing, individually, three parameters associated with the vegetation, namely albedo, roughness length and surface resis-

tance. The influence of such changes upon the surface fluxes is then calculated from both the Penman Monteith equation, and a fully coupled PBL simulation. Intercomparison of the two models is used to argue whether PBL feedbacks enhance (or otherwise) changes in surface fluxes induced by changes in land surface characteristics. Broadly speaking, changes in roughness length and surface resistance are found to damped by PBL feedbacks, whilst changes in albedo are found to be enhanced by the PBL.

The opportunity exists to revisit the characterisation of CBL feedbacks. This may be done in the joint context of the simple relation given in Huntingford and Monteith (1998) (which characterises the full land surface-PBL system) and the study of Jacobs and DeBruin (1992). However, in this paper, the CBL model is compared against just the land surface boundary condition (namely, evaporative flux is linear in vapour pressure deficit and inversely proportional to stomatal resistance) as opposed to the full Penman Monteith equation. This elimates any dependency upon a reference height within the intercomparisons.

2 Analysis

2.1 Model overview

The governing equations follow those presented in McNaughton and Spriggs (1989), although with two modifications. First, the model is now driven by incoming shortwave radiation, $S_{\downarrow}$ (W m^{-2}), and with longwave radiation components solved explicitly. Second, the surface layer is modelled as simply one-tenth of boundary-layer height (De Bruin and Jacobs, 1989 and Garratt, 1992). The governing equations are given in Appendix A.

An short overview of the coupled model is as follows. The land surface is assumed to be uniform, and is described in terms of a bulk surface conductance g_S (m s^{-1}) which is invariant during any modelled diurnal period. However, its value may be changed, reflecting possible changes in soil moisture status. In addition a roughness length for momentum z_{0m} (m) and for heat z_{0h} (m) are given. The surface energy balance is solved using the Penman Monteith combination equation, applied across the surface layer. The driving microclimatic variables are those from the fully-mixed layer, and this equation determines the partitioning of available radiative energy into sensible and latent heat fluxes. The fully-mixed layer extends from the top of the surface layer to a capping inversion, above which a stable layer is assumed. The governing equations for the mixed-layer assume a layer of constant potential temperature and humidity. The layer absorbs heat and vapour from the land surface and further entrains these quantities from the stable layer aloft. In the absence of fronts or formation of clouds, then this model will be representative of the behaviour of the CBL for a diurnal period. Model closure is given by an equation for entrainment that follows the work of McNaughton and Spriggs (1989).

2.2 THE CHARACTERISATION OF FEEDBACK STRENGTH

A simple methodology is needed to describe the importance of the CBL (and surface layer) feedbacks that arise due to prescribed variation in land surface characteristics (through r_S). In this paper, the Priestley-Taylor coefficient is regarded as the main diagnostic of surface energy partitioning. The method outlined below is similar in principle to that given by Betts *et al.*, 19XX, where they quantify the impact of different land surface schemes within climate models.

There are three steps to the analysis, as follows.

1. A fully coupled boundary-layer and land surface simulation is undertaken for an initial form of $r_S(t)$. The time dependent values of the Priestley-Taylor coefficient are retained, and labelled $\alpha_1(t)$. This first numerical run may be regarded as a control simulation.

2. A new form for bulk surface resistance is suggested, $r_S^*(t)$, and the Priestley-Taylor coefficient calculated (now called $\alpha_2(t)$) but using the surface climatology as saved from simulation (1). This "off-line" simulation calculates α_2 as

$$\alpha_2 = \left(\frac{\epsilon + 1}{\epsilon}\right) \frac{\rho \lambda D}{A r_S^*} \tag{1}$$

   where the microclimate of surface temperature θ_c (K), surface humidity q_c (kg kg^{-1}) and ϵ are saved from the first run. This simulation represents the new value of the Priestley-Taylor coefficient that may be expected should the land surface be unaffected by changes in CBL feedbacks.

3. A new fully coupled run is undertaken, using the new form of bulk surface resistance $r_S^*(t)$. Values of the Priestley-Taylor coefficient are calculated, and named $\alpha_3(t)$. This simulation represents to effect of a different surface behaviour upon surface energy fluxes when atmospheric feedbacks are included.

The advantage of undertaking the method outline above is that the intermediate "off-line" simulation (2) allows a far better understanding of the direct influence of r_S upon fluxes. In particular, when the change from simulation (1) to (2) is compared that between (1) and (3), then the degree to which changes are enhanced or otherwise by CBL feedbacks may be assessed. A statistic is required that can express the importance of such feedbacks. If, for instance, the model diagnostic of interest is the mean Priestley Taylor coefficient $\overline{\alpha}$, then one such statistic S may be given by

$$S = 100 \left(\frac{\overline{\alpha_3} - \overline{\alpha_1}}{\overline{\alpha_2} - \overline{\alpha_1}}\right) \tag{2}$$

If S has a value of 100%, then this means that the PBL has no effect at all upon the mean Priestley-Taylor co-efficient. A value of, for example, 60% means that the PBL mitigates 40% of the potential change, whilst a value greater than 100% implies that the PBL acts as a positive feedback.

2.3 Variation in fixed r_S

In the first family of simulations, the value of surface resistance is assumed to be invariant throughout any given diurnal period. Variation of such values of r_S may be considered representative of longer term (eg seasonal) changes in surface characteristics. These may include soil water stress (that generally causes an increase in surface resistance through stomatal closure) and changes in biomass (changes in leaf area index affect r_S directly).

For small variations about the original state for r_S (which gives the Priestley-Taylor coefficient of α_0), then

$$\sigma = 100 \left(\frac{\mathrm{d}\alpha_3}{\mathrm{d}r_S} \right)_{(r_s = r_{s,1})} \left(\frac{\mathrm{d}\alpha_2}{\mathrm{d}r_S} \right)^{-1}_{(r_s = r_{s,1})} \tag{3}$$

2.4 Relation to previous work for fixed r_S

In papers by McNaughton and Spriggs (1989) and Huntingford and Monteith (1998), the relation between $\overline{\alpha}$ and a fixed value of r_S is investigated when PBL feedbacks are incorporated. A family of curves yields relationships of the form

$$\frac{1}{\overline{\alpha}} = \frac{1}{\alpha_0} + m r_s \tag{4}$$

and so

$$m = \frac{\mathrm{d}}{\mathrm{d}r_s} \left(\frac{1}{\overline{\alpha}} \right) \tag{5}$$

If the PBL feedbacks are assumed to be invariant, then (in the calculation of α_2), the (time dependent) change in the inverse of the Priestley-Taylor coefficient with r_s will be given by

$$m_0 = \frac{\mathrm{d}}{\mathrm{d}r_s} \left(\frac{1}{\alpha} \right) = \frac{\epsilon A}{(\epsilon + 1)\rho\lambda D_c} \tag{6}$$

Equations (5) and (6) may be compared due to the diurnal conservatism within the Priestley-Taylor coefficient. That is, the boundary-layer feedbacks appear to allow α to be nearly constant throughout the diurnal period, and as such consideration of changes in α at one time, midday say, will be true for most of the daytime. Statistic σ can now be evaluated from m and m_0 by noting that

From Huntingford and Monteith (1998) and for the parameters chosen in their Table I, $m = 0.00326$ m s^{-1}. Their numerical code is also rerun to obtain midday values ($t = t_{day}/2$) of $\epsilon = 2.68$ and $D_c = 6.25^{-3}$ kg kg^{-1}. Hence $m_0 = 0.0108$ m s^{-1}. Noting that $\mathrm{d}(\overline{\alpha})^{-1})/\mathrm{d}r_S = -\overline{\alpha}^2 \mathrm{d}(1/\overline{\alpha})^{-1})/\mathrm{d}r_S$ then from (5) and (6), statistic (2) is given by

$$\sigma = 100 \frac{m}{m_0} = 30.2\% \tag{7}$$

That is, for the initial and boundary conditions prescribed, boundary-layer feedbacks reduce by 70% the potential change in Priestley-Taylor coefficient as a consequence of variation in stomatal resistance.

2.5 Variation in albedo and momentum roughness length

The vegetation albedo, σ, is reduced from 0.3 to 0.2.

The momentum roughness length, $z_{0,m}$, is reduced by an order of magnitude to $z_{0m} = 0.02$m. The roughness length for heat is similarly reduced so as to maintain $\ln(z_{0m}/z_{0T}) = 2$.

2.6 Relation to analysis of Jacobs and DeBruin

Penman Monteith equation. Set temperature for longwave down as temperature at reference height.

3 Discussion and conclusions

Jacobs and DeBruin (1992) provide a formal structure for characterising the importance of PBL feedbacks upon the land surface. The technique is identical in concept to the general method described by Betts *et al.*, (1997) for testing the impact of different land surface schemes upon climate simulations. Jacobs and DeBruin (1992) assess the importance of feedbacks upon surface energy partitioning based upon comparing the sensitivity of the Penman Monteith equation to perturbation of main driving variables and parameterisations, to identical sensitivies but now with coupling of the land surface description to a PBL model. They conclude that, when considering the evaporative fluxes, variation induced by adjusting the net radiation are enhanced by PBL feedbacks. When considering evaporative fraction,

The Penman Monteith equation depends crucially upon the prescription of a reference height. When assessing sensitivites based upon typical microclimate measurements made at such a height, then the analysis outlined by Jacobs and DeBruin (1992) provides a full assessment of PBL feedbacks. However, when considering the true influence of changes in the land surface, and any resultant PBL feedbacks, then such analysis should be independent of prescription of what is effectively an arbitrary height. In this paper, such an approach is pursued, and results are discussed within the context of the earlier analysis. The argument placed forward is as follows. The evaporative flux from the vegetation can only "see" direct stomatal control and specific humidity deficit. Hence structure changes through changes in albedo and roughness height can only influence through the entire system. The hope is that the Huntingford and Monteith (1998) notation encapsulates the entire system.

The work of Jacobs and DeBruin (1992) provides an exceedingly useful tool for understanding the importance of PBL feedbacks when sensitivity studies are undertaken for sites where micrometeorological measurements are known. The sensitivity to structural changes in

the PBL acts as a negative feedback upon variation in stomatal resistance, but as a positive feedback upon variation in net radiation

4 Conclusions

The analysis of Jacobs and DeBruin (1992) characterises the importance of boundary-layer feedbacks in modulating the effect of changes in land surface characteristics, when compared to equivalent variation in the Penman Monteith equation. Here, we reconfirm their analysis that for both the evaporative fluxes, and the Priestley-Taylor coefficient, the PBL acts of a suppressor of changes in stomatal resistance and roughness length at the land surface. However, the PBL acts as a positive feedback, for evaporation from the surface, due to changes in albedo (variability in the Priestley-Taylor coefficient is again suppressed). The latter result may have very important implications in the case of land degradation.

The overriding difficulty of characterising PBL feedbacks through intercomparison with the Penman Monteith equation is that any derived statistic has been shown here to be highly dependent upon selected reference height. Within this paper, the land surface is regarded as the true lower boundary condition to the atmosphere; that is the reference height above the land surface is effectively zero. This "purer" form of intercomparison yields similar conclusions to the work of Jacobs and DeBruin (1992), but reduces the complexity of characterising effects. The surface evaporative flux is dependent upon just prescribed and direct variation in stomatal resistance, or, through PBL feedbacks influencing surface specific humidity deficit (or both simulataneously).

A major development here is the realisation that the summary of coupled surface-PBL "slab" models, given graphically within McNaughton and Spriggs (1989) and reduced to a simple algebraic form within Huntingford and Monteith (1998) contain important information about the strength of PBL feedbacks. The behaviour of coefficients m and α_0 used by Huntingford and Monteith (1998) contain implicit information on the sensitivity of the PBL to land surface changes.

5 Acknowledgement

The authors thank the CEH Integrating Fund for providing financial assistance to undertake this study.

6 References

Betts, R.A., Cox, P.M., Lee, S.E. and Woodward, F.I.: 1997, 'Contrasting physiological and structural vegetation feedbacks in climate change simulations', *Nature*, **387**, 796-799.

Culf, A.D.: 1994, 'Equilibrium evaporation beneath a growing convective boundary layer', *Boundary-Layer Meteorol.*, **70**, 37-49.

De Bruin, H.A.R.: 1983, 'A model for the Priestley-Taylor parameter, α', *J. Cli-*

mate and Applied Meteorol., **22**, 572-580.

De Bruin, H.A.R. and Jacobs, C.M.J.: 1989, 'Forests and regional-scale processes', *Phil. Trans. Roy. Soc. Lond.*, **B 324**, 393-406.

Driedonks, A.G.M.: 1981, 'Dynamics of the well-mixed atmospheric boundary-layer', *Scientific Report W.R. 81-2*, K.N.M.I., De Bilt, The Netherlands.

Garratt, J.R.: 1992, 'The atmospheric boundary layer', *Cambridge University Press, Cambridge.*

Huntingford, C. and Monteith, J.L.: 1998, 'The behaviour of a mixed-layer model of the convective boundary layer coupled to a big leaf model of surface energy partitioning', *Bounday-layer Meteorol.*, **88**, 87-101.

Jacobs, C.M.J. and DeBruin, H.A.R.: 1992, 'The sensitivity of regional transpiration to land-surface characteristics: significance of feedback', *J. Climate*, **5**, 693-698.

McArthur, A.J.: 1990, 'An accurate solution to the Penman equation', *Agric. For. Meteorol.*, **51**, 87-92.

McNaughton, K.G. and Jarvis, P.G.: 1983, 'Predicting effects of vegetation changes on transpiration and evaporation', in: 'Water deficits and plant growth (Kozlowski, T.T., ed.) Vol VII', *Academic Press, New York.*

McNaughton, K.G. and Spriggs, T.W.: 1986, 'A mixed-layer model for regional evaporation', *Boundary-layer Meteorol.*, **34**, 243-262.

McNaughton, K.G. and Spriggs, T.W.: 1989, 'An evaluation of the Priestley and Taylor equation and the complementary relationship using results from a mixed-layer convective boundary-layer', in: 'Estimation of areal evapotranspiration (Black, T.A., Spittlehouse, D.L. and Novak, M.D., eds.)', *IAHS Publication 177, IAHS Press, Wallingford, UK.*

Monteith, J.L.: 1981, 'Evaporation and surface temperature', *Quart. J. Roy. Meteorol. Soc.* **107**, 1-27.

Paulson, C.A.: 1970, 'The mathematical representation of wind speed and temperature profiles in the unstable atmospheric surface layer', *J. Appl. Meteorol.* **9**, 857-861.

Priestley, C.H.B. and Taylor, R.J.: 1972, 'On the assessment of the surface heat flux and evaporation using large-scale parameters', *Mon. Wea. Rev.*, **100**, 81-92.

Raupach, M.R.: 1998, 'Influences of local feedbacks on land-air exchanges of energy and carbon', *Global Change Biology*, Submitted.

Swinbank, W.C.: 1963, 'Long-wave radiation from clear skies', *Quart. J. Roy. Met. Soc.*, **89**, 339-348.

Tennekes, H.: 1973, 'A model for the dynamics of the inversion above a convective boundary-layer', *J. Atmos. Sci.*, **30**, 558-567.

7 Appendix

The complete set of governing model equations are as follows. The surface energy balance satisfies

$$(1-a)R_{S,\downarrow} - R_{L,\uparrow} + R_{L,\downarrow} = H + \lambda E \tag{8}$$

where a is surface albedo, $R_{S,\downarrow}$ (W m^{-2}) is downward shortwave radiation, $R_{L,\downarrow}$ (W m^{-2}) is longwave downward radiation, $R_{L,uparrow}$ (W m^{-2}) is longwave upward radiation, H (W m^{-2}) is upward sensible heat flux and λE (W m^{-2}) is upward latent heat flux. This equation contains the implicit assumption that the land surface has no thermal capacity, and that the soil heat flux is negligible.

Throughout the model, the downward shortwave radiation is prescribed as

$$R_{S,\downarrow} = 4R_{S,\downarrow,max}\frac{t}{t_{day}}\left(1-\frac{t}{t_{day}}\right) \tag{9}$$

where $R_{S,\downarrow,MAX}$ (W m^{-2}) is the maximum available downward shortwave radiation, t (s) is time since sunrise, t_{day} (s) is day length. The longwave radiative fluxes satisfy

$$R_{L,\uparrow} = \sigma T_c^4 \qquad R_{L,\downarrow} = \mu T_{z,s}^6 \tag{10}$$

where $\sigma = 5.67032 \times 10^{-8}$ W m^{-2} K^{-4} is the Stefan-Boltzman constant and T_c (K) is surface temperature. The equation for downward longwave radiation follows that of Swinback (1963), and where $\mu = 5.31 \times 10^{-14}$ W m^{-2} K^{-6}. The temperature required within the equation for $R_{L,\downarrow}$ is approximated by the temperature at the bottom of the mixed-layer, $T_{z,s}$ (K).

The partioning of available radiative energy, A (W m^{-2}) (where $A = (1-a)R_{S,\downarrow} - R_{L,\uparrow} + R_{L,\downarrow}$) into latent and sensible heat flux is calculated using the Penman Monteith combination equation, applied across a surface layer of height z_s (m). This is given by

$$\lambda E = \frac{\epsilon A + \frac{\lambda\rho\{q_{sat}(\theta_m)-q_m\}}{r_{ah}}}{\epsilon + 1 + \frac{r_S}{r_{ah}}} \tag{11}$$

where ϵ is defined as

$$\epsilon = \frac{\lambda}{c_p} \frac{q_{sat}(\theta_c) - q_{sat}(\theta_m)}{\theta_c - \theta_m}. \tag{12}$$

Here λ (J kg^{-1}) is the latent heat of vapourisation, ρ (kg m^{-3}) is the density of air, r_{ah} (s m^{-1}) is the aerodynamic resistance to heat across the mixed-layer, q_m (kg kg^{-1}) is the mixed-layer humidity and c_p (J kg^{-1} K^{-1}) is the specific heat of vapourisation. The resistance r_{ah} contains stability corrections, as given by Paulson (1970). The surface-layer height is prescribed as one-tenth of the CBL height h (m).

The fully-mixed layer is described through three first order differential equations for mixed-layer potential temperautre, θ_m (K), mixed-layer humidity, q_m (kg kg^{-1}) and mixed-layer height. These satisfy

$$\rho c_p h \frac{\mathrm{d}\theta_m}{\mathrm{d}t} = H + \rho c_p \left[\theta_s(h) - \theta_m\right] \frac{\mathrm{d}h}{\mathrm{d}t}, \tag{13}$$

$$\lambda \rho h \frac{\mathrm{d}q_m}{\mathrm{d}t} = \lambda E + \rho \lambda \left[q_s(h) - q_m\right] \frac{\mathrm{d}h}{\mathrm{d}t}, \tag{14}$$

$$\frac{\mathrm{d}h}{\mathrm{d}t} = \frac{H + 0.07\lambda E}{\rho c_p h \frac{\mathrm{d}\{\theta_s(1+0.61q_s)\}}{\mathrm{d}h}}. \tag{15}$$

Temperature $T_{z,s}$ is approximated by $T_{z,s} = \theta_m - (g/c_p)(h/10)$. where g (m s^{-2}) is gravitational acceleration. Variables θ_s (K) and q_s (kg kg^{-1}) correspond to the potential temperature and humidity within the stable layer. For simplicity (as in Huntingford and Monteith, 1998) this are assumed to vary linearly with height, z (m), that is

$$\theta_s(z) = \theta_{s0} + \gamma_\theta z,$$
$$q_s(z) = q_{s0} + \gamma_q z,$$

where θ_{s0} (K), γ_θ (K m^{-1}), q_{s0} (kg kg^{-1}) and γ_q (kg kg^{-1} m^{-1}) are parameters.

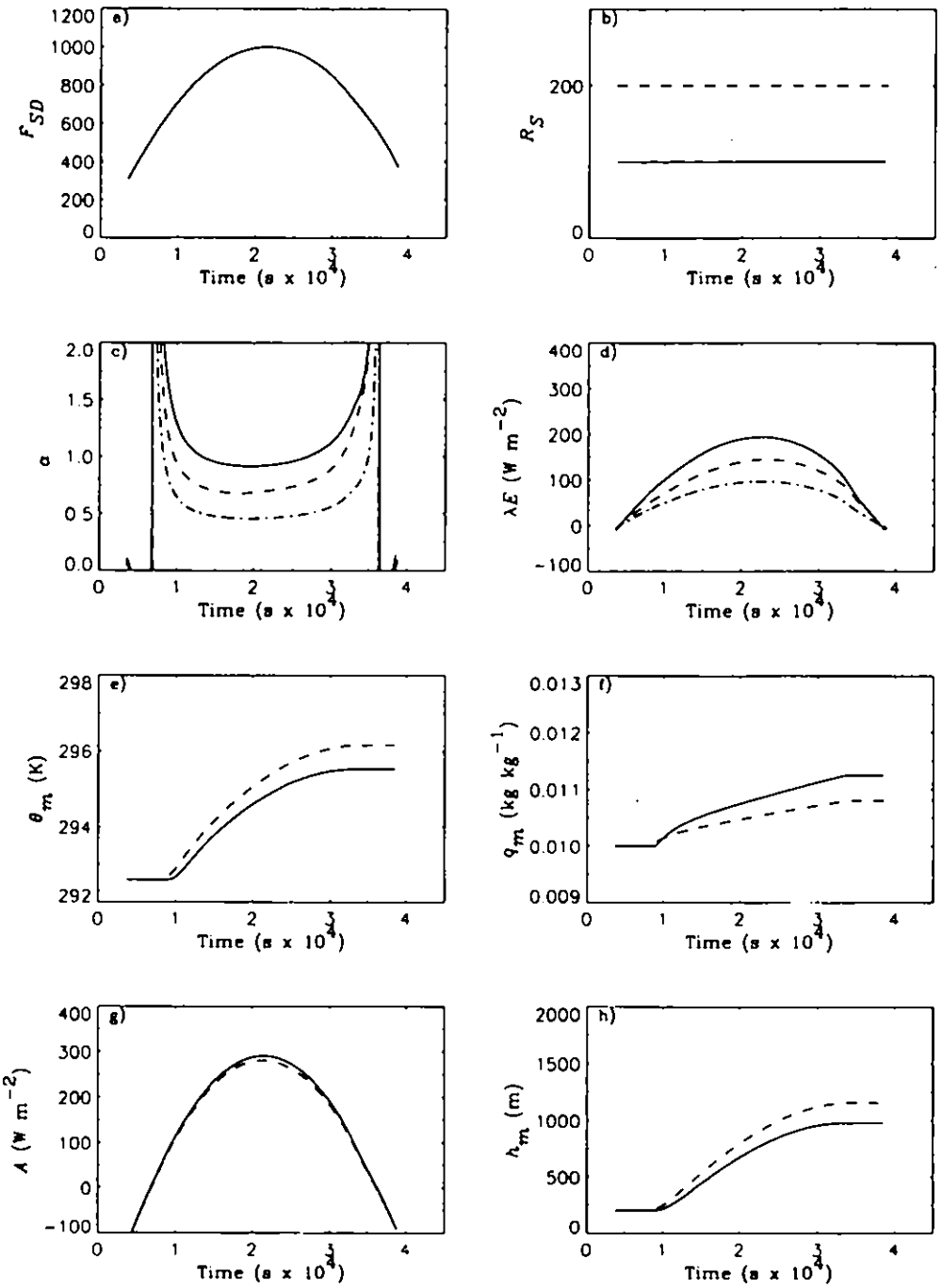

Figure 1. Results from two simulations using the CBL model, with r_S = 100 sm^{-1} (continuous line) and r_S = 200 sm^{-1} (dashed line). Driving and boundary conditions are given in Table I. The individual plots correspond to a) prescribed downward shortwave radiation, b) prescribed value of r_S, and then calculated values of c) Priestley-Taylor coefficient, d) evaporative flux, e) mixed-layer temperature, f) mixed-layer humidity, g) available energy and h) boundary-layer height. Also plotted (dash-dot line) is the value of c) Priestley-Taylor coefficient and d) evaporative flux when using the surface climatology from the first PBL simulation (with r_S = 100 sm^{-1}), and using it to calculate surface fluxes, but with r_S = 200 sm^{-1}.

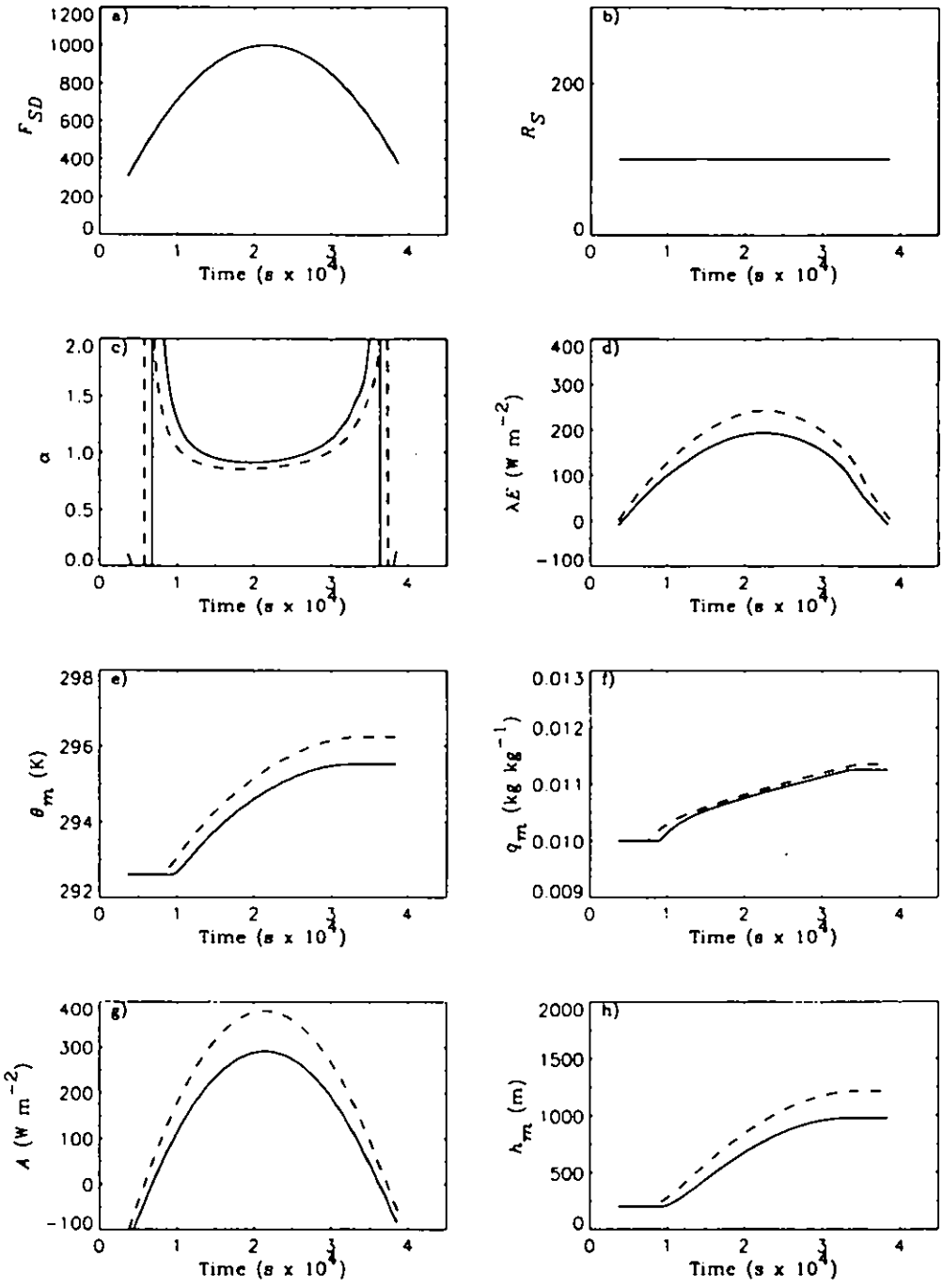

Figure 2. Results from two simulations using the CBL model, both with $r_S = 100$ sm^{-1}, and where $\sigma = 0.3$ (continuous line) and $\sigma = 0.2$ (dashed line). Other driving and boundary conditions are given in Table I. The individual plots are in the same format as Figure 1.

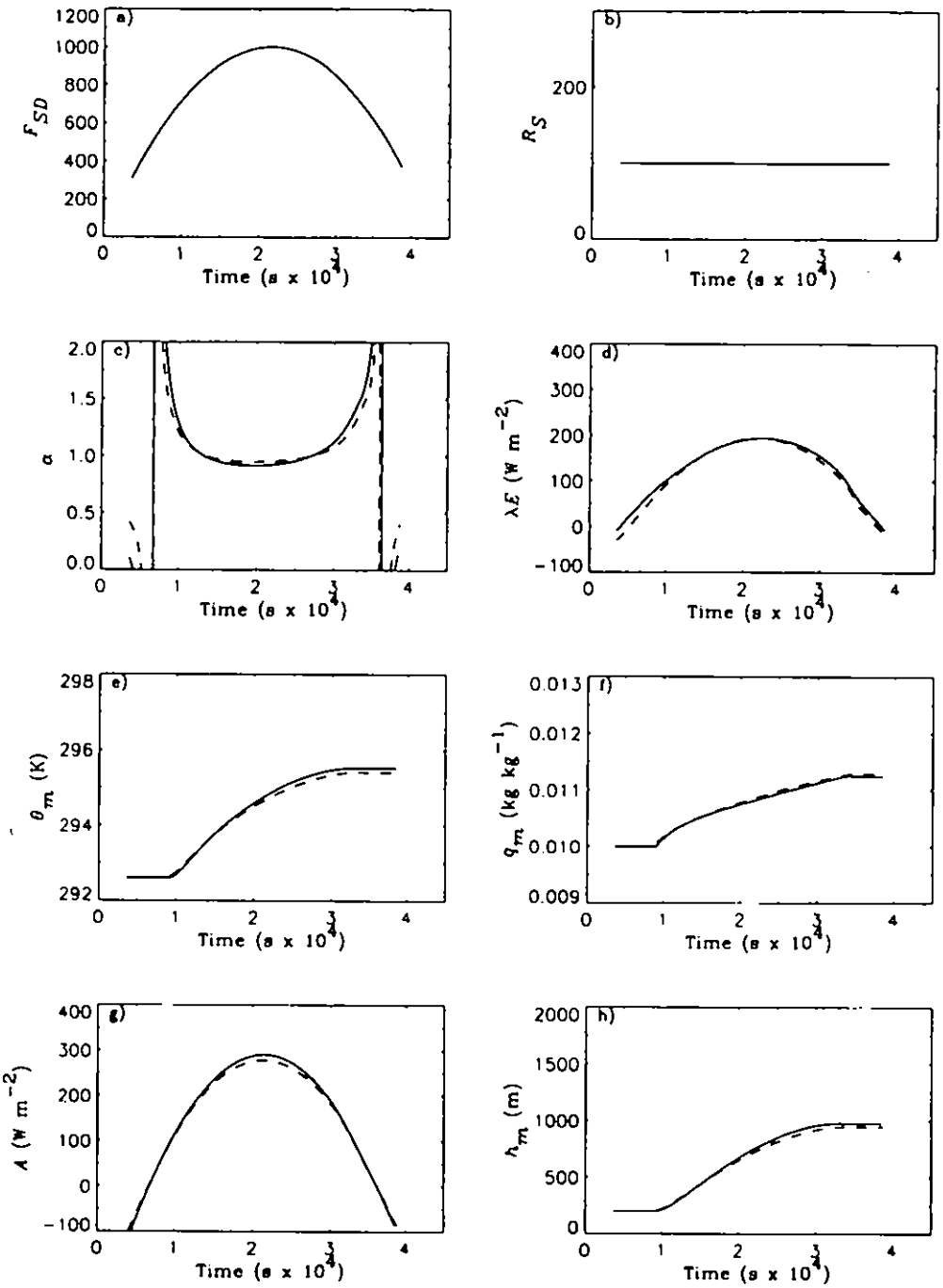

Figure 3. Results from two simulations using the CBL model, both with $r_S = 100$ sm^{-1}, and where $z_{0m} = 0.2$, $ln(z_{0m}/z_{0T}) = 2$ (continuous line) and $z_{0m} = 0.02$, $ln(z_{0m}/z_{0T}) = 2$ (dashed line). Other driving and boundary conditions are given in Table I. The individual plots are in the same format as Figure 1.

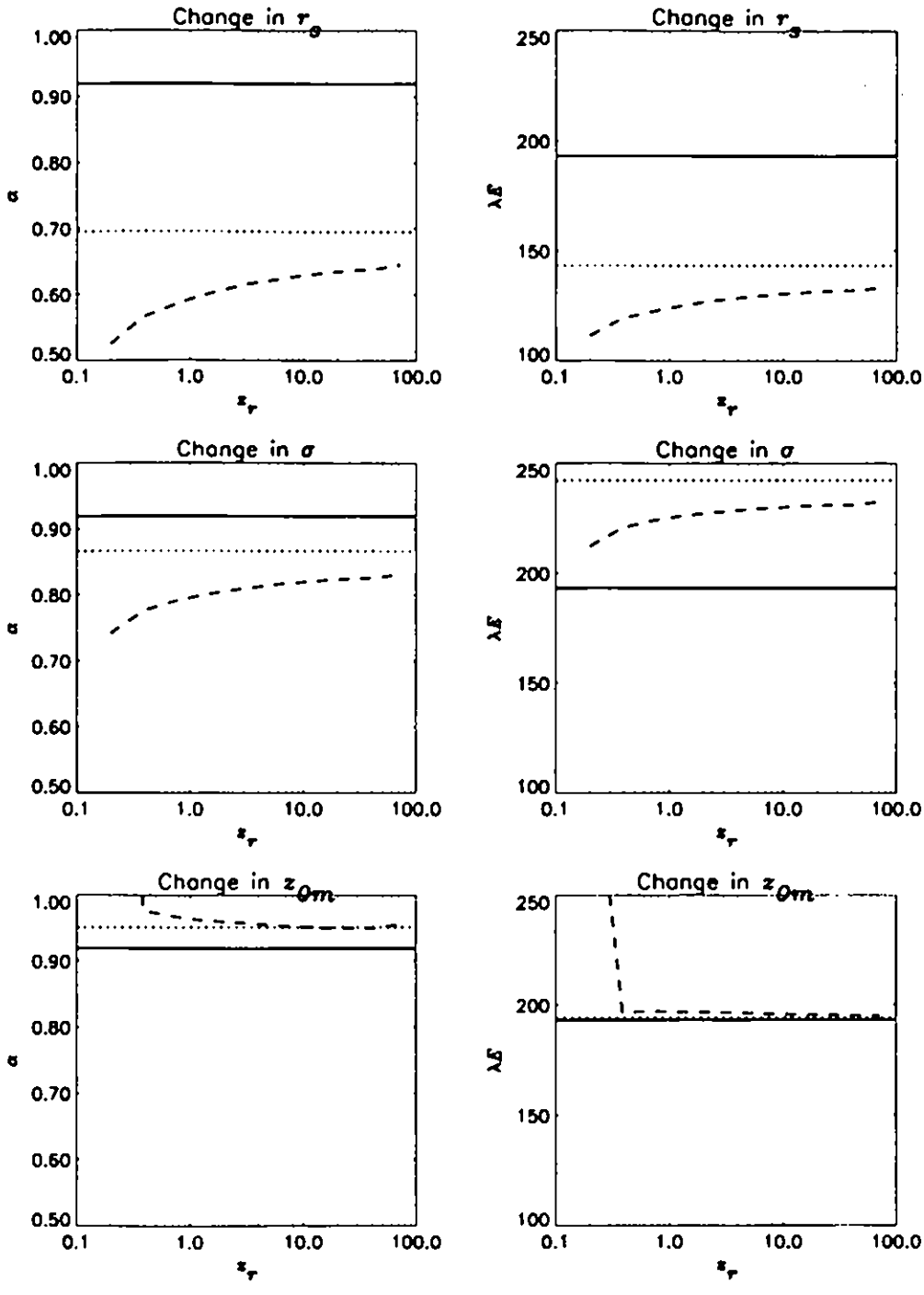
Change in r_s
Change in r_s
Change in σ
Change in σ
Change in z_{0m}
Change in z_{0m}
α
λE
z_r
1.00
0.90
0.80
0.70
0.60
0.50
250
200
150
100
0.1
1.0
10.0
100.0

Figure 4.

A re-interpretation of stomatal behaviour based upon a theoretical analysis of existing descriptions.

Huntingford, C.

Smith, M.

Early notes, but hopefully submitted to Plant Cell and Environment in the New Year

A reinterpretation of stomatal behaviour based upon a theorectical analysis of existing descriptions

C. Huntingford and M. Smith
Institute of Hydrology, Wallingford, OX10 8BB, U.K.

October 21, 1999

Abstract.
A theorectical study is presented to analyze the response of surface conductance to environmental variables. The main model is based upon the emerging hypothesis that chemical signalling provides a mechanism linking stomatal opening to soil moisture status. Through algebraic techniques, this model may be rewritten to be a function of soil moisture and surface humidity deficit. This allows an intercomparison with the more traditional descriptions of stomatal control.

KEYWORDS: Stomatal conductance, ABA, Soil moisture, surface energy balance

1 Introduction

A key control of both photosynthetic uptake of carbon dioxide and transpiration by vegetation is the degree of stomatal opening, which is modelled using the variable stomatal conductance. It is essential that accurate descriptions of stomatal conductance are contained in models of vegetation function and land-surface processes. Rates of carbon fixation in models of plant growth are dependent on stomatal conductance, as is estimation of water use by vegetation. Numerical modelling experiments have shown that stomatal conductance also influences climatic behaviour at a range of spatial scales, because of the effects of stomatal behaviour on partitioning of energy between sensible heat and evaporation at the vegetation surface. For instance, the overview paper, Garratt (1993) demonstrates the importance of the land surface upon climate simulations (of which stomatal control provides a key influence). At the regional scale, conceptual studies demonstrate the importance influence of stomatal control upon atmospheric boundary-layer feedbacks (eg Jacobs and DeBruin, 1992, Raupach, 1998, Huntingford and Monteith, 1998). At the local (plot) scale, surface evaporation is heavily dependent upon stomatal opening, as may be directly observed within the Penman Monteith surface energy partitioning equation (Monteith, 1981).

It is well established, from both laboratory and field experiments, that stomatal conductance appears to respond to environmental conditions. Through testing for correlations between stomatal opening and the prevailing environmental conditions, stomatal conductance may be modelled as a function of light, temperature, humidity deficit and soil moisture. Jarvis (1976) used such a procedure to model stomatal conductance as a series of multiplicative functions of stomatal response to each environmental variable. This approach was used successfully by Stewart (1988) for a UK pine forest and has been used by many others with similar success

for a range of vegetation types. Huntingford and Cox (1997) were able to almost reproduce such functional responses for the pine forest with an unconstrained neural network fitting procedure.

There is now considerable evidence that stomatal response to soil drying is mediated by a chemical signal originating in the roots (Zhang and Davies, 1989). Stomatal opening has been found to decline as the concentration of abscisic acid ([ABA]) in xylem sap increases (Zhang and Davies, 1990; Khalil and Grace, 1993). As xylem [ABA] is thought to be a function of water flux through the root system (Tardieu et al., 1992), stomatal response to [ABA] suggests that stomatal conductance may be dependent on the evaporative flux. There is also experimental evidence that stomatal sensitivity to [ABA] varies with leaf water potential. As leaf water potential declines - for example because of an increase in transpiration - stomata have been found to become more responsive to [ABA] (Tardieu and Davies, 1992). These effects of abscisic acid on stomatal physiology provide a possible mechanism for stomatal response to vapour pressure deficit, which Montieth (1995a) has argued is a surrogate for a dependence on the evaporative flux.

Stomatal opening has also been related to fluxes of carbon dioxide passing through them. Ball et al. (1987) and Leuning (1995) proposed that stomatal conductance is a linear function of net photosynthesis. In these descriptions, the stomatal responses to temperature and light modelled by Jarvis (1976) are surrogates for photosynthetic activity; the effects of temperature and light on stomatal opening are apparent only because of stomatal responses to resultant changes in net photosynthesis.

Tardieu and Davies (1993) developed a model of stomatal control by ABA which can be combined with the Leuning (1995) model of the dependency of stomatal conductance on photosynthesis. The resultant model enables stomatal conductance to be described using just four variables: the evaporative flux, net photosynthesis, soil water content and ambient CO2 concentration. Here, we derive this new flux dependent model and test whether it is able to reproduce responses to environmental variables that are functionally equivalent to the model of Jarvis (1976).

2 Stomatal response to soil moisture and re-interpretation of response to vapour pressure deficit

2.1 Rationale

Tardieu and Davies (1993) provide a model for stomatal response to drought stress that is based upon both direct hydraulic control and chemical signalling. This is by responding to leaf water potential, Ψ_{leaf} (MPa) and xylem concentration, ABA (mol m^{-3}) respectively. Here, through combination of the model with the Clapp and Hornberger (1978) relations for soil parameterisation and the big leaf model for surface energy partitioning, it is demonstrated that the model may be expressed in terms of a response to soil moisture concentration, θ (m^3 H_2O m^{-3} soil) and

specific humidity deficit at leaf level, D (kg kg^{-1}).

2.2 Governing equations

2.2.1 The model of Tardieu and Davies (1993) for stomatal control

The model of Tardieu and Davies is described here for completeness, including the units used within this study, and parameters chosen. Root water potential, Ψ_r (MPa) satisfies

$$\Psi_r = \Psi_s - J_w R_{root}. \tag{1}$$

where J_w (mg m^{-2} s^{-1}) (mg m^{-2}) s^{-1}) is the water flux and R_{root} (MPa m^2 s mg^{-1}) is the resistance within the soil. This latter resistance is as given in Tardieu, 1993 as

$$R_{root} = \frac{1}{4\pi K L_a} \ln \frac{d^2}{r^2} \tag{2}$$

where L_a (m m^{-2}) is root length per unit area of ground, d (m) is the half mean distance between roots (m) and r (m) is the mean radius of the roots. Here, values are prescribed as $L_a = 10^4$ m m^{-2}, $r = 5 \times 10^{-4}$ m and $d = 5.6 \times 10^{-3}$. The leaf water potential, Ψ_{leaf} (MPa), satisfies a further resistance formulation

$$\Psi_{leaf} = \Psi_{root} - J_w R_{plant} \tag{3}$$

where R_{plant} (MPa m^2 s mg^{-1}) is a plant resistance. Following Tardieu and Davies (1993), this corresponds to $R_p = 7.2 \times 10^{-3}$ MPa s m^{-1}.

The ABA concentration, c_{ABA} (mol m^{-3} water) is modelled as dependent upon both the root water potential and the evaporative flux as

$$c_{ABA} = -\frac{a\Psi_{root}}{J_w + b} \tag{4}$$

where $a = 1.4 \times 10^{-3}$ mol ABA m^{-2} s^{-1} Pa^{-1} and $b = 4.0$ mg m^{-2} s^{-1}. Following Tardieu (1993), stomatal conductance, g_s, is then modelled as a function of leaf water potential and ABA concentration thus

$$g_s = g_{s,min} + \alpha e^{c_{ABA}\beta e^{\delta\Psi_{leaf}}}. \tag{5}$$

Variable $g_{s,min}$ (m s^{-1}) is a minimum stomatal conductance, set at 8.93×10^{-4} m s^{-1} (corresponding to a value of 0.02 mol m^{-2} s^{-1}; see Tardieu *et al.* (1993)). Similarly constant α is given a value of 0.0112 m s^{-1}, which corresponds to a value of 0.25 mol m^{-2} s^{-1} (again, see Figure x of Tardieu *et al.*, 1993). The other constants are $\beta = -2.69 \times 10^3$ (m^3 mol^{-1}) and $\delta = -0.183$ MPa^{-1}.

By combining Equations (1) to (5), it is possible to write the form for stomatal control as $g_s = g_s(\Psi_s, J_w)$.

2.2.2 Soil moisture behaviour

Soil properties are related to the prescribed soil water content, θ. Soil water potential, Ψ_s (MPa) and hydraulic conductivity K ($m^2\ s^{-1}\ MPa^{-1}$) are given by the Clapp and Hornberger (1978) relations thus:

$$\Psi_s = \Psi_{sat}\theta_f^{-b_{CH}}, \qquad K = K_{sat}\theta_f^{2b_{CH}+3}. \tag{6}$$

Here $\theta_f = \theta/\theta_{sat}$, and θ_{sat} ($m^3\ H_2O\ m^{-3}$ soil) is the saturated soil moisture content, Ψ_{sat} (MPa) is the saturated soil water potential, K_{sat} ($m^2\ s^{-1}\ MPa^{-1}$) is the saturated hydraulic conductivity and b_{CH} is the Clapp-Hornberger coefficient. Values are adopted for a medium soil, as given by Cosby *et al.* (1984) and further given in Table 2 of Cox *et al.* 1999. Hence $\theta_s = 0.458$, $b = 6.63$, and so converted into the units of this paper, $\Psi_{sat} = -4.86 \times 10^{-4}$ MPa and $K_{sat} = 4.81 \times 10^{-4}\ m^2\ s^{-1}\ MPa^{-1}$. Combining these equations with those of Section 2.2 implies that the equations so far may be written as

$$g_s = g_s(J_w, \theta) \tag{7}$$

2.2.3 Surface energy balance

Atmospheric demand on evaporation is given by the 'big leaf model' thus:

$$J_w = \rho_a D g_s 10^{-6} \tag{8}$$

where ρ_a ($kg\ m^{-3}$) is the density of air.

2.3 Equation solution

The entire set of equations (1) to (8) are solved for g_s, and require the prescription of just two driving variables, namely leaf level specific humidity deficit and soil moisture content. That is, Equations (7) and (8) are two equations in four unknowns g_s, J_w, θ, D, and so the prescription of D and θ reduce by two the degrees of freedom, thereby allowing solution. In particular, this implies that the full set of equations may be written as

$$g_s = g_s(\theta, D). \tag{9}$$

A direct comparison may therefore be made with the models of Jarvis (1976) and Stewart (1988).

3 Comparison with previous work

3.1 Relation to the work of Jarvis (1976) and Stewart (1988)

The model of Jarvis (1976) and Stewart (1988) assumes that controlling influences upon stomatal conductance may be expressed multiplicatively. In particular, their model may be written as

$$g_s = g_{s,min} + \gamma f_1(\theta) f_2(D) f_3(T) f_4(I) \tag{10}$$

where T (K) is leaf level temperature and I (W m^{-2}) is incoming solar radiation. Each multiplicative parameter $f_i, 1 \leq i \leq 4$ satisfies $0 \leq f_i \leq 1$ whilst γ (m s^{-1}) is a constant. In particular, the function forms for θ and D are given by

$$f_1 = \begin{cases} 1 & \theta < \theta_c \\ \frac{\theta - \theta_w}{\theta_c - \theta_w} & \theta_c \leq \theta < \theta_w \\ 0 & \theta \geq \theta_w \end{cases} \tag{11}$$

$$f_2 = 1 - a_1 \delta q, \tag{12}$$

for parameters θ_c (m^3 water m^{-3} soil) (the critical point), θ_w (m^3 water m^{-3} soil) (the wilting point) and a_2 (kg kg^{-1}).

Eqns (1) to (8) are solved for a range of values of θ and D, to give a contour plot for g_s (Figure 7). Two features are noticeable. The response of stomatal conductance to soil moisture content is such that g_s drops rapidly to $g_{s,min}$ over a small range of values of θ during the onset of drought conditions. The dependence upon proxy variable D is, however, far weaker.

The particular form given in Figure 7a indicates that the (effective) dependence upon θ and D is fairly uncoupled (except for a slight variation appearing within the 0.006 contour, and that at high soil moisture values, there appears to be almost no response of changes in D). This is similar in concept to the independence of functions $f_1(\theta)$ and $f_2(D)$ in Equation (10). Since $0 \leq \exp(c_{ABA}\beta \exp(\delta\Psi_{leaf})) \leq$, then parameter α (in Equation (5) may be regarded as equivalent to $\gamma f_3(T) f_4(T)$ where there is little temperature or light stress. A visual inspection of the contour plot within Figure 7 suggests that, at least in the regions of high dependency upon θ, that this would correlate to the approximate values of $\theta_c = 0.28$, $\theta_w = 0.15$ and $a_1 = 7.0$ kg^{-1} kg within Equations (11) and (12).

A further check is required. The model of Jarvis (1976) assumes an independence of responses to all climatic conditions. For this to be analagous to Equation (5) requires that the implicit form of the dependence upon θ and D is independent of the α. This would allow for the possibility that α can incorporate the effects of temperature and light stress. In Figure 1b, α is decreased to just one quarter of its value given in Section 2.2.1. It may be observed that although some slight differences do exist between the structures of Figures 1a and 1b, they do retain similarities, suggesting that the values of θ_c, θ_w and a_1 are fairly robust in the intercomparison with the work of the Jarvis (1976) and Stewart (1988).

In summary, it may be concluded that the model outlined within Section 2.2.1 is comparable to the more established descriptions of stomatal response given by Jarvis (1976) and Stewart (1988), and that to a quite high degree, Equation (5) may be rewritten as $g_s = g_{s,min} + \alpha(T, I) f_1(\theta) f_2(D)$.

3.2 Comparison with the work of Monteith (1995)

Monteith (1995) reconsidered the supposed dependence of stomatal conductance upon specific humidity deficit, and re-interpreted the response to this microclimatic

variable as a dependence upon the rate of transpiration (or water flux) itself. The suggestion is that with no light or temperature stress, then

$$g_s = g_{s,min} + g_{max}\left[1 - \frac{J_w}{J_{w,max}}\right] \tag{13}$$

for an assumed maximum conductance g_{max} (m s^{-1}) and maximum water flux $J_{w,max}$ (mg m^{-2} s^{-1}). Variable $J_{w,max}$ is considered to be a function of the soil moisture content θ, and such that in drought conditions, $J_{w,max}$ will decrease. Monteith (1995) assumes that $g_{s,min} = 0.0$

It is remarked in Section 2.3 that the Tardieu and Davies (1993) equations may be written as $g_s = g_s(D,\theta)$. The water flux J_w is calculated as a diagnostic from Equation (8), that is $J_w = J_w(g_s, D)$. Hence with two equations for four unknowns (J_w, g_s, D, θ), then the specification of two should yield the other two variables. This means that the model described throughout Section 2.2 can be rewritten as $g_s = g_s(J_w, \theta)$, which is the hypothesis of Monteith (1995). This is presented in Figure 2, whereby each curve corresponds to different values of $0.1 \leq \theta \leq 0.3$,increasing in jumps of 0.01. The implicit values of specific humidity deficit satisfy $0.003 \leq D \leq 0.015$, and so the curves within Figure 2 correspond to "vertical slices" in Figure 1. Quantitatively, the curves are similar to those predicted by Equation (13). They exhibit a decrease in g_s for increasing values of J_w, and with extrapolation of the curves to $g_s = g_{s,min}$ indicates that $J_{w,max}$ is a decreasing function of soil moisture content. However, the main gradients in g_s responding to water flux J_w only occur within the regions where g_s is sensitive to soil moisture content (that is $0.18 \leq \theta \leq 0.22$). Nevertheless, the model of Tardieu and Davies (1993), combined the a big leaf model of surface energy partitioning and the Clapp and Hornberger (1978) relations for soil parameterisation do reveal a structure similar to Equation (13). This is further evidence that the hereto assumed dependence of stomatal conductance upon surface humidity deficit may in fact be a direct response to the water flux.

3.3 Linkage to the model of Ball *et al.* (1987) and Leuning (1995)

Based upon the work of Ball *et al.* (1987), Leuning (1995) propose a model for stomatal conductance with an explicit dependence on net assimilation, a_n (mol CO_2 m^{-2} s^{-1}). This is given by

$$g_s = g_{min} + \frac{\nu a_n}{(c_a - c_*)\left(1 + \frac{D}{D_0}\right)} \tag{14}$$

where ν and D_0 (kg kg^{-1}) are parameters, c_a (mol CO_2 m^{-3}) is atmospheric CO_2 concentration and variable c_* (mol CO_2 m^{-3}) is the CO_2 compensation point. This model has been tested extensively against FIFE data, and incorporated within the latest GCMs (eg Cox *et al.*, 1998). Net photosynthesis contains a dependence

upon surface temperature, T, incoming solar radiation, I and intercellular CO_2 concentration, c_i (mol CO_2 m^{-3}). The latter is calculated from the flux gradient across the stomata thus:

$$a_n = \frac{g_s}{1.6}(c_a - c_i). \tag{15}$$

A well established model of photosynthesis are those given by Collatz *et al.*, 1991 and Collatz *et al.*, 1992. These exhibit a peak in temperature response and saturate in incoming solar (PAR?) radiation. It is noted that the functional forms of the responses to T and I (see Cox *et al.*, 1998) are similar to those proposed by Jarvis (1976) within $f_3(T)$ and $f_4(I)$ of Eqn (10).

In Cox *et al.*,, there is a discussion of how a soil water dependence may enter within the Leuning (1995) model given by (14), given the observation that a_n itself appears to be very sensitive to θ. Two mechanisms are proposed. These are either that net photosynthesis itself is directly dependent upon θ (see Equation (29) of Cox *et al.*, 1998), or that g_s decreases for water stress, which in turn decreases c_i (through Equation (15) thereby reducing a_n. The latter possibility was rejected due to the relative insensitivity of a_n to c_i, and as such changes within g_s would only weakly affect photosynthetic activity. However, the model of Tardieu and Davies (1993), as presented within the framework above, show (Figure 1) a vary strong dependence upon θ within certain regions. This effect is sufficient to influence c_i, and so the second (direct water control of g_s) may in fact be valid on the basis of this model for stomatal opening.

4 A new formulation for stomatal control

It is noted that the Leuning model contains a dependence upon D that is similar to that of Jarvis (1976). Combining this information with the discussion of soil dependence above, then it is possible to see an equivalence between the hydrological aspects of Equation (14) and the full model given in Equations (1) to (9). That is, it may be appropriate to replace $\nu(1+D/D_0)^{-1}$ with the full (normalised) Tardieu and Davies (1993) model, which (from (7)) is a dependence upon J_w and θ. The temperature, light and intercellular CO_2 concentrations that may impact upon stomatal opening come in through a_n (effectively adjusting α within Equation (5). It is therefore possible to make the unifying hypothesis that the models may be combined to give a single description that is dependent upon both carbon and water fluxes. That is:

$$\begin{aligned} g_s &= g_{s,min} + \left(\frac{\kappa}{c_a - c_*}\right) e^{c_{ABA}\beta e^{\delta\Psi_{leaf}}} a_n \\ &\equiv g_s(J_w, a_n; \theta, c_a) \end{aligned} \tag{16}$$

for some constant κ.

To do - plot out the functional forms for this model.

5 Discussion and conclusions

This is a theorectical study that has shown the equivalence of a family of "closures" for stomatal control. The undoubted success of many of these descriptions against data also validates the new equivalent descriptions in the absence of any particular preference on the absolute dependencies. Models such as Ball *et al.* (1987), which contain an explicit dependence upon net photosynthetic activity, a_n, have been adopted by the modelling community. Other researchers, most notably Monteith (1995), argue the case for a direct dependence upon water flux, J_w. Tardieu and Davies (1993) provide evidence that stomata respond directly to hydrological status of the vegetation, and ABA concentration, itself a function of J_w. In this study, most features of all these representations have been shown to contain striking similarities. This therefore raises the possibility that the majority of responses to local climate observed by stomatal control are in fact dependencies upon the fluxes themselves. In this paper, a new formalism is presented that describes stomatal opening as a function of both net assimilation, a_n and water flux, J_w, and with the only explicit dependence upon microclimate occurring as a response to atmospheric CO_2 concentration, c_a and soil moisture content, θ. Both c_a and θ are slowly varying whereas the faster (diurnal) timescales of response to local conditions can all be incorporated within a dependence upon the fluxes themselves. The new formulation $g_s = g_s(J_w, a_n; \theta, c_a)$ as a new description for stomatal conductance has potentially important implications for the ease of incorporation within climate models. It is also noted that the work of Farquhar (19xx) suggests that the entire responsive form for stomatal conductance is to allow an optimisation of carbon uptake for a given water usage. The proposed structure given by Equation (17) may allow significant new insights into this hypothesis.

6 Acknowledgement

The authors thank the CEH Integrating Fund for providing financial assistance to undertake this study.

7 References

Ball, J.T., Woodrow, I.E. and Berry, J.A.: 1987. 'A model predicting stomatal conductance and its contribution to the control of photosynthesis under different environmental conditions', in: 'Progress in photosynthesis research (ed. I. Biggins)', *Martinun Nijhoff Publishers, Netherlands*, 221-224.

Clapp, R. and Hornberger, G.: 1978. 'Emperical equations for some soil hydraulic properties', *Water Resources Res.*, **14**, 601-604.

Collatz, G.J., Ball, J.T., Grivet, C. and Berry, J.A.: 1991. Physiological and environmental regulation of stomatal conductance, photosynthesis and transpiration:

a model that includes a laminar boundary-layer. Agr. For. Met., **54**, 107-136.

Collatz, G.J., Ribas-Carbo, M. and Berry, J.A., 1992. Coupled photosynthesis-stomatal conductance model for leaves of C_4 plants. Aust. J. Plant Physiol., **19**, 519-538.

Cox, P.M., Betts, R.A., Bunton, C., Essery, R.L.H., Rowntree, P.R. and Smith, J.: 1999, The impact of new land surface physics on the GCM simulation of climate and climate sensitivity, J. Climate **15**, 183-203.

Cox, P.M., Huntingford, C. and Harding, R.J., 1998b. A canopy conductance and photosynthesis model for use in a GCM land surface scheme. J. Hydrol., **213**, 79-94.

Garratt, J.R.: 1993. Sensitivity of climate simulations to land-surface and atmospheric boundary-layer treatments - a review. J. Climate, **6**, 419-449.

Huntingford, C. and Cox, P.M.: 1997. Use of statistical and neural network techniques to detect how stomatal conductance responds to changes in the local environment. *Ecol. Mod.*, **97**, 217-246.

Huntingford, C. and Monteith, J.L.: 1998, 'The behaviour of a mixed-layer model of the convective boundary layer coupled to a big leaf model of surface energy partitioning', *Bounday-layer Meteorol.*, **88**, 87-101.
Jacobs, C.: 1994. Direct impact of atmospheric CO_2 enrichment on regional transpiration'. PhD Thesis, Wageningen Agricultural University.

Jacobs, C.M.J. and DeBruin, H.A.R.: 1992, 'The sensitivity of regional transpiration to land-surface characteristics: significance of feedback', *J. Climate*, **5**, 693-698.

Jarvis, P.G.: 1976. The interpretation of the variations of leaf water potential and stomatal conductance found in canopies in the field. *Phil. Trans. R. Soc. Lond. B*, **273**, 593-610.

Khalil A.A.M. and Grace, J.: 1993. Does xylem sap ABA control stomatal behaviour of water-stressed sycamore (Acer psuedoplatanus L.) seedlings? *J. Exp. Bot.* **44**, 1127-1134.

Leuning, R., 1995. A critical appraisal of a combined stomatal-photosynthesis model for C3 plants. *Plant, Cell and Enviro.* **18**, 357-364.

Monteith, J.L.: 1981, 'Evaporation and surface temperature', *Quart. J. Roy.*

Meteorol. Soc. **107**, 1-27.

Monteith, J.L.: 1995, 'A reinterpretation of stomatal responses to humidity', *Plant, Cell and Environ.* **18**, 339-355.

Raupach, M.R.: 1998, 'Influences of local feedbacks on land-air exchanges of energy and carbon', *Global Change Biology*, Submitted.

Schulze, E.D., Kelliher, F.M., Korner, C. and Lloyd, J., 1994. Relationships among maximum stomatal conductance, ecosystem surface conductance, carbon assimilation rate and plant nitrogen nutrition: a global ecology scaling exercise. *Ann. rev. of ecol. systems*, **25**, 629-660.

Shuttleworth, W.J., Gash, J.H.C., Lloyd, C.R., McNeil, D.D., Moore, C.J. and Wallace, J.S., 1988. An integrated micrometeorological system for evaporation measurements. Agri. For, Met., **43**, 295-317.

Stewart, J.B., 1988. Modelling surface conductance of a pine forest., Agri. For. Met.. **43**, 19-35.

Tardieu, F.: 1993, 'Will increases in our undertanding of soil-root relations and root signalling substantially alter water flux models?' *Phil. Trans. R. Soc. Lond.* **B, 341**, 57-66.

Tardieu, F. and Davies, W.J.: 1993, Integration of hydraulic and chemical signalling in the control of stomatal conductance and water status of droughted plants, *Plant, Cell and Environ.* **16**, 341-349.

Tardieu, F., Zhang, J. and Davies, W.J., 1992. What information is conveyed by an ABA signal from maize roots in drying field soil? *Plant Cell Environ.* **15**, 185-191.

Tardieu, F., Zhang, J. and Gowing, D.J.G.: 1993, 'Stomatal control by both [ABA] in the xylem sap and leaf water status: a test of a model for droughted or ABA-fed field-grown maize', *Plant, Cell and Environ.* **16**, 413-420.

Tardieu, F. and Simonneau, T.: 1998, 'Variability among species of stomatal control under fluctuating soil water status and evaporative demand: modelling isohydric and anisohydric behaviours', *J. Expt. Botany* **49**, 419-432.

Zhang, J. and Davies, W.J., 1989. Abscisic acid produced in dehydrating roots may enable the plant to measure the water status of the soil. *Plant Cell Environ.* **12**, 73-81.

Zhang, J. and Davies, W.J., 1990. Changes in the concentration of ABA in xylem sap as a function of changing soil water status can account for changes in leaf

conductance and growth. *Plant Cell Environ.* **13**, 277-285.

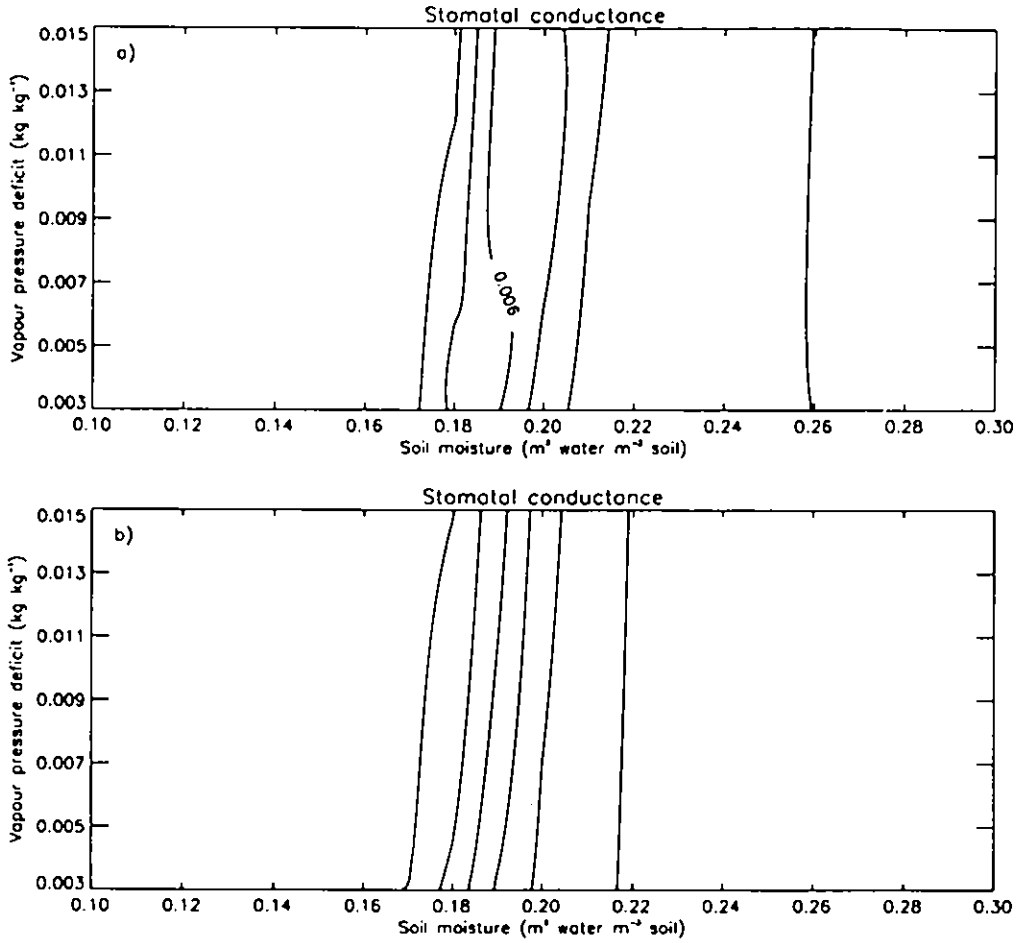

Figure 1. Predictions of stomatal conductance, following the model of Tardieu and Davies (1993), as a function of soil moisture content and specific humidity deficit. Plot a) is for $\alpha = 0.0112$ ms^{-1} and plot b) for the light or temperature stressed case with $\alpha = 0.00279$ ms^{-1}.

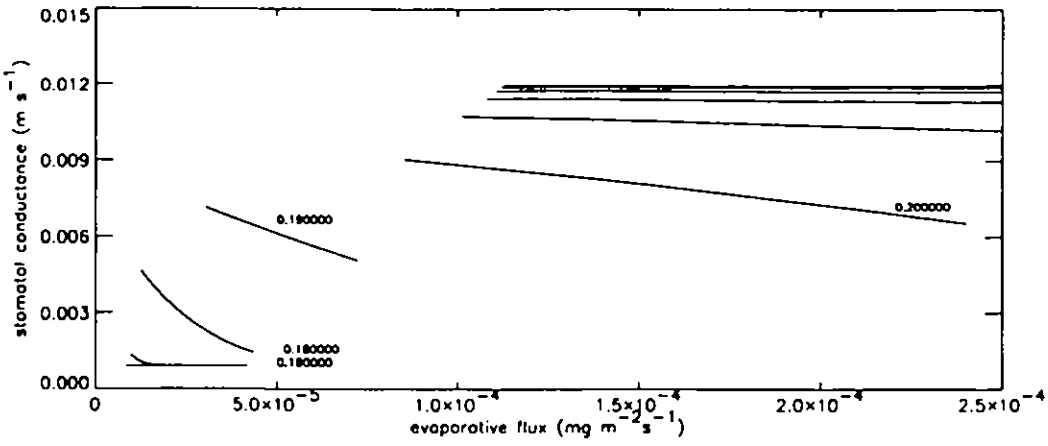

Figure 2. Predictions of stomatal conductance as a function of water flux, J_w. The individual plots are for diferent soil moisture concentrations, θ. Multiplication of the water flux by 10^6 gives the evaporative flux in units of W m^{-2}.

Dual versus single source models for estimating surface temperature of African savannah.

Huntingford, C.

Verhoef, A.

Stewart, J.

ACCEPTED, SUBJECT TO MINOR REVISION
"AGRICULTURE & FOREST METEOROLOGY"

Dual versus single source models for estimating surface temperature of African savannah.

Chris Huntingford[1], Anne Verhoef[1] and John Stewart[2]

1 Institute of Hydrology, Wallingford, OX10 8BB, UK

2 Department of Geography, Southampton University, SO17 1BJ, UK

Abstract

Predictions of average surface temperature of a sparsely vegetated West-African savannah by both single and dual source models of surface energy partitioning are compared. Within the single source model, the "excess resistance" to heat transfer away from the canopy (compared to momentum absorption) is characterised by parameter kB^{-1}, where k is the von Kármán constant and B is the Stanton number. Two values of this parameter are used; first $kB^{-1} = 2$ (a value often used within surface energy balance models but primarily applicable to permeable vegetation types) and then 12.4 (a value applicable to the savannah in question, which consists more of bluff roughness elements). As expected, the latter parameterisation generates better predictions of surface temperature.

To make accurate predictions of surface temperature using a dual source model, then an increase must be made to that model's in-canopy aerodynamic resistance. Information on this increase is found through direct model intercomparison with the single source model parameterised with $kB^{-1} = 12.4$.

Keywords: Penman-Monteith equation, Surface temperature, Canopy resistance, Savannah, Dual-Source model.

1. Introduction

The reliability of numerical weather models to predict climate change depends critically on the correct modeling of the surface vegetation atmosphere interaction. Surface temperature is a sensitive diagnostic of the success of land surface energy partitioning modes, since the surface temperature indicates how the modelled energy fluxes have been adjusted to the given conditions. So comparisons of the predictions of surface temperature by surface-atmosphere transfer models against measurements is a very stringent test of the models.

There are a number of types of surface vegetation-atmosphere transfer models. For homogeneous land cover, a single source (Big Leaf) model (Monteith, 1965) is suitable. To represent more complex canopies, dual source models with an explicit upper canopy and an understorey composed of, for example, distinct plant types and bare soil have been developed (Shuttleworth and Wallace, 1985; Dolman, 1993; Huntingford *et al.*, 1995). Recently, the dual source approach has evolved to a multi-component approach (Verhoef and Allen, 1998).

Dual source models have two sets of aerodynamic resistances across which individual, local, single source models are applied and an in-canopy point where such resistances meet, allowing interaction between the soil/vegetation components. A single aerodynamic resistance connects the combined canopy with the free atmosphere. A single source model uses only one aerodynamic resistance and assumes that all the surfaces are at an identical temperature and humidity.

For complex vegetation communities a dual source model with its extra physical realism should replicate the overall surface energy balance with greater accuracy than a single source model. However, in spite of the over simplification of reality intrinsic to a single source model, many authors have found, after appropriate tuning of the model parameters, that it satisfactorily describes the surface energy balance of the complex vegetation (REFS). Analogous parameters exist within the dual source model and these also require calibration. A failure to do this could result in a simple but correctly calibrated single source model performing better than an ill-parameterised dual source model - this issue has been raised by Kustas (1990).

The comprehensive data set available from the HAPEX-Sahel project provides an opportunity to assess the relative merits of single and dual source models for estimating the surface vegetation atmosphere exchange for a spatially complex vegetation community - savannah consisting of shrubs (20%) with an understorey of sparse grasses and forbs.

The aim of this paper is to assess whether the greater physical realism of a dual source model for savannah vegetation provides improved estimates of the mean surface temperature and hence of the fluxes. Initially both models were run using the best estimates from the literature of their parameters for "general" vegetation and the estimates of the mean surface temperature compared. Then the parameters of the models were individually changed to be appropriate for this particular location, before again comparing their outputs.

2. Theory

2.1. The single source model

The single source model (Monteith, 1965) is driven by values of windspeed, temperature and humidity at a reference height, and a prescribed available energy (net radiation minus soil heat flux), A. The model contains an aerodynamic resistance to momentum, r_a (sm^{-1}), and to heat transfer, r_{ah} (sm^{-1}). The difference between these two resistances satisfies

$$\frac{B^{-1}}{u^*} = r_{ah} - r_a \qquad (1)$$

where B is a nondimensional parameter (Stanton number) and u^* ($s\ m^{-1}$) is the friction velocity. For historical reasons, the difference is described by parameter kB^{-1} where k is the Von Kármán constant. For permeable rough surfaces such as grasses, Brutsaert (1982) and Garratt (1992) suggest $kB^{-1} \approx 2$. However, bluff rough surfaces such as the relatively rigid shrubs and bushes found in the Sahelian savannah have larger values of kB^{-1}; between 10 and 15 (see Garratt and Hicks, 1973; Stewart *et al.* 1994, Verhoef *et al.*, 1997).

2.2. *The dual source model*

The dual source model is based upon the aerodynamic resistance structure of Dolman (1993) and Huntingford *et al.* (1995), whereby such resistances influence the transfer of heat both within the canopy, and up into the atmosphere. Here the vegetation types are indexed (by i) as "1" for the canopy and "2" for the understorey. The canopy and understorey have heights h_i (m), stomatal resistances r_{ST_i} ($s\ m^{-1}$), local leaf area indices L_i and the vegetation is assumed to be clumped at heights $d_i + z_{0m_i}$ (m) where

$d_i = 0.75\ h_i$ (m) and $z_{0m_i} = 0.1\ h_i$ (m). Vegetation "1" has a fractional coverage α of the ground, and vegetation "2" a fractional coverage of 1-α. The in-canopy resistance, r_{au} (s m^{-1}), plus resistance from canopy to reference height and the boundary-layer resistances follow Eqns (15), (16) and (17) of Huntingford *et al.* (1995). Both vegetation surfaces receive an available energy, A_i.

2.3. Linkages between the single and dual source models

Predictions of surface temperature for the single source model, T_{SS} (°C) and the spatially averaged surface temperature of the dual source model T_{TS} (°C) are compared, where

$$T_{TS} = \alpha T_1 + (1-\alpha) T_2 \qquad (2)$$

and T_i are individual surface temperatures as calculated by the dual source model. For the single source model, an available energy $A = \alpha A_1 + (1-\alpha) A_2$ and stomatal resistance $r_{ST} = \alpha r_{ST_1} / LAI_1 + (1-\alpha) r_{ST_2} / LAI_2$ are prescribed (see McNaughton, 1994, for example, for alternative aggregation schemes of stomatal resistance).

For the dual source model, variations within boundary-layer resistances and in-canopy aerodynamic resistance, r_{au} can perform a similar role to adjusting kB^{-1} within the single source model. However, the (thin laminar) boundary-layer resistances close to the leaves are well defined (see for example Jones, 1983). Variations to modelling heat transfer (and associated surface temperatures) within the dual source model are therefore placed within the less understood in-canopy aerodynamic resistance. Resistance r_{au} (Huntingford *et al.*, 1995) is replaced by fr_{au} whereby f may be adjusted.

3. The experimental data

The data used to calculate values of the effective model parameters were made by the Department of Meteorology, Wageningen Agricultural University, The Netherlands as part of the HAPEX-Sahel experiment (Goutorbe *et al.*, 1994). The experimental location was at 13°32'N, 02°60'E which is within the Central West Supersite (Kabat *et al.*, 1996 and Gash *et al.*, 1997). The savannah consisted of 2-2.5 m high shrubs (*Guiera senegalensis*), with an undergrowth of sparse grasses and forbs. The shrubs covered about 20% of the ground area (hence $\alpha = 0.2$).

The data are from the period 16 September (Day 260) to 9 October, 1992 (Day 283). This corresponds to the start of the dry season, and the last rainfall (0.5 mm) was observed on 20 September.

Windspeed, temperature and humidity were measured at a height of 4.5m using an anemometer and a psychrometer, respectively. For details of the day to day variation of the microclimate, see Verhoef *et al.* (1996b). Values for A_i were obtained from the difference between net radiation, R_{ni} (W m^{-2}) (obtained from two Funk radiometers, installed at a height of 10.2 and 1.6 m) and soil heat flux, G_i, (i = 1,2) (W m^{-2}) for both surface components. Here, G_1 is the average of nine thermopile flux plates that were installed under a shrub at an average depth of 40 mm. Soil temperature measurements were used to correct G_1 for the heat storage in the soil layer overlying the plates. G_2 was found from the Calorimetric method using a soil temperature profile, measured with horizontally inserted PT-100 resistance thermometers and corresponding estimates of soil heat capacity (see Verhoef *et al.*, 1996a).

The stomatal resistances are parameterised using Jarvis-Stewart type of equations (Jarvis, 1976, Stewart, 1988), where r_{ST} is dependent on environmental variables. The parameters for r_{ST_1} were derived from porometry (by Verhoef, 1995) which then allowed the parameters for the calculation of r_{ST_2} to be derived from inversion of the dual source model (Huntingford *et al.*, 1995) for known surface evaporative fluxes (by Verhoef, 1995). While r_{ST_1} represents the stomatal resistance of bushes, r_{ST_2} is meant to give an average surface resistance value of the total understorey, that is a combination of grasses, forbs and bare soil.

The effective displacement and roughness length for the total surface were obtained from wind profile measurements as described by Verhoef (1995), giving the values z_{0m} = 0.25 m and d = 1.14 m. Estimates of L_1 and L_2 were taken from Hanan *et al.* (1997).

For model verification, values of the canopy and understorey surface temperatures were obtained using two infra-red thermometers, IRTs (Heimann KT15, Wiesbaden, Germany), with a field of view of 15 °, following the procedure described below (see also Verhoef *et al.* (1997). For continuous measurement of surface temperature two fixed IRTs were used. One at a height of 1.60 m which was vertically oriented above the grass/soil surface between the shrubs. The other, with a horizontal inclination, was trained on the north-facing side of a bush. Furthermore, surface temperature has been measured by using a manually tended IR sensor (Comet 8000, Mawi-therm, Monheim, Germany).

The fixed IRT representing the understorey appeared to overestimate the surface temperature because of its vertical installation (90 °), causing the instrument to 'see' between the upright blades of grass (see also Malhi 1993). The readings for the total

understorey, as recorded with the fixed IRT, were found to be very close to the surface temperatures of the bare patches of soil, whereas the values of T measured for the herb/grass layer (from a horizontal angle) were close to the bush temperatures. The hand-held instrument, operated at an angle of 45 °, indicated that understorey temperatures should roughly be between the values measured for bare soil and the herb layer. Therefore, continuously measured surface temperatures were corrected with the help of the readings recorded with the hand-held Comet using a linear relationship developed by Verhoef (1995). Finally, the average surface temperature, was found using the relative coverage of both surface components: $T = 0.2T_1 + 0.8T_2$.

Applying the condition that incoming solar radiation is positive, 411 data values are available.

4. Results of model intercomparison

Three intercomparisons are made between the single and dual source models (Case 1 - Case 3). In each intercomparison, the two models are driven by the single control data point presented in Table I. These data are time-averages of the 411 half-hourly data points, along with relevant vegetation parameters. This provides a first indication of model differences. Then the models are driven by the full set of savannah driving data, and with the diurnally varying stomatal resistances r_{ST_i} (see Section 3).

Case 1 sets $kB^{-1} = 2.0$ within the single source model. The difference between model predictions of surface temperature T_{ss} and T_{rs} for this control data point is small (Table II), suggesting that the dual source in-canopy aerodynamic resistance with $f = 1.0$ is similar to setting $kB^{-1} = 2$ within the single source model. With these

values of kB^{-1} and f, the single source (Figure 1a, closed circles) and dual source (Figure 1b, closed circles) model predictions of surface temperature are compared against the half-hourly diurnally varying savannah measurements. In both cases, there is little scatter, and so each model is responding in a similar fashion to the driving data. However, there is a systematic under estimation of surface temperature, suggesting that both kB^{-1} and f are incorrect.

Case 2 is identical to Case 1 except that now kB^{-1} = 12.4. This particular value was found empirically using simultaneous measurements of surface temperature and sensible heat flux for the savannah site by Verhoef *et al.*, 1997, and is towards the top of values found for a family of semiarid rangeland sites (Stewart et al., 1994). From Figure 1a (open circles), it is seen that this change results in far better predictions of surface temperature by the single source model, with the points generally clustered about the 1:1 line.

Case 3 adjusts parameter f so as to allow a similar improvement in the prediction of mean surface temperature by the dual source model. This is achieved with f = 3.9 where this value is such that the dual source model makes an identical prediction of mean surface temperature, for the control driving data, as that of the single source model with kB^{-1} = 12.4 (see Table II). The new dual source model predictions of mean surface temperature, T_{rs} are compared against data in Figure 1b (open circles). There exists a small tendency to overestimate at high temperatures and underestimate at low temperatures (although, from visual inspection, this is less than for the single source model in Figure 1a). However, the systematic bias has been almost eliminated when compared to Case 1 and Case 2 (filled circles, Figure 1b).

Case 3 is considered to be a better parameterisation of the dual source model. Further evidence of this is the good performance, with f = 3.9, of the dual source

model's predictions of bush and understorey temperatures (see Figure 2a and Figure 2b). By definition, the single source model cannot differentiate between such temperatures, but the earlier understanding of savannah behaviour through the use of the single source model has allowed a transfer of parameterisations such as to improve the more complicated dual source model's output.

5. Discussion

This analysis shows that using either the single source or the dual source model with literature values appropriate to "average" vegetation gives poor results compared to the measured values of average surface temperature for the savannah site. In particular, the greater physical realism of the dual source model does not improve predictive ability. Work undertaken by others indicates that for the savannah, within the single source model, a parameter value of $kB^{-1} = 12.4$ is appropriate. This greatly improves the performance of the single source model, although there is some underestimation of the surface temperature at low values and overestimation at higher surface temperatures. Since surface temperature is a very stringent check on the accuracy of any surface energy partitioning model, this implies that the model, using the new parameterisation for kB^{-1} can be expected to provide reliable estimates of the fluxes of sensible and latent heat. This also shows that an incorrectly calibrated dual source model will make predictions that are worse than those of a properly tuned but simpler single source model.

The dual source model can also be adjusted for savannah by varying the in-canopy aerodynamic resistance until the average surface temperature simulated agrees with that predicted by the single source model, the latter with the revised kB^{-1} value. Now

the dual source model also performs well, giving the added benefit that temperatures of the two components of shrubs and understorey can be predicted explicitly. Comparison with measured surface temperatures of the individual components confirms that such predictions are accurate. The ability to differentiate between and model the different surface temperatures is of importance in designing agroforestry experiments, and may also influence surface-atmosphere exchanges of CO_2 (eg Huntingford *et al.*, 1998).

6. Conclusions

From this analysis it is concluded that the greater physical realism of the dual source model does no better at simulating the savannah surface temperature than the single source model when using parameters taken from the literature for "typical" vegetation – both models underestimate the surface temperature by about five degrees. However, as may be expected, the simulations of the single source model can be greatly improved by using literature values of the parameters appropriate to the savannah vegetation. Similar improvements can then be obtained using the dual source model following calibration against the better parameterised single source model. The advantage of the adjusted dual source model is that it can provide good simulations of the surface temperatures of the two components.

Many studies of the surface energy balance reported in the literature use the single source model. From this analysis, it has been demonstrated that parameterisations found in such studies have the potential to be reused to calibrate more complex and more physically representative surface schemes such as the dual source model.

Acknowledgements

Chris Huntingford has been funded by the Natural Environment Research Council's Centre for Ecology and Hydrology Integrating fund. Anne Verhoef has been funded by an EU fellowship (contract No: ENV4-CT95-5007). The comments of Simon Allen, Eleanor Blyth, Alistair Culf, John Gash and the two anonymous referees on early drafts of this work are gratefully acknowledged.

References

Brutsaert, W.H.: 1982. Evaporation into the atmosphere. D. Reidel, Norwell, Mass., 299 pp.

Dolman, A.J., 1993. A multiple-source land surface energy balance model for use in general circulation models. Agric. For. Meteorol. 65: 21-45.

Garratt, J.R., 1992. The atmospheric boundary layer. Cambridge University Press, Cambridge, 316pp.

Garratt, J.R. and Hicks, B.B., 1973. Momentum, heat and water vapour transfer to and from natural and artificial surfaces. Quart. J. R. Meteorol. Soc. 99: 680-687.

Gash, J.H.C., Kabat, P., Monteny, B.A., Amadou, M., Bessemoulin, P., Billing, H., Blyth, E.M., deBruin, H.A.R., Elbers, J.A., Friborg, T., Harrison, G., Holwill, C.J., Lloyd, C.R., Lhomme, J.-P., Moncrieff, J.B., Puech, D., Soegaard, H., Taupin, J.D., Tuzet, A. and Verhoef, A., 1997. The variability of evaporation during the HAPEX-Sahel intensive observation period. J. Hydrology 188-189: 385-399.

Goutorbe, J-P., Lebel., T., Tinga, A., Bessemoulin, P., Brouwer, J., Dolman, A.J., Engman, E.T., Gash, J.H.C., Hoepffner, M., Kabat, P., Kerr, Y.H., Monteny, B., Prince, S., Said, F., Sellers, P. and Wallace, J.S., 1994. HAPEX-Sahel: a large scale study of land atmosphere interactions in the semi-arid tropics. Annales Geophysicae 12: 53-64.

Hanan, N.P., Prince, S.D. Bégué, A. (1997) Modelling vegetation primary production during HAPEX-Sahel using production efficiency and canopy conductance model formulations. Journal of Hydrology 188-189, 651-675.

Huntingford, C., Allen, S.J. and Harding, R.J., 1995. An intercomparison of single and dual-source vegetation-atmosphere transfer models applied to transpiration from Sahelian savannah. Boundary-Layer Meteorol. 74: 397-418.

Huntingford, C., Hall, R.L. and Verhoef, A., 1998. An argument for the use of two-layer SVAT schemes to simulate terrestrial carbon dioxide fluxes. Hydrol. Earth System Sci. 2, 299-302.

Jarvis, P.G., 1976. The interpretation of variations in leaf water potential and stomatal conductance found in canopies in the field. Phil. Trans. Roy. Soc. London, Ser. B. 273: 593-610.

Jones, H.G., 1983. Plants and microclimate. Cambridge University Press, Cambridge, U.K. 323 pp.

Kabat, P., Prince, S.D. and Prihodko, L., (Editors), 1996. HAPEX-Sahel West Central Supersite: Methods, Measurements and Selected Results. Report 130, DLO Winard Staring Centre, Wageningen.

Kustas, W.P., 1990. Estimates of evapotranspiration within a one- and two-layer model of heat transfer over partial canopy cover. J. Appl. Meteorol. 29: 704-715.

Malhi, Y.S., 1993. Sensible heat flux from heterogeneous surfaces. PhD Thesis, University of Reading, 261pp.

McNaughton, K.G., 1994. Effective stomatal and boundary-layer resistances of heterogeneous surfaces. Plant Cell and Environ. 17: 1061-1068.

Moncrieff, J.B., Monteny, B., Verhoef, A., Friborg, Th., Elbers, J., Kabat, P., de Bruin, H., Soegaard, H., Jarvis, P.G., and Taupin, J.D., 1997. Spatial and temporal variations in net carbon flux during HAPEX-Sahel. J. Hydrol. 188-189: 563-588.

Monteith, J.L., 1965. Evaporation and environment. In G. E. Fogg, (ed.) The State and Movement of Water in Living Organisms, Sympos. Soc. Exper. Biol., Vol. 19, Academic Press, N.Y., pp. 205-234.

Paulson, C.A., 1970. Mathematical representation of wind speed and temperature profiles in the unstable atmospheric surface layer. J. Appl. Meteorol. 9: 857-861.

Shuttleworth, J.W. and Wallace, J.S., 1985. Evaporation from sparse crops - an energy combination theory. Quart. J. R. Meteorol. Soc. 111: 839-855.

Stewart, J.B, 1988. Modelling surface conductance of pine forest. Agric. For. Meteorol. 43: 19-35.

Stewart, J.B., Kustas, W.P., Humes, K.S., Nichols, W.D., Moran, M.S., De Bruin, H.A.R., 1994. Sensible heat flux-radiometric surface temperature relationship for eight semi-arid areas. J. Appl. Meteorol. 33: 1110-1117.

Verhoef, A., 1995. Surface energy balance of shrub vegetation in the Sahel. PhD-thesis, Dept. of Meteorology, WAU, Wageningen, the Netherlands, ISBN 90-5485-458-8, 247 pp.

Verhoef, A., Van den Hurk, B.J.J.M, Jacobs, A.F.M, and Heusinkveld, B.G., 1996a. Thermal soil properties for vineyard (EFEDA-I) and savanna (HAPEX-Sahel) sites. Agric. For. Meteorol. 78: 1-18.

Verhoef, A., Allen, S.J., De Bruin, H.A.R., Jacobs, C.M.J. and Heusinkveld, B.G., 1996b. Fluxes of carbon dioxide and water vapour from a Sahelian savanna. Agric. For. Meteorol. 80: 231-248.

Verhoef, A., De Bruin, H.A.R. and Van den Hurk, B.J.J.M., 1997. Some practical notes on the parameter kB^{-1} for sparse canopies. J. Appl. Meteorol. 36: 560-572.

Verhoef, A., Allen, S.J., 1998. The relative importance of surface and aerodynamic resistances in a multi-source energy-CO_2 model. Physics and Chemistry of the Earth 23: 459-463.

Tables

Table I.

Variable/Parameter		Mean Value	Standard Deviation
Reference height windspeed	u_r (m s^{-1})	2.4	(0.7)
Reference height temperature	T_r (C)	30.6	(3.4)
Reference height humidity	e_r (kPa)	2.3	(0.13)
Canopy available energy	A_1 (W m^{-2})	380	(218)
Understorey available energy	A_2 (W m^{-2})	250	(105)
Canopy height	h_1 (m)	2.3	
Understorey height	h_2 (m)	0.5	
Fractional cover	α	0.2	
Canopy leaf area index	L_1	1.5	
Understorey leaf area index	L_2	1.1	
Canopy stomatal resistance	r_{ST_1} (s m^{-1})	128	(53)
Understorey stomatal resistance	r_{ST_2} (s m^{-1})	386	(122)
Roughness length for momentum	z_{0m} (m)	0.25	
Displacement height	d (m)	1.14	

Table II

Case	Coefficient		Surface temperature (°C)	
	kB^{-1}	f	T_{SS}	T_{TS}
1	2.0	1.0	33.2	33.8
2	12.4	1.0	37.6	33.8
3	12.4	3.9	37.6	37.6

Table captions

Table I. The mean of daytime meteorological variables, measured half-hourly and at 411 separate times, over Sahelian savannah (standard deviations in brackets). Also presented are model parameters applicable to the savannah vegetation.

Table II. Values of parameters kB^{-1} (as required to evaluate the roughness length for heat within the single source model) and f (as used in the parameterisation of the in-

canopy resistance of the dual source model) relevant to three model intercomparisons (Case 1 - Case 3). Also presented are values of surface temperature for the single source model, T_{SS}, and spatially averaged surface temperature for the dual source model, T_{TS}, at the control environmental data point (see Table I). By definition there is equality for Case 3.

Figure captions

Figure 1. The relation between a) single source model predictions of surface temperature, T_{SS}, and savannah measurements and b) dual source model predictions of mean surface temperature, T_{TS}, and savannah measurements. In Figure 1a), the closed circles correspond to Case 1 (kB^{-1} = 2) and the open circles correspond to Case 2 and Case 3 (kB^{-1} = 12.4). In Figure 1b), the closed circles correspond to Case 1 and Case 2 (f = 1.0) and the open circles correspond to Case 3 (f = 3.9).

Figure 2. A plot of dual source model predictions (for Case 3) of a) the upper canopy temperature, T_1 and b) the understorey T_2 against measurements.

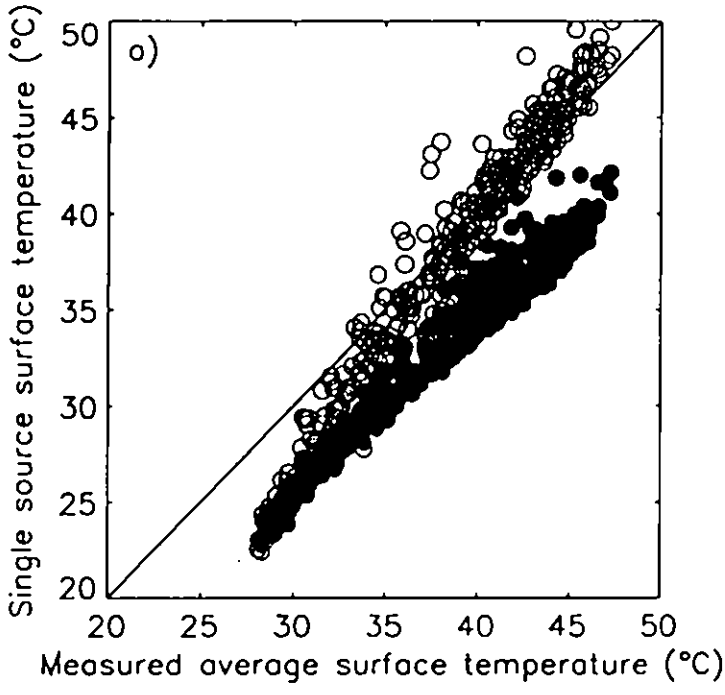
a)
Single source surface temperature (°C)
Measured average surface temperature (°C)
20
25
30
35
40
45
50

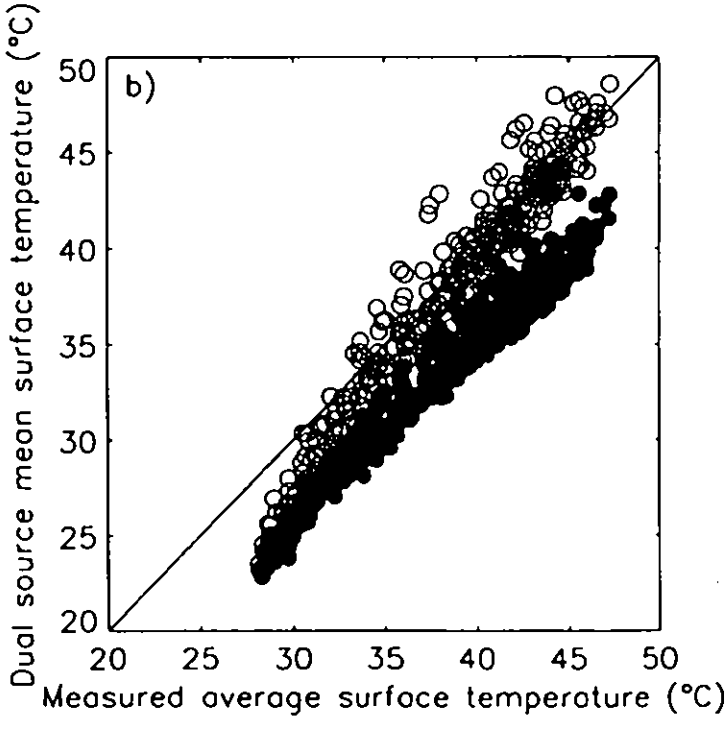
b)
Dual source mean surface temperature (°C)
Measured average surface temperature (°C)
20
25
30
35
40
45
50

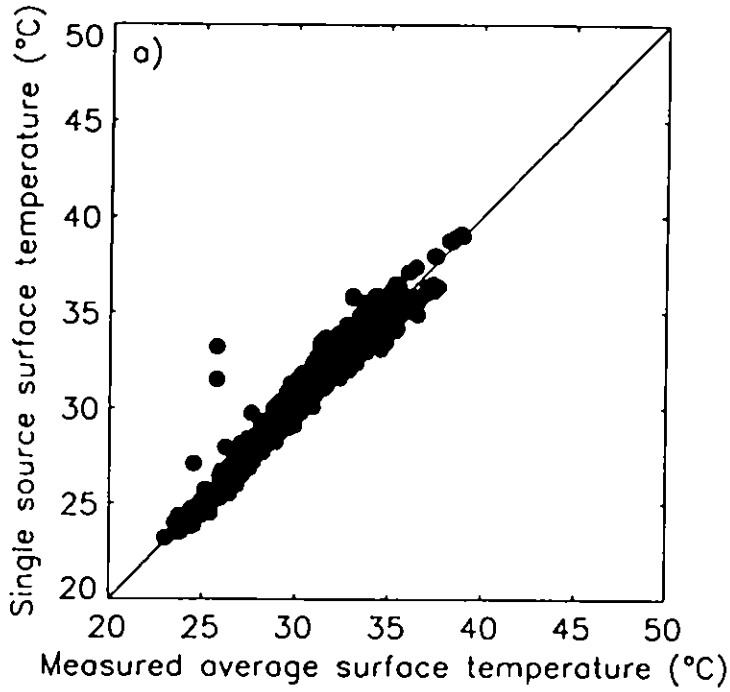
a)
Single source surface temperature (°C)
Measured average surface temperature (°C)
20
25
30
35
40
45
50

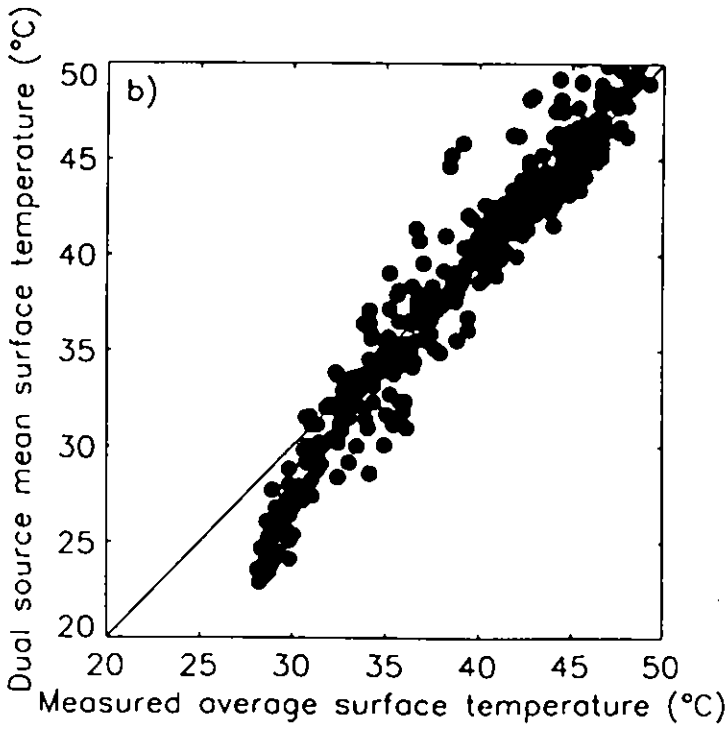
b)
Dual source mean surface temperature (°C)
Measured average surface temperature (°C)
20
25
30
35
40
45
50

The behaviour of a mixed-layer model of the convective boundary layer coupled to a big leaf model of surface energy partitioning.

Huntingford, C.

Monteith, J.L.

GALLEY PROOFS CHECKED
MAY '98

THE BEHAVIOUR OF A MIXED-LAYER MODEL OF THE CONVECTIVE BOUNDARY LAYER COUPLED TO A BIG LEAF MODEL OF SURFACE ENERGY PARTITIONING

C. HUNTINGFORD
Institute of Hydrology, Wallingford, OX10 8BB, U.K.

J. L. MONTEITH
Institute of Terrestrial Ecology, Penicuik, EH26 0QB, U.K.

(Received in final form, 17 March, 1998)

Abstract. Daily mean values of the Priestley-Taylor coefficient, $\bar{\alpha}$, are derived from a simple model of the daily growth of a convective boundary layer. For a particular control set of driving environmental variables, $\bar{\alpha}$ is related to the prescribed bulk surface resistance, r_S by $1/\bar{\alpha} = 1/\alpha_0 + mr_S$ for parameters α_0 and m. The dependence of the parameters α_0 and m on weather is explored and a potential use of this linear relation to provide information about regional values of r_S is indicated.

Keywords: Atmospheric boundary layer, Diurnal variability, Latent heat flux, Priestley-Taylor coefficient, Surface resistance

1. Introduction

In models of the convective boundary layer (CBL), the state of the underlying surface is dominated by specification of a bulk surface resistance, r_S, a quantity that plays a central role in the partitioning of energy between sensible and latent heat (Monteith, 1981). McNaughton and Spriggs (1989) used climate records from Cabauw in The Netherlands to drive a CBL model and obtained daily mean values of the nondimensional Priestley-Taylor coefficient, α (Priestley and Taylor, 1972). They found that $\bar{\alpha}$ was a sigmoidal function of the logarithm of r_S, assumed constant during the day. Using the same CBL model, it is demonstrated here that the reciprocal of $\bar{\alpha}$ increases almost linearly with r_S and the extent to which the constants of this regression depend on climate is explored.

2. The Governing Equations

The CBL model developed by McNaughton and Spriggs (1989) consists of (a) a uniform surface at the ground endowed with the properties of a vegetation canopy, (b) a "surface" layer, the height of which is identified as the Obukhov length, L and (c) a "fully-mixed" layer extending from height L to a capping inversion, above which a stable layer exists.

Boundary-Layer Meteorology **88**: 87–101, 1998.

2.1. THE CANOPY AND SURFACE LAYER

Canopy behaviour is described through the bulk surface resistance, r_S. If θ_c (K) and q_c (kg kg^{-1}) are, respectively, effective values at the vegetation surface of temperature and specific humidity, then the upward latent heat flux, λE (W m^{-2}), may be defined as

$$\lambda E = \frac{\lambda\rho\{q_{sat}(\theta_c) - q_c\}}{r_S} \tag{1}$$

where q_{sat} (kg kg^{-1}) is the temperature dependent saturated specific humidity, λ (J kg^{-1}) is the latent heat of vaporisation of water and ρ (kg m^{-3}) is the density of air at the surface. Energy closure is satisfied by

$$A = \lambda E + H \tag{2}$$

where A (W m^{-2}) is the available energy (net radiative flux minus downward soil heat flux) and H (W m^{-2}) is the upward sensible heat flux.

The surface layer is assumed to have height $|L|$ (for consistency with McNaughton and Spriggs, 1989), across which fluxes of momentum, vapour and heat are constant. This height is a somewhat arbitrary choice, but for most hours of the diurnal cycle is similar in size to heights proposed by other authors (for instance De Bruin and Jacobs (1989) and Garratt (1992) suggest one-tenth of the boundary-layer height, and Raupach (1998) suggests a fixed height of 50 m). The aerodynamic resistances to momentum, r_{am} (s m^{-1}), heat r_{ah} (s m^{-1}) and vapour r_{av} (s m^{-1}), across the surface layer are then defined by

$$r_{am} = \frac{\ln\left(\frac{|L|}{z_{0m}}\right) - \psi_1}{ku_*}, \tag{3}$$

$$r_{ah} = r_{av} = \frac{\ln\left(\frac{|L|}{z_{0m}}\right) + \ln\left(\frac{z_{0m}}{z_{0T}}\right) - \psi_2}{ku_*} \tag{4}$$

where $L = -\rho c_p u_*^3 \theta_c / \{kg(H + 0.07\lambda E)\}$. Here, $\psi_1 = 1.12$ and $\psi_2 = 1.88$ are stability corrections applied at $z = |L|$ (Paulson, 1970). It is assumed that $\ln(z_{0m}/z_{0T}) = 2$ (e.g. see Garratt, 1992) where z_{0m} (m) is the roughness length for momentum and z_{0T} (m) is the roughness length for both heat and vapour; $k = 0.41$ is the von Kármán constant, u_* (m s^{-1}) is the friction velocity, g (m s^{-2}) is the gravitational acceleration and c_p (J kg^{-1} K^{-1}) is the specific heat capacity of air. If, throughout the fully-mixed layer, u_m (m s^{-1}) is wind velocity, θ_m(K) potential temperature and q_m (kg kg^{-1}) is specific humidity, then these values provide boundary conditions at the top of the surface layer so that

$$u_*^2 = \frac{u_m}{r_{am}}, \tag{5}$$

$$\lambda E = \frac{\lambda\rho(q_c - q_m)}{r_{ah}}, \tag{6}$$

$$H = \frac{\rho c_p(\theta_c - \theta_m)}{r_{ah}}. \tag{7}$$

For specified values of u_m, θ_m, q_m and A, simultaneous solution to Equations (1) - (7) gives values of u_*, r_{am}, r_{ah}, canopy level states, θ_c, q_c and surface energy fluxes, λE and H. Elimination of variables means the latent heat flux may be written as

$$\lambda E = \frac{\epsilon A + \dfrac{\lambda\rho\,[q_{sat}(\theta_m) - q_m]}{r_{ah}}}{\epsilon + 1 + \dfrac{r_S}{r_{ah}}} \tag{8}$$

where ϵ is defined as

$$\epsilon = \frac{\lambda}{c_p}\frac{q_{sat}(\theta_c) - q_{sat}(\theta_m)}{\theta_c - \theta_m}. \tag{9}$$

If ϵ is linearised as $\epsilon \approx (\lambda/c_p)\mathrm{d}q_{sat}/\mathrm{d}\theta$, evaluated at $\theta = \theta_m$, then Equation (8) is formally identical to the Penman-Monteith combination equation (Monteith, 1981). However, such linearisation could produce significant errors if applied across the entire surface layer (McArthur, 1990). For this paper (as in McNaughton and Spriggs, 1989), the exact solution to Equations (1)–(7) is calculated.

2.2. THE FULLY-MIXED LAYER

In the absence of advection, the daily evolution of θ_m and q_m is determined by the behaviour of the evolving CBL, the surface fluxes λE and H, and the thermodynamic conditions within the stable layer above the inversion capping. The fully-mixed layer model (McNaughton and Spriggs, 1989) is based on budget equations (Tennekes, 1973 and McNaughton and Spriggs, 1986) for heat and vapour (assuming $L \ll h$), viz.

$$\rho c_p h\frac{\mathrm{d}\theta_m}{\mathrm{d}t} = H + \rho c_p\,[\theta_s(h) - \theta_m]\,\frac{\mathrm{d}h}{\mathrm{d}t}, \tag{10}$$

$$\lambda\rho h\frac{\mathrm{d}q_m}{\mathrm{d}t} = \lambda E + \rho\lambda\,[q_s(h) - q_m]\,\frac{\mathrm{d}h}{\mathrm{d}t}. \tag{11}$$

Here h (m) is the CBL height, and $\theta_s(h)$ (K) and $q_s(h)$ (kg kg^{-1}) are respectively the potential temperature and humidity within the stable layer directly above the inversion capping. A third equation is required to close the system. The rate of increase in height of the fully-mixed layer is assumed directly proportional to the

virtual heat flux and inversely proportional both to h and to the gradient of potential virtual temperature (McNaughton and Spriggs, 1989) so that

$$\frac{dh}{dt} = \frac{H + 0.07\lambda E}{\rho c_p h \dfrac{d\{\theta_s(1 + 0.61 q_s)\}}{dh}}. \tag{12}$$

Given stable layer profiles of $\theta_s(z)$ and $q_s(z)$ above the CBL, and fluxes of λE and H, the time dependent behaviour of θ_m, q_m and h may be calculated.

2.3. A NUMERICAL MODEL OF THE FULL CBL AND ASSOCIATED BOUNDARY CONDITIONS

The canopy, surface layer and fully-mixed layer are coupled. Fluxes of sensible and latent heat, evaluated within the canopy and surface layer, depend on the mixed-layer temperature and humidity. Simultaneously, the diurnal course of mixed-layer variables depends on the integrated behaviour of such surface energy fluxes. This paper explores a numerical model that combines all these components of the CBL.

Specified initial and driving boundary conditions are required. The diurnal course of available energy is assumed to be parabolic as

$$A = 4A_{max}\frac{t}{t_{day}}\left(1 - \frac{t}{t_{day}}\right)$$

where t (s) is time since sunrise, t_{day} (s) is day length and A_{max} (W m^{-2}) is the maximum available energy (at midday). Potential temperature and humidity within the stable layer are assumed to vary linearly with height, that is

$$\theta_s(z) = \theta_{s0} + \gamma_\theta z,$$

$$q_s(z) = q_{s0} + \gamma_q z,$$

where θ_{s0} (K), γ_θ (K m^{-1}), q_{s0} (kg kg^{-1}) and γ_q (kg kg^{-1} m^{-1}) are lapse rates that require specification.

To allow for the collapse of the nocturnal boundary layer and the development of convection, boundary conditions of h_0 (m), $\Delta\theta_0$ (K) and Δq_0 (kg kg^{-1}) are specified at $t = t_0 = 3600$ s after sunrise, when $h(t_0) = h_0$, $\theta_m(t_0) = \theta_s(h_0) - \Delta\theta_0$ and $q_m(t_0) = q_s(h_0) - \Delta q_0$. The mixed-layer windspeed, u_m, is specified and assumed constant both in height and time. The numerical model generates values of λE, θ_m, q_m and h_m as functions of time after sunrise.

TABLE I

A control set of driving conditions for the full CBL model

Variable	Units	Value
A_{max}	W m^{-2}	300
θ_{s0}	K	293.0
γ_θ	K m^{-1}	0.003
q_{s0}	kg kg^{-1}	0.01
γ_q	kg kg^{-1} m^{-1}	0.0
u_m	m s^{-1}	4.0
z_{0_m}	m	0.2
h_0	m	200
$\Delta\theta_0$	K	1.0
Δq_0	kg kg^{-1}	0.01
t_{day}	s	43200

2.4. DIAGNOSTICS

The Priestley-Taylor coefficient (Priestley and Taylor, 1972) can be expressed as

$$\alpha = \frac{\epsilon + 1}{\epsilon} \times \frac{\lambda E}{A}. \tag{13}$$

From Equation (8), Equation (13) may be written as

$$\alpha = \frac{1 + \dfrac{\lambda\rho\,\{q_{sat}(\theta_m) - q_m\}}{\epsilon r_a A}}{1 + \dfrac{r_s}{r_a(\epsilon + 1)}} \equiv \frac{1 + C}{1 + S} \tag{14}$$

where C and S are nondimensional and referred to here as the climate number and surface number respectively.

The Priestley-Taylor coefficient has often been reported as having only a small diurnal range for both open water and freely transpiring vegetation (see for instance Davies and Allen (1973), Bailey and Davies (1981) and Driedonks (1981)). Such conservatism gives significance to a mean diurnal value of this variable, $\bar{\alpha}$. A fully coupled model of the CBL allows investigation of the dependence of $\bar{\alpha}$ on r_S and any prescribed driving environmental conditions. Such a model could also allow comparison with the equilibrium approach, as presented by McNaughton and Jarvis (1983) and Culf (1994).

3. Numerical Results

3.1. A SINGLE MODEL RUN

The control set of driving conditions in Table I provides input for the CBL model and Figure 1 plots the daily evolution of the model diagnostics λE, θ_m, q_m, h_m, α, C and S with the bulk surface resistance set at $r_S = 100$ s m^{-1}. The Priestley-Taylor coefficient demonstrates a high degree of conservatism throughout much of the day, as identified and explored by De Bruin (1983). There is a period both at the very beginning and end of each day, whereby $H + 0.07\lambda E < 0$ (corresponding to $L > 0$) and so the virtual potential heat flux is downwards. For such stable atmospheric conditions, Equations (3) and (4) are not meaningful, and generate singularities. The beginning of such a response may be seen in the anomalous behaviour of variable C late in the day.

3.2. THE DEPENDENCE OF $\bar{\alpha}$ UPON BULK SURFACE RESISTANCE, r_S

The dependence of $\bar{\alpha}$, $\overline{C}$ and $\overline{S}$ on r_S is analysed for the conditions in Table I, where the averaging is performed for $0.2t_{day} \leq t \leq 0.8t_{day}$, that is the middle three-fifths of each day. The numerical code is run for twenty values of $r_S = 10, 20, \ldots, 200$ s m^{-1} (a range of surface resistance corresponding to well-watered to moderately stressed vegetation) and results are presented in Figure 2. The correlation between $1/\bar{\alpha}$ and r_S is nearly linear, so that $\bar{\alpha}$ and r_S may be related by

$$\frac{1}{\bar{\alpha}} = \frac{1}{\alpha_0} + mr_S. \tag{15}$$

A simple least squares regression, for the runs in Figure 2, gives $\alpha_0 = 1.391$, $m = 0.00326$ m s^{-1} and a correlation coefficient of $r = 0.998$.

Also plotted in Figure 2 is the behaviour of $\bar{\alpha}$ for far higher values of r_S. The sigmoidal dependence of $\bar{\alpha}$ upon $\log(r_S)$, as observed by McNaughton and Spriggs (1989), is now apparent. A linear relation between $1/\bar{\alpha}$ and r_S is again present, although this is not described well with the values of m and α_0 valid for $r_S \leq 200$ s m^{-1}. A linear fit for the wider range would be at the expense of accuracy at the more important low r_S values.

3.3. A CALIBRATION OF α_0 AND m AGAINST INDIVIDUAL DRIVING ENVIRONMENTAL CONDITIONS

The dependence of α_0 and m in Equation (15) upon the parameters listed in Table I is examined. Each parameter of Table I is varied individually and the numerical CBL model re-run for the range $10 \leq r_S \leq 200$ s m^{-1}. The "best fit" values of

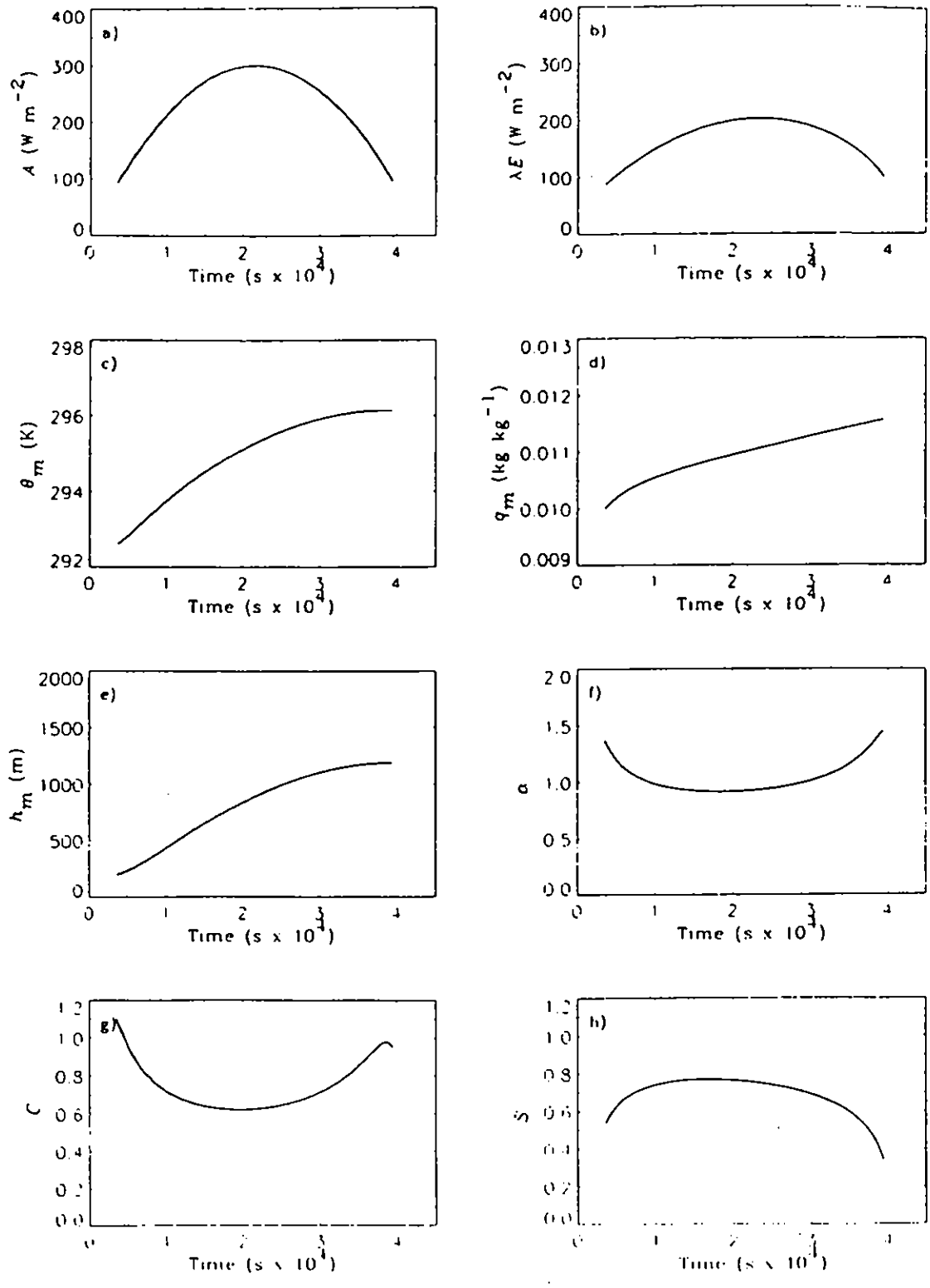

Figure 1. Results from a single run of the CBL model using driving environmental conditions described in Table I and with $r_S = 100$ s m^{-1}. Individual plots are of the prescribed diurnal variation of (a) available energy, A and calculated variations of (b) evaporative flux, λE, (c) fully-mixed layer temperature, θ_m, (d) fully-mixed layer humidity, q_m, (e) boundary-layer height, h_m, (f) Priestley-Taylor coefficient, α, (g) climate variable, C and (h) surface variable, S.

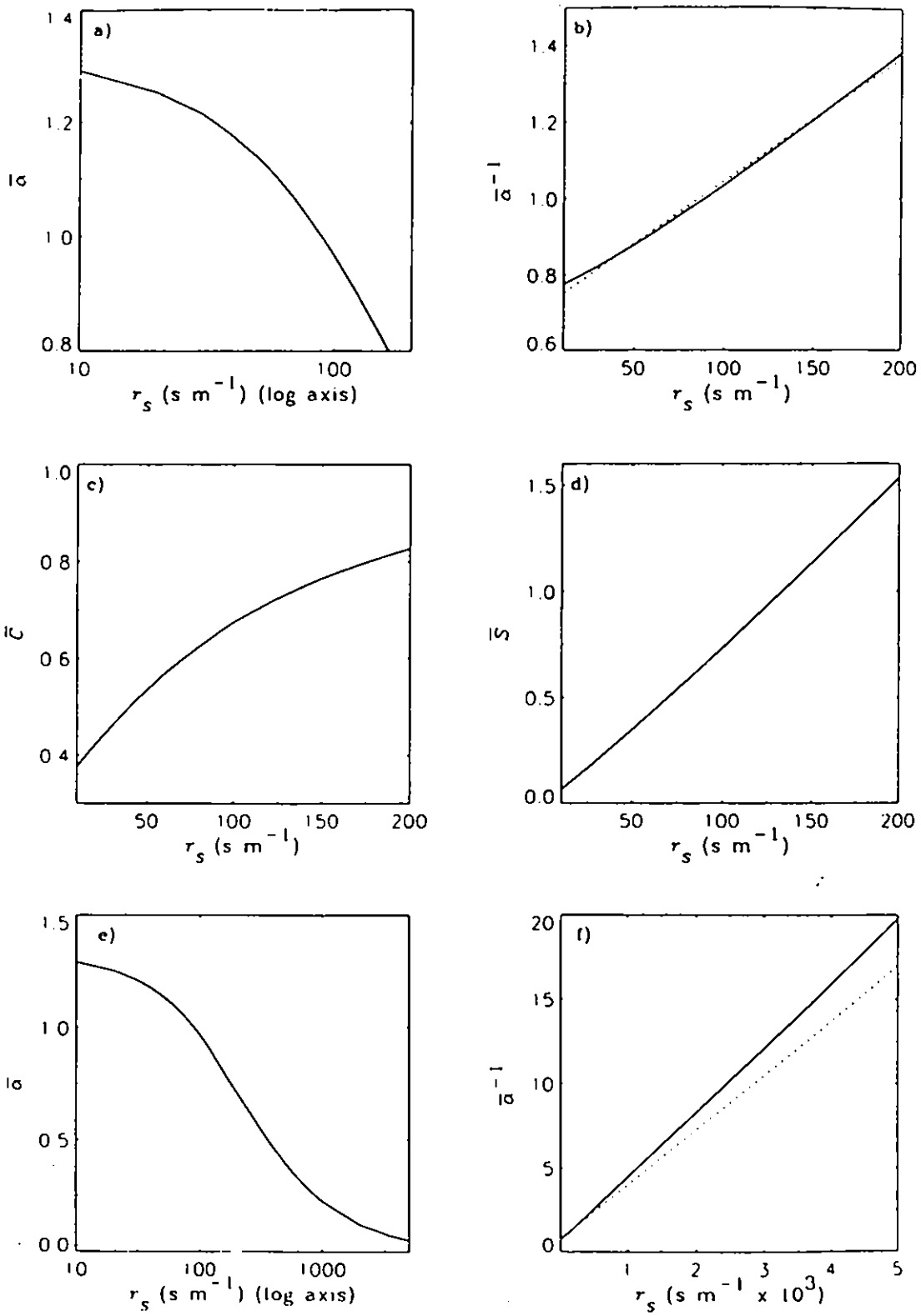

Figure 2. Results from multiple runs of the full CBL model using driving environmental conditions described in Table I and values of bulk surface resistances in the range $10 \leq r_S \leq 200$ s m^{-1}. Plots are of (a) $\tilde{\alpha}$ vs. r_S (logarithmic axes), (b) $1/\tilde{\alpha}$ vs. r_S, (c) $\overline{C}$ vs. r_S and (d) $\overline{S}$ vs. r_S. Also plotted are (e) $\tilde{\alpha}$ vs. r_S (logarithmic axes) and (f) $1/\tilde{\alpha}$ vs. r_S over an extended range of r_S, up to values of $r_S = 5000$ s m^{-1}. Also plotted (dotted line) in both (b) and (f) is $\tilde{\alpha}^{-1} = \alpha_0^{-1} + mr_S$ with $\alpha_0 = 1.391$ and $m = 0.00326$ m s^{-1} (see Section 3.2).

m and α_0 against r_S are calculated, and then plotted against the adjusted parameter (see Figure 3a and Figure 3b). In each example, the correlation coefficient r was nearly unity, indicating that the reduction of the canopy, surface layer, and fully-mixed layer description of the CBL to Equation (15) is robust. For the range prescribed to each parameter, there is relatively little variation in either α_0 or m, except for the dependence on θ_{s0} and q_{s0}. The dependence on initial conditions h_0, $\Delta\theta_0$ and Δq_0 are particularly weak. However, prescribed changes in individual parameters are not directly comparable, so it is unwise to order sensitivities.

Because of the relatively small sensitivity of α_0 and m to each parameter, regression coefficients associated with multiple changes in driving parameters may be predicted with acceptable accuracy by a linear imposition of the results in Figures 3a and 3b. As an example, with $A_{max} = 400$ W m^{-2}, $\theta_0 = 293$ K and other parameters as in Table I, then $\alpha_0 = 1.344$ and $m = 0.00384$ m s^{-1}. Similarly, with $A_{max} = 300$ W m^{-2}, $\theta_0 = 298$ K then $\alpha_0 = 1.464$ and $m = 0.00187$ m s^{-1}. With the values for α_0 and m as given in Section 3.2, then for both $A_{max} = 400$ W m^{-2} and $\theta_0 = 298$ K, linearisation predicts

$$\alpha_0 = 1.391 + (1.344 - 1.391) + (1.464 - 1.391) = 1.417,$$

$$m = 0.00326 + (0.00384 - 0.00326) + (0.00187 - 0.00326) = 0.00245.$$

As a check to obtain precise values, running the numerical model with $A_{max} = 400$ W m^{-2} and $\theta_0 = 298$ K (other parameters as in Table I) gives $\alpha_0 = 1.427$ and $m = 0.00241$. As the error in prediction of α_0 and m is significantly smaller than the overall changes in these parameters, linearisation appears valid to a first approximation. However, there are an unlimited number of possible combinations of parameter changes, and some "cross" terms may be important.

4. A Methodology to Infer Regional Values of r_S and α

4.1. Theory

Suppose at height $z = z'$, standard microclimatological measurements of windspeed, temperature, θ' (K) and humidity, q' (kg kg^{-1}) are recorded, and a measurement or estimate of energy A' (W m^{-2}) is available. Variable $\epsilon' = \epsilon(z')$, and an approximation, without stability corrections, of the aerodynamic resistance to heat and vapour from the surface to $z = z'$, r'_{ah} (s m^{-1}), may be calculated. All variables needed to calculate α within Equation (14) are known except r_S. If $\tilde{\alpha} \approx \alpha$, then Equation (15) also holds; Equation (14) represents the Big Leaf model driven by point meteorological measurements and Equation (15) summarises CBL behaviour.

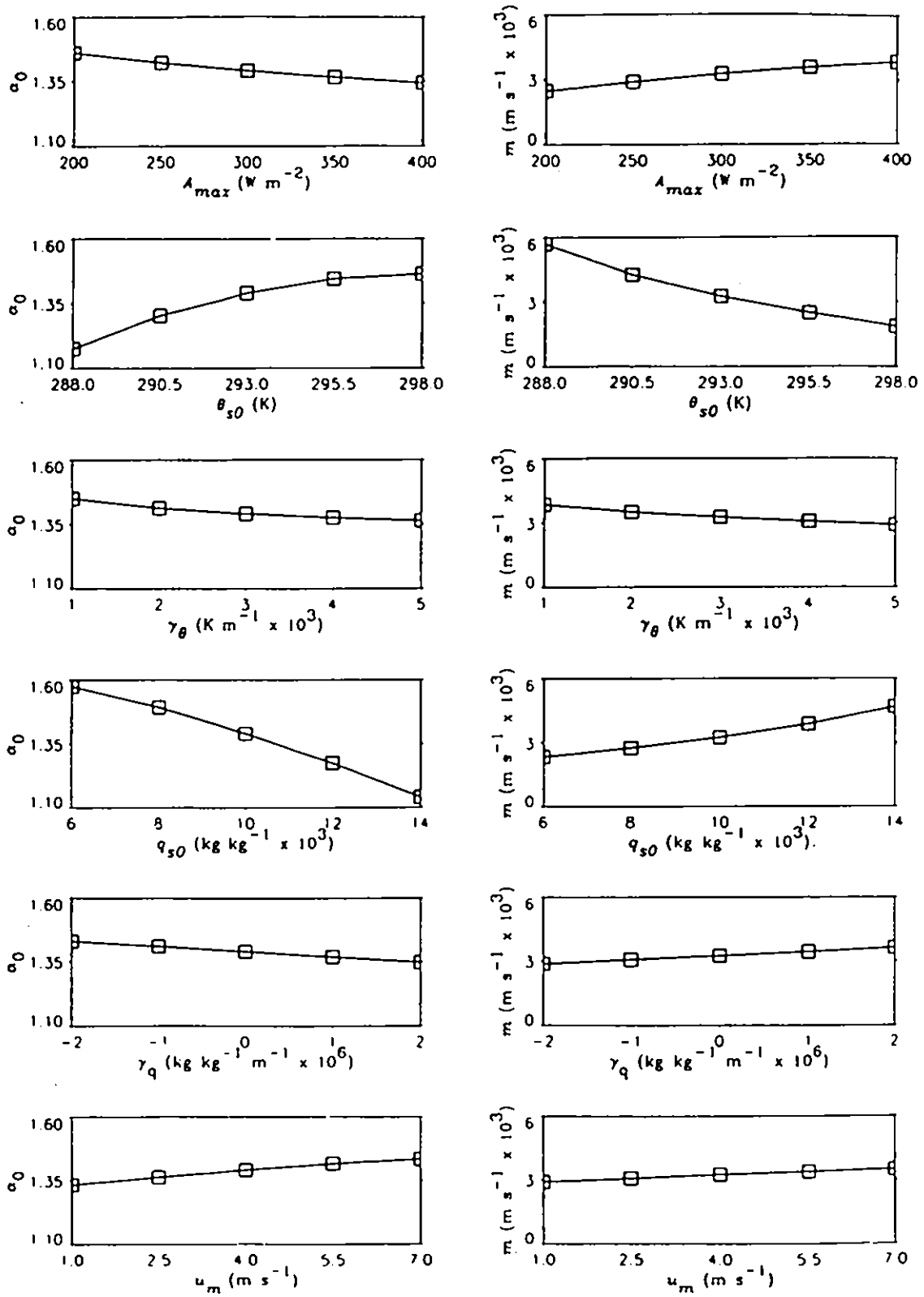

Figure 3a. The dependence of α_0 (left-hand plots) and m (right-hand plots) on variation of individual parameters (top-to-bottom) of A_{max}, θ_{s0}, γ_θ, q_{s0}, γ_q and u_m. In each case, the remaining driving variables are fixed as given in Table I. Each model run is represented by the □ symbol.

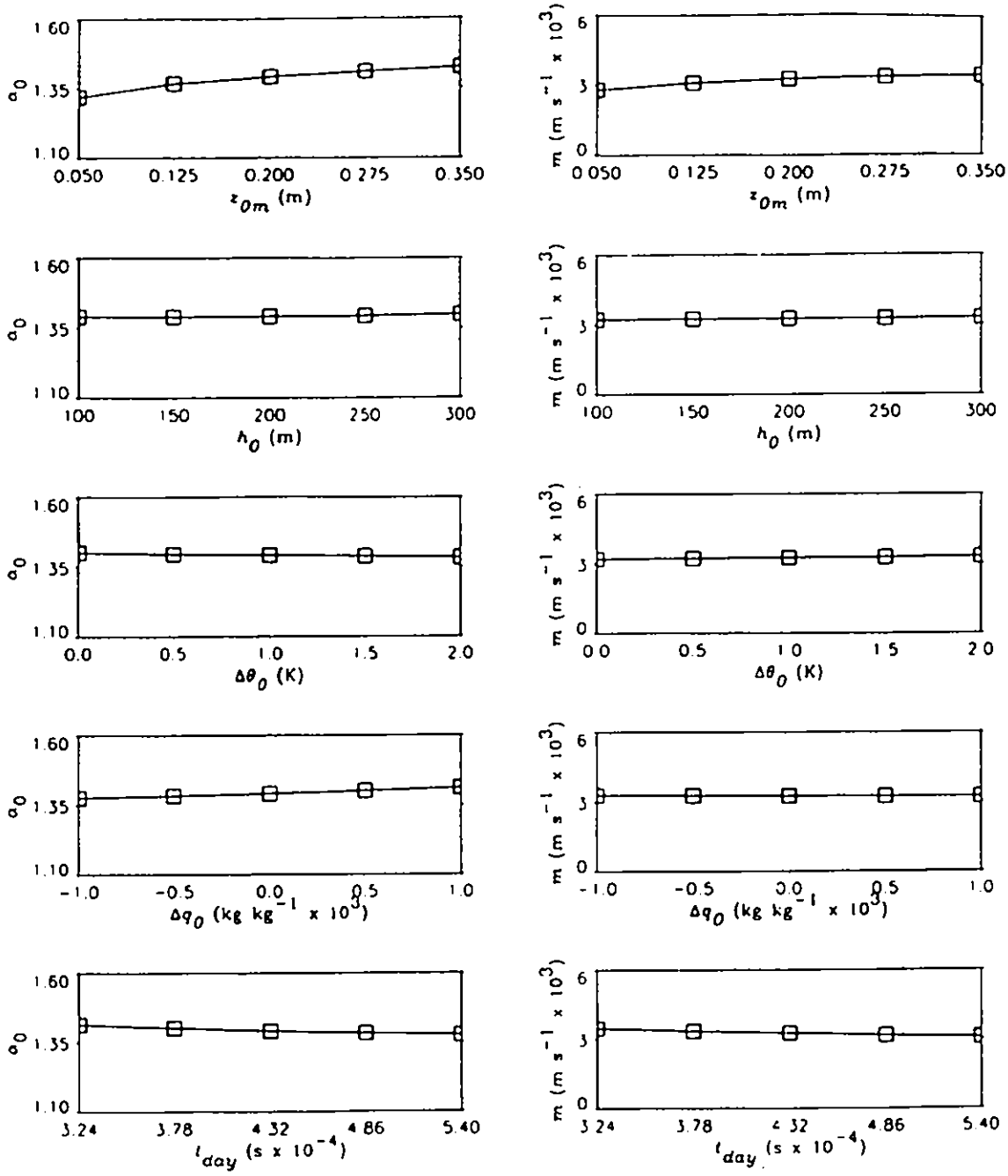

Figure 3b. The dependence of α_0 (left-hand plots) and m (right-hand plots) on variation of individual parameters (top-to-bottom) of z_{0m}, h_0, $\Delta\theta_0$, Δq_0 and t_{day}. In each case, the remaining driving variables are fixed as given in Table I. In the first case, z_{0T} is varied simultaneously such that $\ln(z_{0m}/z_{0T}) = 2$. Each model run is represented by the □ symbol.

Variable α may be eliminated between these two equations, to derive an estimate for r_S:

$$r'_S = \frac{1 - \dfrac{1}{\alpha_0}\left[1 + \dfrac{\lambda\rho\left\{q_{sat}(\theta') - q'\right\}}{\epsilon r'_{ah} A'}\right]}{\left[m\left(1 + \dfrac{\lambda\rho\left\{q_{sat}(\theta') - q'\right\}}{\epsilon r'_{ah} A'}\right) - \dfrac{1}{r'_{ah}(\epsilon' + 1)}\right]} \tag{16}$$

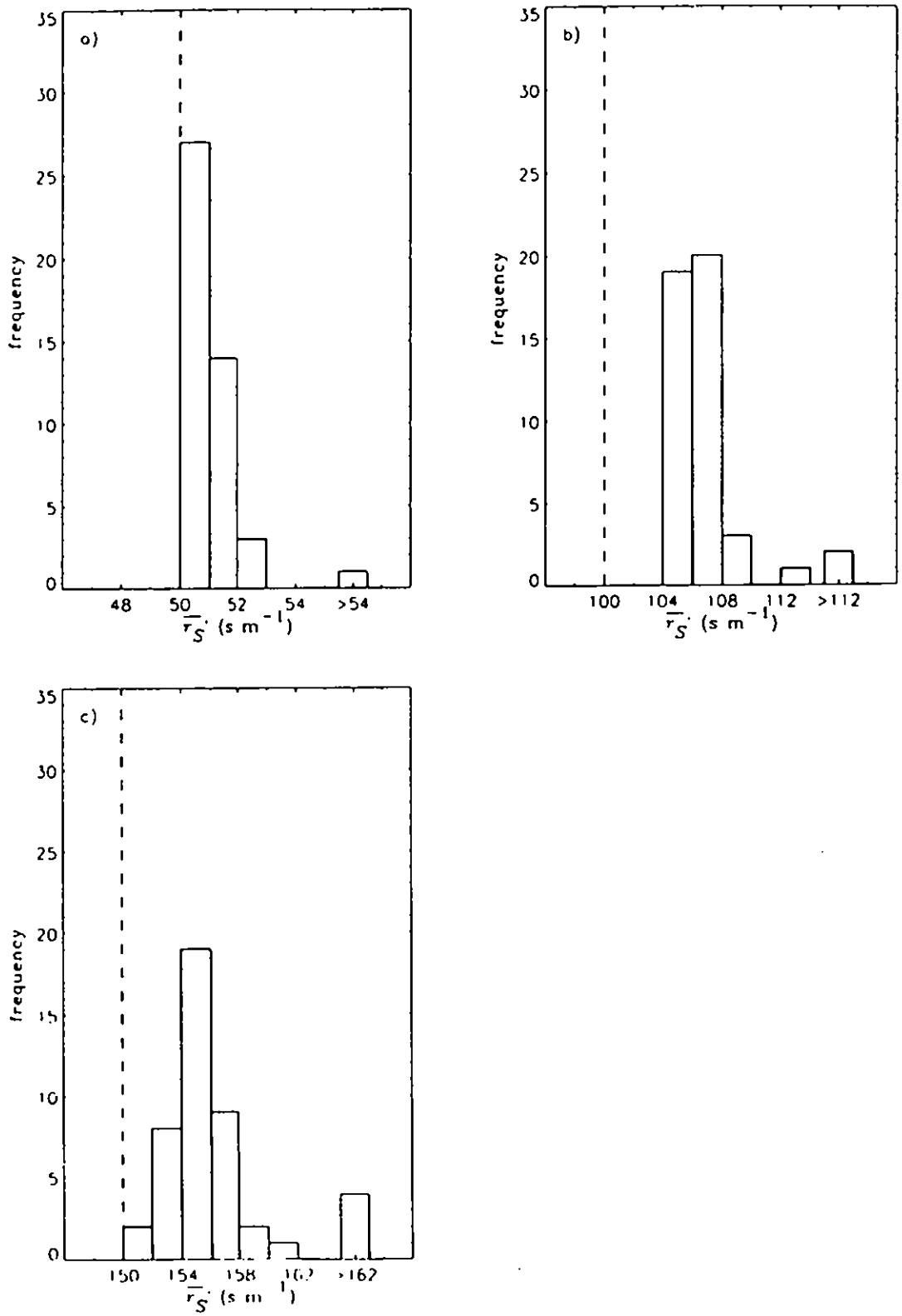

Figure 4. A histogram of values of $\overline{r'_S}$ (45 points) to provide estimates of r_S (dashed line) for the cases (a) $r_S = 50$ s m^{-1}, (b) $r_S = 100$ s m^{-1} and (c) $r_S = 150$ s m^{-1}.

An iterative procedure may be developed to include stability corrections within r'_{ah}. The Priestley-Taylor coefficient can now be estimated as $(1/\alpha_0 + mr'_S)^{-1}$.

4.2. THE PERFORMANCE OF EQUATION (16)

For the single run in Section 3.1, the numerical model calculates hourly values of r'_{ah}, D', ϵ' and A' at $z' = 2$m for the middle three-fifths of the day. Substitution of these values within Equation (16) for each of the hours, and with the values of α_0 and m from Section 3.2, yields a wide range of values for r'_S. However, their mean value is $\overline{r'_S} = 106.5$ s m^{-1}, which is very close to the prescribed value of 100 s m^{-1}. To assess whether this good estimate of r_S is merely fortuitous, and to obtain error estimates for Equation (16), this exercise is repeated for the values of driving variables and α_0 and m as presented in Figure 3a and Figure 3b. Including the control values of Table I, this corresponds to 45 points, and each numerical test is repeated for prescribed values of $r_S = 50$, 100 and 150 s m^{-1}. Values of $\overline{r'_S}$ are presented in histogram form in Figure 4 and it is seen that in all cases, there is a bias towards an overestimation of r_S. The spread is lowest for $r_S = 50$ s m^{-1}, but in all three cases the majority of values of $\overline{r'_S}$ lie within 10 % of r_S. Provided estimates are available of all parameters within Table I (such that m and α_0 may be calculated), then through Equation (16), hourly standard meteorological measurements may be used to estimate r_S on a given day without the additional requirement of surface flux measurements.

5. Conclusions

It has been demonstrated that, over a range of values of bulk surface resistance, r_S, and for a particular control set of driving conditions, a linear relation exists between the inverse of the mean diurnal value of the Priestley-Taylor coefficient and the (fixed) bulk stomatal resistance (Equation (15)). Such a relation is shown to be general over a range of driving variables, albeit with different α_0 and m values. This simple relation encapsulates much of the behaviour of a growing CBL. For a homogeneous surface, away from strong advection, and where r_S is known, this model could eliminate the need to use the Big Leaf model (and associated prescription of climate variable C) to determine surface energy partitioning.

The dependence of α_0 and m on individual changes of environmental driving conditions is shown to be generally weak. The presented dependence upon different stable-layer profiles represents an explicit technique for characterising the effect of nocturnal conditions on subsequent daytime behaviour. The weak sensitivity of parameters α_0 and m to most environmental driving conditions suggests that an acceptable estimate of these parameters values may be obtained through a simple linear superposition of known dependencies. Such calculations reveal values of driving conditions where the Priestley-Taylor coefficient departs from the often quoted range of $1.2 < \alpha < 1.3$.

The linear relation between $1/\bar{\alpha}$ and r_S can be used in conjunction with separate calculations of the Penman-Monteith equation such that estimates of r_S may be made using data from a meteorological station (Equation (16)). For the numerical runs performed, the mean of these estimates accurately predict the prescribed value of r_S. This inverse technique may be especially useful when information on the daily variation in r_S is required (for instance, during "dry-down" between rainfall events), but measurements of the evaporative flux are not available.

Acknowledgement

The authors thank E.M. Blyth, A.D. Culf, R.J. Harding and J.S. Wallace for valuable suggestions during the preparation of this manuscript.

References

Bailey, W. G. and Davies, J. A.: 1981, 'Evaporation from Soybeans', *Boundary-layer Meteorol.* **20**, 417–428.

Culf, A. D.: 1994, 'Equilibrium Evaporation Beneath a Growing Convective Boundary Layer', *Boundary-Layer Meteorol.* **70**, 37–49.

Davies, J. A. and Allen, C. D.: 1973, 'Equilibrium, Potential and Actual Evaporation from Cropped Surfaces in Southern Ontario', *J. Appl. Meteorol.* **12**, 649–657.

De Bruin, H. A. R.: 1983, 'A Model for the Priestley-Taylor Parameter, α', *J. Climate and Appl. Meteorol.* **22**, 572–580.

De Bruin, H. A. R. and Jacobs, C. M. J.: 1989, 'Forests and Regional-Scale Processes', *Phil. Trans. Roy. Soc. Lond.* B **324**, 393–406.

Driedonks, A. G. M.: 1981, 'Dynamics of the Well-Mixed Atmospheric Boundary-Layer', *Scientific Report W.R. 81-2*, K.N.M.I., De Bilt, The Netherlands.

Garratt, J. R.: 1992, *The Atmospheric Boundary Layer*, Cambridge University Press, Cambridge, 316 pp.

McArthur, A. J.: 1990, 'An Accurate Solution to the Penman Equation', *Agric. For. Meteorol.* **51**, 87–92.

McNaughton, K. G. and Jarvis, P. G.: 1983, 'Predicting Effects of Vegetation Changes on Transpiration and Evaporation', in T. T. Kozlowski (eds.), *Water Deficits and Plant Growth. Vol VII, Academic Press, New York.*

McNaughton, K. G. and Spriggs, T. W.: 1986, 'A Mixed-Layer Model for Regional Evaporation', *Boundary-Layer Meteorol.* **34**, 243–262.

McNaughton, K. G. and Spriggs, T. W.: 1989, 'An Evaluation of the Priestley and Taylor Equation and the Complementary Relationship using Results from a Mixed-Layer Convective Boundary-Layer', in T. A. Black, D. L. Spittlehouse and M. D. Novak, (eds.), *Estimation of Areal Evapotranspiration*, IAHS Publication 177, IAHS Press, Wallingford, UK.

Monteith, J. L.: 1981, 'Evaporation and Surface Temperature', *Quart. J. Roy. Meteorol. Soc.* **107**, 1–27.

Paulson, C. A.: 1970, 'The Mathematical Representation of Wind Speed and Temperature Profiles in the Unstable Atmospheric Surface Layer', *J. Appl. Meteorol.* **9**, 857–861.

Priestley, C. H. B. and Taylor, R. J.: 1972, 'On the Assessment of the Surface Heat Flux and Evaporation using Large-Scale Parameters', *Mon. Wea. Rev.* **100**, 81–92.

Raupach, M. R.: 1998, 'Influences of Local Feedbacks on Land-Air Exchanges of Energy and Carbon', *Global Change Biology* 4, 477–494.

Tennekes, H.: 1973, 'A Model for the Dynamics of the Inversion above a Convective Boundary-Layer', *J. Atmos. Sci.* 30, 558–567.

Centre for Ecology & Hydrology

Component Institutes
Institute of Freshwater Ecology
Institute of Hydrology
Institute of Terrestrial Ecology
Institute of Virology & Environmental Microbiology

Natural Environment Research Council